Université Paris 13 – Institut Galilée

Ecole Doctorale Galilée – ED 146

Thèse

pour l'obtention du grade de

Docteur de l'Université Paris 13

Discipline : **Sciences de l'Ingénieur**

Mention : **Génie Biologique et Médical**

Development of polymer nano/micro-systems as contrast agents for ultrasound molecular diagnosis of cardiovascular pathologies

Présentée et soutenue publiquement par

M. Bo LI

Le 18 janvier 2017

Directeur de Thèse : Dr. Cédric CHAUVIERRE

Co-Directeur de Thèse : Dr. Didier LETOURNEUR

Membre du Jury

Dr. Olivier COUTURE	Rapporteur
Dr. Nicolas TSAPIS	Rapporteur
Pr. Laurence MOTTE	Examinateur
Dr. Cédric CHAUVIERRE	Directeur de Thèse

Laboratory for Vascular Translational Science (LVTS) – INSERM U1148

ACKNOWLEDGEMENTS

First, I would like to warmly thank Olivier Couture and Nicolas Tsapis for agreeing to evaluate my manuscript as well as Laurence Motte for agreeing to judge my work.

Moreover, I would like to express my heartfelt gratitude to my supervisor, Didier Letourneur for giving me such a good opportunity to become part of his laboratory team. It was a great pleasure and privilege for me to join his group and to get the necessary training required to pursue a future career in this research field.

Then, I would like to owe my deepest gratitude to Cedric Chauvierre for the outstanding leadership he provided daily. He gave me independence while guiding me through the rough patches. His dedication, energy and generous support at a professional level during these four years are highly commendable. I have appreciated and enjoyed working with him.

Huge thanks to my colleagues Maya Junenet, Véronique Ollivier and Rachida Aid-Launais. They assisted me during the experiments, and without their help some of this work probably would not have been completed. I also would like to thank my previous colleague Thomas Bonnard, Pierre Saboural and Denis Arnaud for teaching me most of the technical methods in the field of their research.

Many thanks to all other collaborators for providing me reagents, rats and letting me use their equipments. In particular, Martine Jandrot-perrus, Benoit Ho-Tin-Noé and Stéphane Loyau for her experience in platelets research and equipment, Brigitte Escoubet and Clément Journé for their technical support in ultrasonic imaging, Frédéric Chaubet and Murielle Maire for their technical assistance about fucoidan, Lucas Chollet for providing fucoidan samples, Antonino Nicoletti and Francesco Andreata for their technical help in flow cytometry. I would also like to thank to the other members of our laboratory, Joana Antunes, Alexis Gillet, Louis Hatte, Marisol

Zuluaga Tamayo, Jessica Pereira, Graciela Pavon-Djavid, Anne Pelle, Angélique Levoye and Sophie Vo for their kind assistance throughout my project.

It is also a pleasure to thank some of my close friends: Peng Jiang, Xuefeng Wang, Zhaojun Sheng, Shihui Shi and Jun Hai for their insightful advice and continuous encouragement.

I would also like to thank you my parents from my heart for their unconditional love and heartfelt encouragement.

Finally, a huge thank you to my wife for her love, support and the patience she has shown during these four years. This achievement could never happen without your constant “sacrifice and understanding”, there is no word that can describe my gratitude. Thank you for giving up the opportunity to work in the US and accompanying me here. Most of all, I am grateful to your positive outlook in life and work hard mentality, which were the driving forces that helped me in crossing the finish line.

GENERAL CONTENTS

LIST OF FIGURES

LIST OF TABLES

ABBREVIATIONS

^{201}T1: Thallium-201	mLp: modified Lipoproteins
^{99m}Tc-MIBI: Tc-99m 2 methoxy-isobutyl-isonitrile	MMP: Matrix Metallo Proteinase
AAA: Abdominal Aortic Aneurysm	MRI: Magnetic Resonance Imaging
ADP: Alpha-D-ribose-1-phosphate 5-kinase	NO: Nitric Oxide
B-Mode: Brightness Mode	PACA: Poly (Alkyl Cyanoacrylate)
CR: Complement Regulatory	PBCA: Poly (n-butyl Cyanoacrylate)
CT: Computerized Tomography	PET: Positron Emission Tomography
CVD: Cardiovascular Disease	PFCs: Perfluorinated Chemicals
EC: Endothelial Cells	PFOB: Perfluorooctyl Bromide
EGF: Epidermal Growth Factor	PIBCA: Poly (Iso-butyl Cyanoacrylate)
GPVI: Glycoprotein VI	PLGA: Poly (Lactide-co-Glycolide)
HDL: High Density Lipoproteins	PLLA: Poly (L-lactide)
ICAM-1: Intercellular Cell Adhesion Molecule-1	PSGL-1: P-selectin glycoprotein ligand-1
IL: Interleukin	PVA: Poly (vinyl-alcohol)
Kd: Dissociation Constant	SLeX: Sialyl LewisX
LDL: Low Density Lipoprotein	SMC: Smooth Muscle Cells
Lp: Lipoproteins	VCAM: Vascular Cell Adhesion Molecule
MB: Microbubble	VCAM-1: Vascular Cell Adhesion Molecule-1
MCP-1: monocyte chemoattractant protein 1	vWF: von Willebrand Factor
MI: Mechanical Index	

GENERAL INTRODUCTION

Most of cardiovascular diseases, such as thrombosis, Abdominal Aortic Aneurysm, are chronic pathogenic processes that happen imperceptibly and progress silently over decades in the body. The morbidity and mortality rates of acute cardiovascular incidents and their consequences remain high in the developed countries. The reason is that traditional diagnosis and treatment of these diseases are limited by the lack of technology that enables early detection and prediction of the extent and location of vascular diseases. A recent strategy involves production of molecular imaging probes to target key biological markers, such as P-selectin, which are involved in the early pathogenesis of atherosclerotic cardiovascular disease.

Molecular imaging relies on different contrast agents to detect biochemical changes processed in vascular diseases at the molecular scale. Currently, the techniques involved in molecular imaging development almost cover all medical imaging advices. In these imaging modalities, ultrasonography is widely used as a screening tool in cardiovascular diseases because of its several obvious advantages: ease of procedure, low cost, quickly and no radiation exposure. The only drawback is low resolution. Therefore, big companies (GE Healthcare, Philips, Agilent, etc.) are highly interested by the development of new ligands and new acoustic agents for cardiovascular molecular imaging.

Fucoidan, a type of poly sulfated polysaccharide mainly found in brown seaweed, has shown strong binding ability with P-selectin in previous research. Due to this property, it has been considered as a good candidate to image vascular diseases and has gotten much attention from many researchers in the past few years.

The aim of my project was to develop high echogenic contrast agents functionalized with fucoidan, which allow molecular imaging of cardiovascular pathologic processes as efficient acoustic tracers. Here, we plan to design and synthesize three kinds of contrast agents, and subsequently assess their properties respectively. We hope that stable high echogenic targeting contrast agents could be recognized as potential diagnostic tools for vascular diseases.

The thesis is divided in two parts:

The introduction part presents the related literature reviews as background information. We briefly outlined the physiology structure of the artery and introduced relevant diseases and their underlying pathogenic mechanism. We also reviewed the difficulties that traditional diagnostic technologies are facing and described the current research orientations and achievements in addressing this challenge. Molecular imaging techniques associated with vascular pathologies, which are based on targeted contrast agents, were emphatically mentioned in this part. Then we introduced basic principle of medical ultrasound molecular technology and summarized the major types of ultrasound contrast agents. Finally, an overview of synthetic methods and applications of poly cyanoacrylate nanoparticles was provided.

In the experimental part, the results obtained in this work would be divided in 3 chapters and written in the form of publications:

- In the 1st chapter, we developed and designed the polysaccharides-coated poly (isobutyl cyanoacrylate) perfluorooctyl bromide nanoparticles, which were characterized by physical and chemical techniques. Their ability to detect P-selectin was also evaluated *in vitro* and *in vivo*.

- In the 2nd chapter, biodegradable microcapsules consist of poly (isobutyl cyanoacrylate) and polysaccharide were designed and synthesized based on emulsion solvent evaporation method. The microcapsule surface could be easily functionalized by fucoidan, which gives them specific property to bind to P-selectin expressed by human activated platelets under arterial flow conditions.

- In the 3rd chapter, we synthesized, functionalized and characterized polysaccharide-decorated microbubbles. Subsequently, their echogenicity and binding abilities to thrombi are investigated *in vitro*. The results indicated that these constructs were good candidates as contrast agents for targeted molecular ultrasound imaging of cardiovascular diseases.

INTRODUCTION

1. Arterial diseases

1.1 Physiology of the artery

The arteries are the vessels that carry blood from the heart to other tissues and organs. In humans, their diameter can vary by several tens of micrometers for smaller arterioles, about 2.7 cm for the aorta. They are characterized by a thicker wall and stiffer than the veins and are well adapted to blood pressure changes resulting from the cardiac ventricles. The arterial wall is primarily composed of 3 tunicae that surround the luminal cavity as illustrated in **Figure 1**.

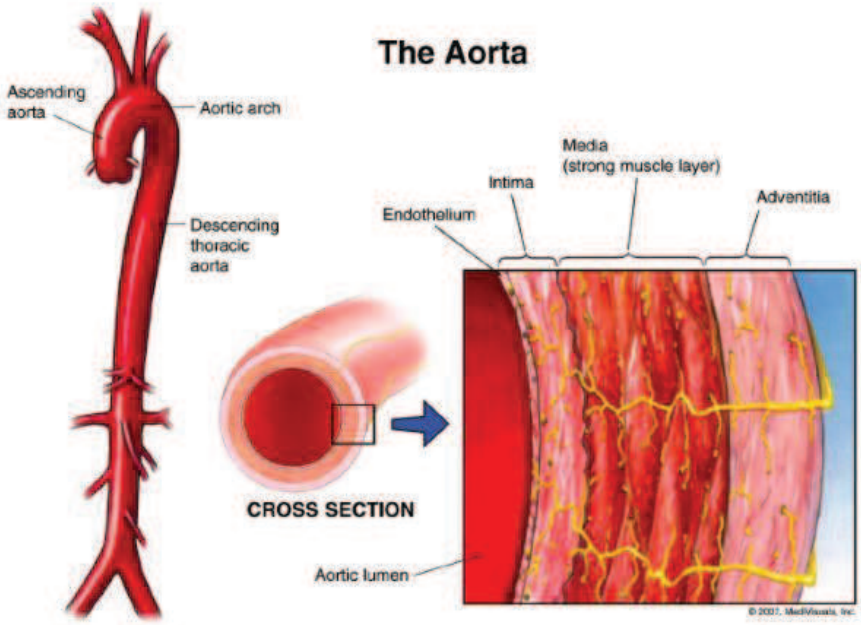

Figure 1. Structural composition of an artery.

-Tunica Intima: It forms the inner lining of a blood vessel and is in direct contact with blood as it flows through the lumen. This layer has three parts: innermost layer is a tight monolayer of endothelial cells, which are active participants in a variety of vessel-related activities; the second components is a basement membrane, which provides support base for the endothelial layer; the third part is the internal elastic lamina, which forms the boundary between the tunica intima and tunica media.

-Tunica Media: It is the thickest layer in arteries and consists mainly of extensive concentric layers of smooth muscle cells (SMC) and substantial amounts of elastic fibers. The primary role of the smooth muscle cells is to regulate blood flow and blood pressure by altering the extents of their contraction. In addition, smooth muscle cells help limit loss of blood when vessel is damaged.

-Tunica Adventitia: It consists of elastic and collagen fibers. Particularly, the external adventitia of large vessel contains numerous nerves and tiny blood vessels that supply the tissues of the vessel wall. The tunica adventitia also helps anchor the vessels to surrounding tissues.

1.2 The main diseases of the arteries

1.2.1 Atherosclerosis

Atherosclerosis is the complex process that culminates in blood vessels being narrowed and eventually occluded. It is sometimes triggered by subtle physical or chemical insults to the endothelial cell layer of arteries. The "response to injury theory" now has widespread acceptance among scientific and medical scholars, which includes several steps:

1. Endothelial dysfunction in atherosclerosis. The earliest changes in atheroma formation consist in the endothelium. These changes include increased endothelial permeability to plasma lipoproteins (Lp), especially low density lipoprotein (LDL) in the subendothelium. LDL changes itself and becomes the highly atherogenic, oxidized modified lipoproteins (mLp) by interacting with extracellular matrix components (**Figure 2A**). Affected on subtle changes of plasma lipid homoeostasis and the subendothelial accrual of mLp, the endothelial cells (EC) further trigger a multipart inflammatory process, such as expression of new or more cell adhesion molecules, cytokines and chemokines that assist in the recruitment of specific blood inflammatory cells (**Figure 2B**).

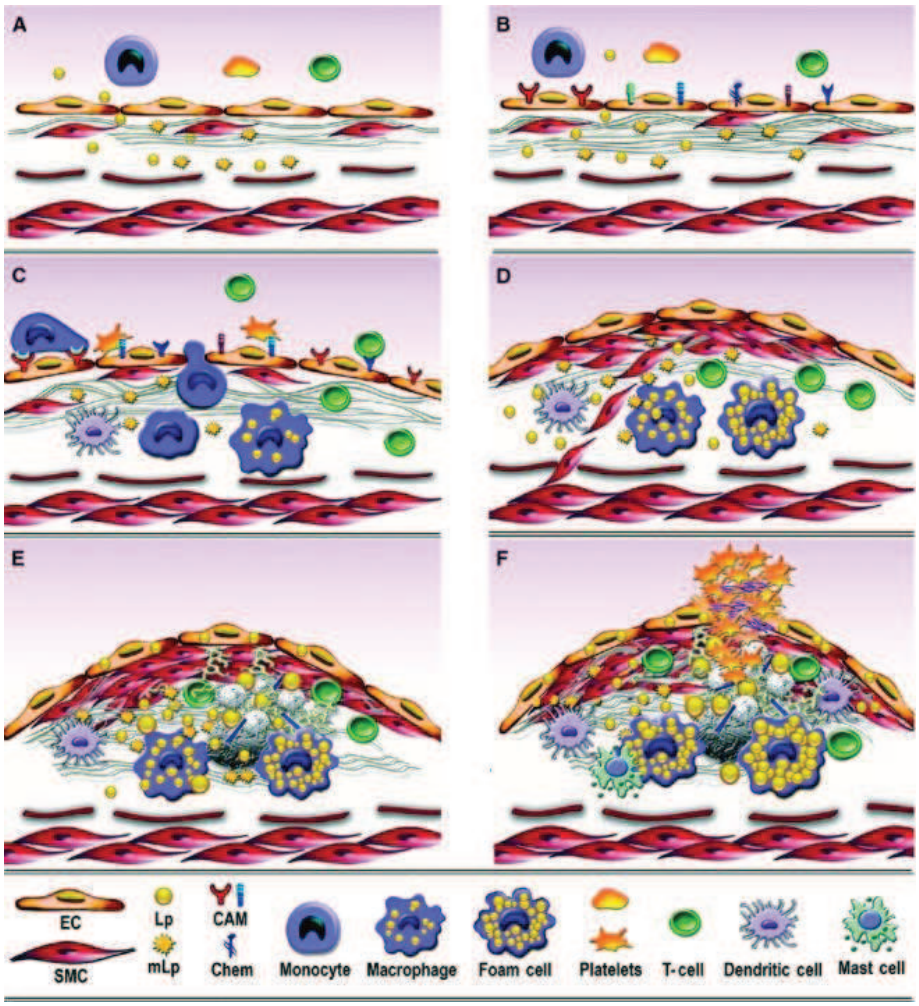

Figure 2. Stages in the development of atherosclerotic lesions.[1]

2. Recruitment of inflammatory cells and initiation an inflammatory reaction. Molecular warning signals sent by dysfunctional EC are decoded by specific immune cells (monocytes, T lymphocytes, neutrophils, mast cells) and by the resident vascular cells (SMC, dendritic cells), that respond by initiating the inflammatory process, which has a major contribution to the escalation of the atheromatous plaque formation and fate (**Figure 2C**).

3. SMC-key participants to fibrous plaque formation. Atherosclerosis progression involves the proliferation of intima-resident SMCs and migration of SMCs from the vessel's media to the intima, the latter partially degraded internal elastic leads to the formation of fibrous cap that is accompanied by increased synthesis of extracellular matrix components (**Figure 2D**).

4. Formation of an advanced calcified fibro-lipid plaque. The fibrous cap covers a mixture of leukocytes, lipid, and debris, which contributes to the formation of the calcified fibro-lipid plaque. Combined with macrophages, SMC-, macrophage-derived foam cells and extracellular lipid droplets, calcification cores may develop into large calcification centers occupying a sizeable sector of the arteries (**Figure 2E**).

5. Unstable fibro-lipid plaques in Atherosclerosis. Thinning of the fibrous cap, cell apoptosis and macrophages generate the physical rupture of the plaque, which enables blood coagulation components to directly come in contact with tissue factors, triggering the thrombus formation that extends into the vessel lumen, where it can partially or totally impede the blood flow (**Figure 2F**).

1.2.2 Arterial thrombosis

Arterial thrombosis is the process of a blood clot, also known as a thrombus, developing in an artery vessel. This thrombus is the result of sequential events involving platelet adhesion, activation and subsequent aggregation. Notably, arterial thrombi are typically composed mainly of platelet aggregates, giving the appearance of 'white clots'.[2] It can block or obstruct blood flow in the affected area. In some cases, the thrombi may break free and move around the blood stream until it reaches vessels too small to let it pass, this process is known as embolization, which causes severe diseases. For example, when it happens within in heart, lung or brain, infarction, pulmonary embolism and accident cerebrovascular (stoke) occur as a result of embolism happened within heart, lung or brain, respectively.

The formation of arterial thrombi induced by vulnerable human has been studied in detail and shown to occur in two distinct stages: the rapid first phase of GPVI and GP Ia/IIa (also known as integrin $\alpha_2\beta_1$)-mediated platelet adhesion and aggregation onto plaque collagen components (such as fibronectin, collagen, and vWF) occurred within 1 min after rupture of atherosclerotic plaques (**Figure 3A**). The second phase of coagulation started after a delay of 3 min, the thrombus is characterized by the

formation of thrombin and fibrin, and by the activation of coagulation, which is driven entirely by plaque tissue factor, moreover, fibrin fiber were observed only at sites where platelet aggregates had formed (**Figure 3B**).[3]

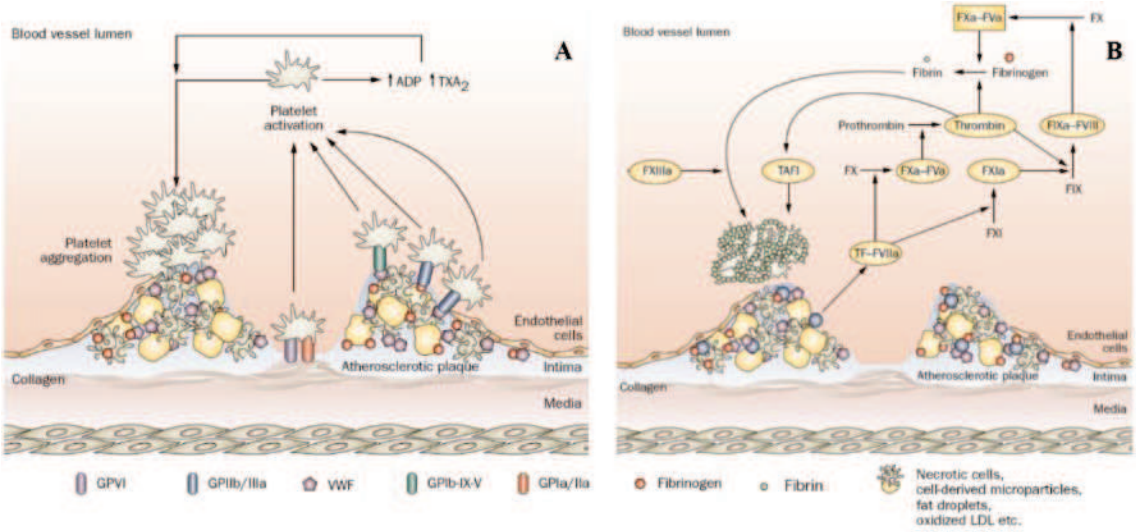

Figure 3. Summary of the formation of thrombus.[2]

1.2.3 The aneurysm

An arterial aneurysm is a permanent localized dilation of an artery encompassing all three layers of the vessel wall that has at least a 50% increase in diameter compared to the normal diameter of the artery.[4] The prevalence of aneurysm in the abdominal aorta exists in 82% of the aneurysm and affects 5% of the population in western countries. Abdominal Aortic Aneurysms (AAA) usually go undetected until they rupture, and the mortality from ruptured aneurysms is as high as 90%. AAA pathophysiology is multifactorial process involving degenerative disease of the abdominal aorta with a natural history of progressive dilatation and ultimate rupture. The mechanisms of AAA are complex and involve vascular inflammation, metalloproteinase activity and increased reactive oxygen species (ROS) production in the vessel wall.[5] Many studies published over the past decade support the view that inflammation actually plays a key role in the pathogenesis of the AAA.[6] The pathophysiology of aortic aneurysms is characterized by four events (**Figure 4**):[7]

1. Infiltration of the vessel wall. The initial stage of AAA is associated with recruitment of inflammatory cells, particularly lymphocytes and macrophage in the aortic media and the production of proinflammatory cytokines.

2. Destruction of elastin and collagen. The aortic lumen shows intraluminal thrombus formation and adhesion of inflammatory cells due to these inflammatory responses. Increased cytokines trigger the expression of matrix metalloproteinases and serine and cathepsin proteases, which degrade structural proteins such as elastin, collagen, and laminin.

3. Loss of smooth-muscle cells. Inflammatory cell infiltration exacerbates tissue injury via the production of cytokines (e.g., interleukin (IL)-6, MCP-1 and osteopontin), leading to further recruitment of immune cells and promoting smooth muscle cell apoptosis, elastin degradation, and collagen turnover either directly or indirectly. Dying SMC releases proteases, which further contribute to matrix degradation.

4. Presence medial neovascularization at aneurysm rupture edge. Neovascularization of the medial layer showed strong and consistent spatial correlation with abdominal aortic aneurysms.[8]

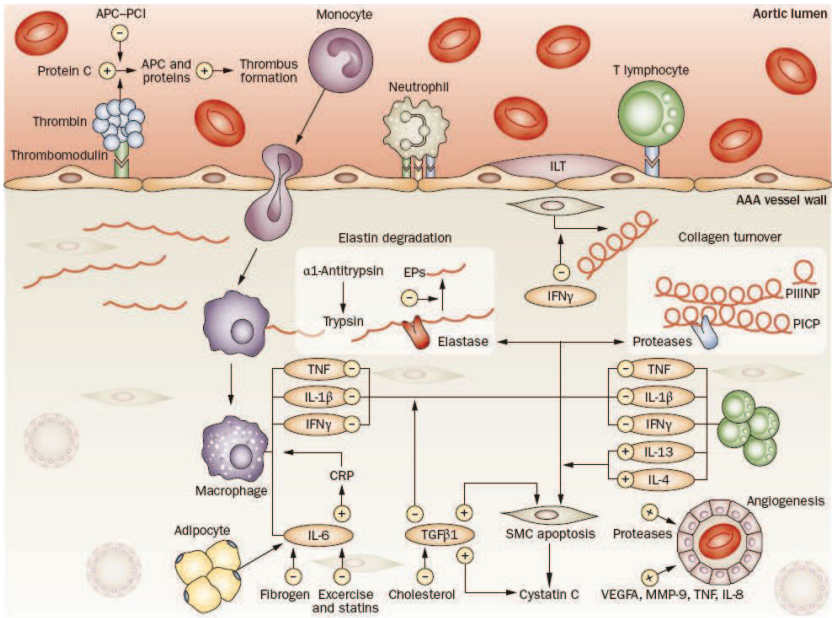

Figure 4. Summary of the mechanisms implicated in abdominal aortic aneurysm.[9]

1.3 Current diagnostic techniques

Imaging is the cornerstone in diagnosing cardiovascular disease.[10]

Most of cardiovascular diseases are chronic process that occurs stealthily and silently over decades in the body. Despite tremendous progress in diagnosis and treatment techniques advances in recent years, cardiovascular diseases due to atherosclerosis and rupture of AAAs are still the leading cause of mortality and morbidity in western countries.[11] Conventional diagnostics using ultrasound, Computed Tomography (CT), Magnetic Resonance Imaging (MRI) and contrast enhanced angiography provide valuable anatomical and morphological information about cardiovascular disease, and these techniques also can be used to estimate biomechanical stresses acting within the arterial system, which are essential to everyday clinical practice and cardiovascular research (**Figure 5**).[12] However, such cardiovascular diseases as, atherosclerotic and AAAs, can only be diagnosed at advanced stages by traditional methods, either by directly revealing the narrowing of the arterial lumen or by evaluating the effect of arterial stenosis on organ perfusion.[13]

Mounting clinical data revealed that the simply measuring the vessel is insufficient for predicting the rupture of AAA and the risk of CVD. The present and future challenge for cardiovascular medicine is to identify critical cellular and molecular mechanisms of atherosclerotic disease, and to prevent some of its manifestations and subsequently reduce its impact on health. Therefore, imaging the pathophysiological process of the disease from the molecular and cellular points of view before the onset of symptoms can make a decisive contribution in this regard.[10, 14]

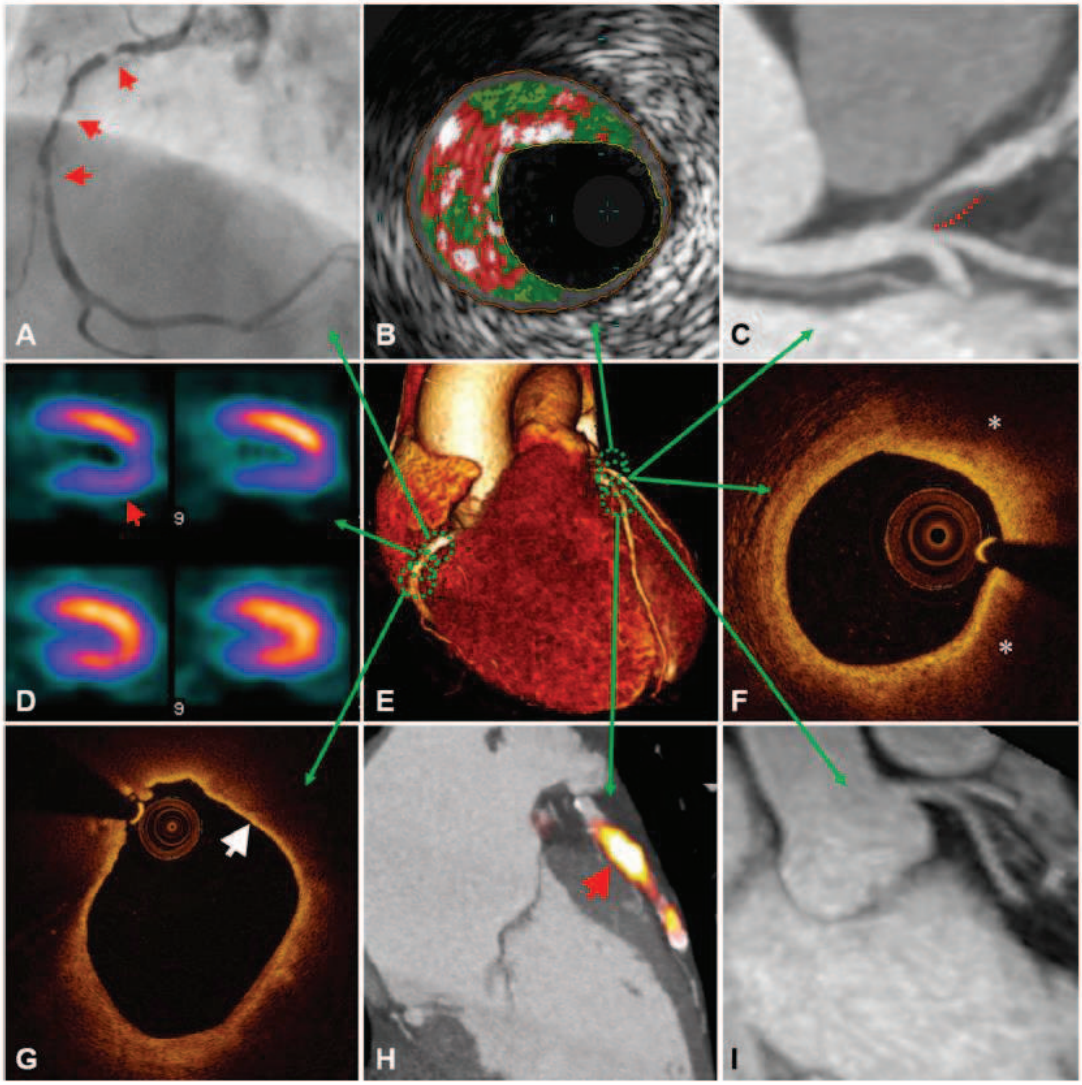

Figure 5. Multimodal approach to atherosclerosis imaging. A representative illustration of current and emerging atherosclerosis imaging modalities. A, X-ray angiography showing coronary artery atherosclerotic lesions (arrows); B, virtual histology intravascular ultrasound showing the structure of coronary plaque (red: necrotic core, white: dense calcium and dark/light green: fibro-fatty regions); C, CT angiography showing no calcified plaque with positive remodeling (dashed line); D, SPECT myocardial perfusion scan with stress-induced perfusion defect (arrow); E, 3D volume rendered CT whole-heart image; F, OCT image of a coronary plaque showing lipid (*), characterized as signal-poor regions with poorly demarcated borders; G, OCT image of a lipid-rich coronary plaque displaying thin overlying fibrous cap (arrow); H, (PET)-CT image revealing active plaque microcalcification due to high tracer uptake; I, MR angiography showing clear delineation of the proximal left coronary vessels.[12]

2. New angle of imaging cardiovascular disease

To fulfill the above-mentioned requirements, new imaging approaches should not only assess the morphology of blood vessels, but also monitor the composition of the vessel walls, enable diseases-associated abnormalities in the arteries to be observed, down to the cellular and molecular level in some cases.[13]

2.1 Functional imaging

Functional imaging techniques can detect changes in the metabolism, blood flow, regional chemical composition and absorption. Using specific tracers or probes, such as radiolabeled blood cells, lymphocytes, platelet or LDL, functional imaging is able to track their spatial distribution and reveal physiological activities within a certain tissue or organ in humans.[15]

To date, various functional imaging tools have been developed with the aim to follow

the accumulation of red blood cells, LDL, leukocytes or platelets. All of these methods based on the same strategy: combine an *ex vivo* contrast agent to one of these individual components and then inject he patient before moving the imaging. Red blood cells radiolabeled with ^{99m}Tc are injected in humans and bring a contrast signal at aneurysms of the abdominal, which is simple, non-invasive and has been used for over 30 years.[16] Thereafter, the feasibility of localizing human atherosclerotic plaques by imaging with radio-labeled LDL were assessed, results revealed that focal accumulation of radiolabel was consistent with ^{99m}Tc-LDL sequestration by plaques in the human atherosclerotic lesions.[17] Moreover, ^{111}In-labeled platelets and leukocytes have also been used for the imaging of an AAAs.[18] Furthermore, ^{99m}Tc-sestamibi (or ^{99m}Tc-MIBI) is lipophilic monovalent cations, which has been used for imaging the myocardium.[19] Perfusion imaging with SPECT most often utilizes thallium-201 (^{201}T1).[20]

Although these imaging techniques can offer valuable information in the diagnosis and management of artery diseases, they are insufficient to track the cellular/molecular event that may occur in the aortic wall long before any structural/functional changes become detectable.[15] This limitation makes it impossible for us to study a developing vessel disease through imaging or to predict future clinical risk. Therefore, there is still a huge requirement for developing novel non-invasive methods that will enable early identification and evaluation of the cardiovascular diseases progression. A recent strategy is focused on using the molecular imaging to fulfill these demands.

2.2 Molecular imaging

- What and why we need molecular imaging?

Molecular imaging is one of the most frequently used diagnostic methods. It aims to non-invasively visualize, characterize, and measure normal and pathological biological processes at the cellular and molecular levels in humans and other living organism.[21] Several different techniques used include radiotracer imaging/nuclear medicine, MRI, MRS, optical imaging, ultrasound and others. In the case of cardiovascular pathology, molecular imaging combined with specific targeting contrast agent will hopefully provide insight into potential disease mechanisms, including:

a) Diagnosis of pathologies at the early maturing stages. When anatomical deformation isn't enough to be visualized, the targeting of key molecules presented in the early stages of atherosclerosis, arterial thrombosis or aneurysm could help to evaluate the risks.

b) Observing the molecular characterization of artery. By demonstrating the presence of a certain molecule, these techniques will bring more in-depth understanding of the pathophysiological processes that underlie aneurysm development, expansion, and rupture and allow us to better predict its evolution.[22]

2.2.1 Cardiovascular disease biomarkers

To target vascular pathologies, it is necessary to identify the cells or key molecules that are only present in sufficiently large quantities during the first pathological signs of the artery. In **Figure 6**, we summarize main biomarkers involved in the development of atherosclerosis. They can be used to characterize vascular diseases status or to predict disease behavior. The molecular imaging of these biomarkers emerged as novel tool that offers many enticing prospects, such as diagnosing aneurysm early, monitoring vascular pathologies and evaluating the treatment.

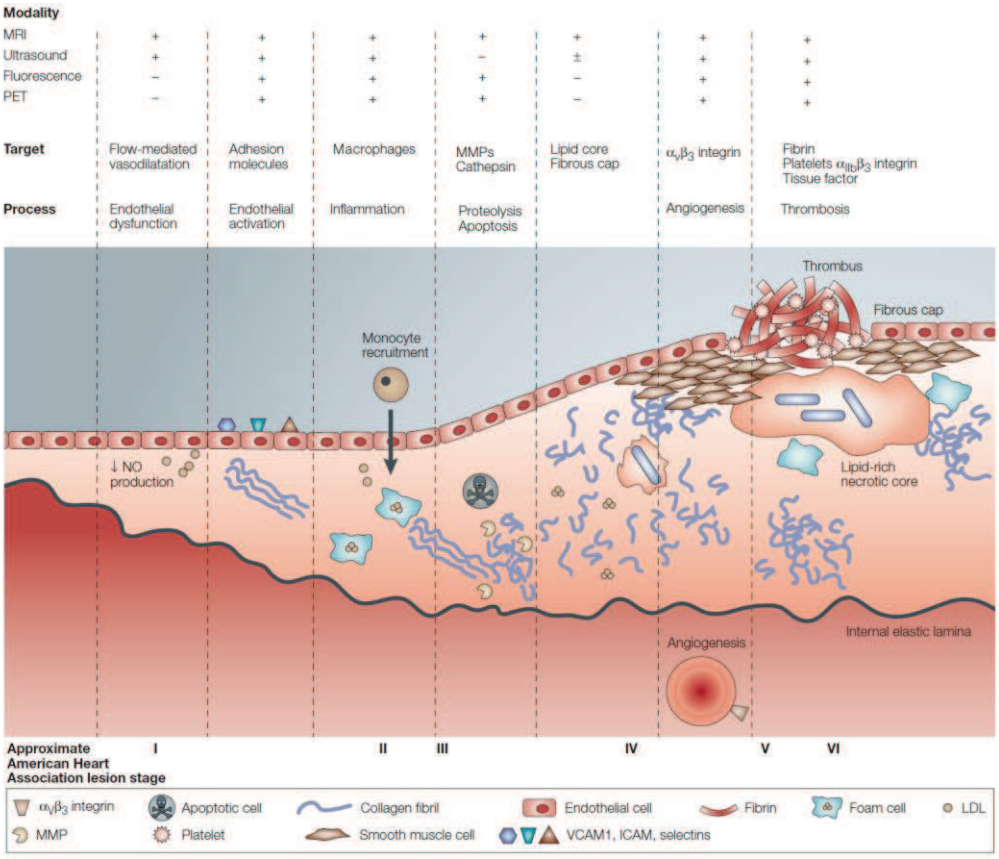

Figure 6. Imaging targets in atherothrombosis. Illustration of processes of an atherosclerotic lesion. The biomarkers could be used for molecular imaging at each stage also listed. Symbols reveal the feasibility of imaging method using each of the modalities listed.

Inflammation is currently regarded as a crucial step in the pathogenesis of atherosclerotic cardiovascular disease and is therefore an attractive target for molecular imaging techniques.[23] Vascular inflammation characterized by the release

of soluble signaling factors, including chemokines, and by the expression of endothelial cell adhesion molecules, e.g, VCAM-1, ICAM-1 and the selectin family of molecules (P-, E- and L-selectin) that play critical roles in leukocyte arrest in the vasculature, extravasation and migration to inflamed tissue.[24] The selectins, E-selectins, L-selectins and P-selectins, are a family of type-1 cell surface glycoproteins.[25] They all have 5 domains: a short cytoplasmic tail, a transmembrane region and a long extracellular portion. This last part strongly glycosylated consists of several CR (Complement Regulatory) proteins, an EGF (Epidermal Growth Factor)-like domain and a calcium-dependent lectin domain (**Figure 7**).

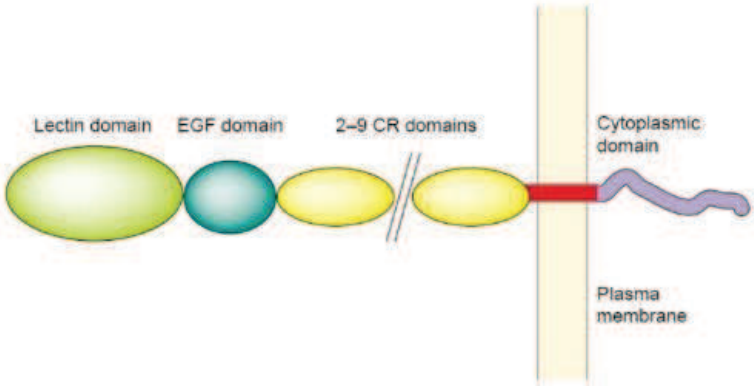

Figure 7. Selectin structure. Selectins are composed of a lectin domain (lime green), an epidermal growth factor (EGF) domain (dark green), two (L-selectin), six (E-selectin) or nine (P-selectin) consensus repeats with homology to complement regulatory (CR) proteins (yellow), a transmembrane domain (red) and a cytoplasmic domain (purple).[26]

L-selectin is expressed on all granulocytes and monocytes and on most lymphocytes, it is now implicated in many instances of inflammatory leukocyte trafficking.[27] E-selectin is not normally expressed, but is upregulated expressed on the surface of endothelial cells in the presence of inflammatory cytokines.[28] P-selectin, which is expressed by activated platelets and endothelial cells, play a mediator role in platelet-leukocyte and leukocyte-endothelium interactions and has an important role in the interplay between inflammation and platelets in atherogenesis and its thrombotic complications (**Figure 8**).[29] Exposure of endothelium to mediators including agonists, such as thrombin, histamine, the activator of kinase C or ADP

results in rapid upregulation of P-selectin expression on the cell surface.[30]

Therefore, targeting P-selectin using novel molecular imaging probes is an attractive therapeutic target in vascular disease.[31]

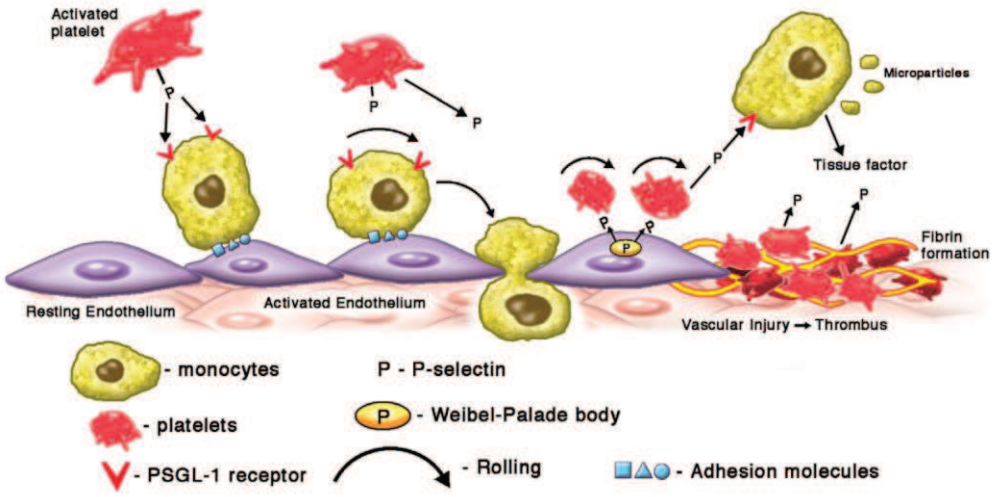

Figure 8. P-selectin in thrombus. Role of P-selectin linking inflammatory and thrombotic pathophysiological pathways at the arterial vessel wall.[32]

2.2.2 P-selectin ligands

- Antibodies

Until now, three kinds of molecules are determined as candidate ligands for P-selectin (**Figure 9**). Among those, antibodies-based agents get good imaging results.[33] However, the production of these tracers is also rather complex and expensive in a quantity that would be demanded for use as a clinical reagent.[34]

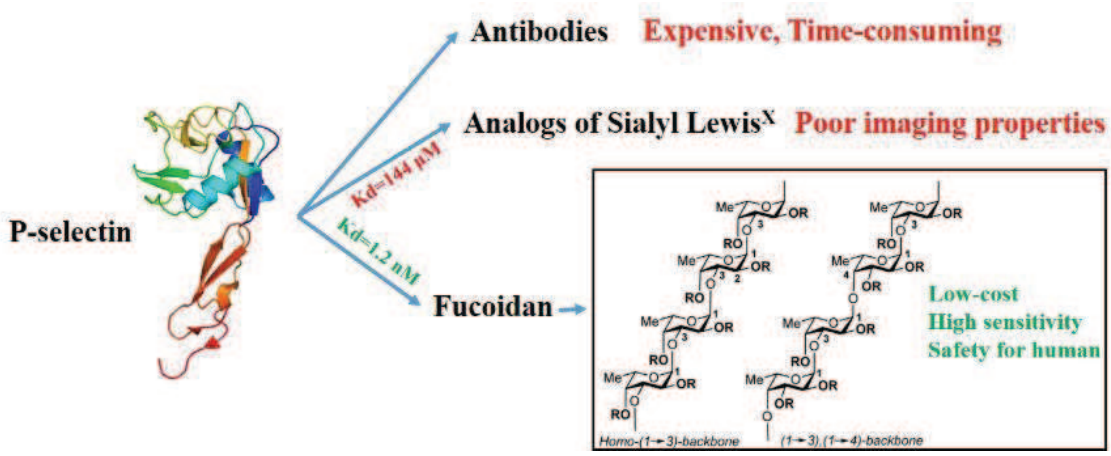

Figure 9. P-selectin ligands for molecular imaging.

- Sialyl Lewis^X

The Sialyl Lewis^X (SLe^X) is a well-known nature ligand for all of three selectins.[35] Structural features of Sialyl Lewis^X are essential for binding with selectins: the hydroxyl functions of L-fucose and D-galactose, and the carboxylic group of sialic acid.[35] Numerous previous studies have shown that synthetic analogs of SLe^X interact with P-selectin. However, its application prospects are limited by their poor imaging properties.

2.2.3 Fucoidan

Fucoidan, first isolated by Kylin in 1913, are a type of fucose-rich sulfated polysaccharides, mainly found in the cell-wall matrix of various brown marine algae.[36] The chemical composition of fucoidan is extremely variable owing to its heterogeneity and irregularity.[37] It contains a linear backbone built up of (1→3)-α-L-Fuc or alternating (1→3)-α-L-Fuc and (1→4)-α-L-Fuc (**Figure 9**), (1→2)-α-L-Fuc sometimes being present in the backbone branching.[38] Sulfate groups in the native polysaccharide occupy positions 4 (mainly) and 2, whereas some 3-linked α-L-fucopyranose residues are acetylated at O-2.[39]

- Biological activity of fucoidan

In recent years, fucoidan has been extensively studied aiming at assessing their potential biological activities. These include antitumor effect, antivirus,[40] anti-inflammatory, anticoagulation and antithrombosis,[41] as well as their effects against various renal, hepatic and uropathic disorders.[42]

The anticoagulant effect of fucoidan is considered to be a complex mechanism involving direct inhibition on the enzyme and indirect inhibition of thrombin through the activation of thrombin inhibitors.[43] Other results confirmed that, like heparin, fucoidan could prolong the clotting time of human plasma *in vitro* and inhibit rat thrombosis *in vivo*.[44] From this base, it has been proposed that fucoidan may represent promising candidate for prevention or treatment of thrombosis-related cardiovascular disease.

Previous studies also have shown fucoidan inhibits cancer cell proliferations by inducing cell cycle arrest, inducing apoptosis, regulating growth signaling molecules and inhibits metastasis and angiogenesis.[42]

- Why choose fucoidan?

Numerous previous studies have shown that polysaccharides, such as heparin and dextran sulfate, interact with P-selectin. Our group has observed fucoidan exhibited the highest affinity for immobilized P-selectin with a Kd of 1.2 nM as compared to 557 nM for heparin, 118 nM for dextran sulfate (**Figure 10A**) and 320 nM for PSGL-1 particularly.[45] Together, fucoidan could be used in biomedical applications as a targeting ligand for P-selectin.

In the past decade, Rouzet *et al.* showed the ^{99m}Tc labeled fucoidan allowing SPECT imaging of thrombosis and heart ischemia thanks to the interaction of fucoidan with P-selectin overexpressed by activated platelet and activated endothelium (**Figure 10B**). Suzuki *et al.* evidenced the capacity of superparamagnetic functionalized with fucoidan to detect *in vivo* the intraluminal thrombus of abdominal aortic aneurysm in

a rat model with a 4.7 T MR Imager. Bonnard *et al.* designed dextran/pullulan/fucoidan microparticles radiolabeled with ^{99m}Tc or were embedded with USPIO to image an aneurysmal thrombus in a rat model. Among these, fucoidan has been evidenced as good candidate to image atherothrombosis *in vivo*.

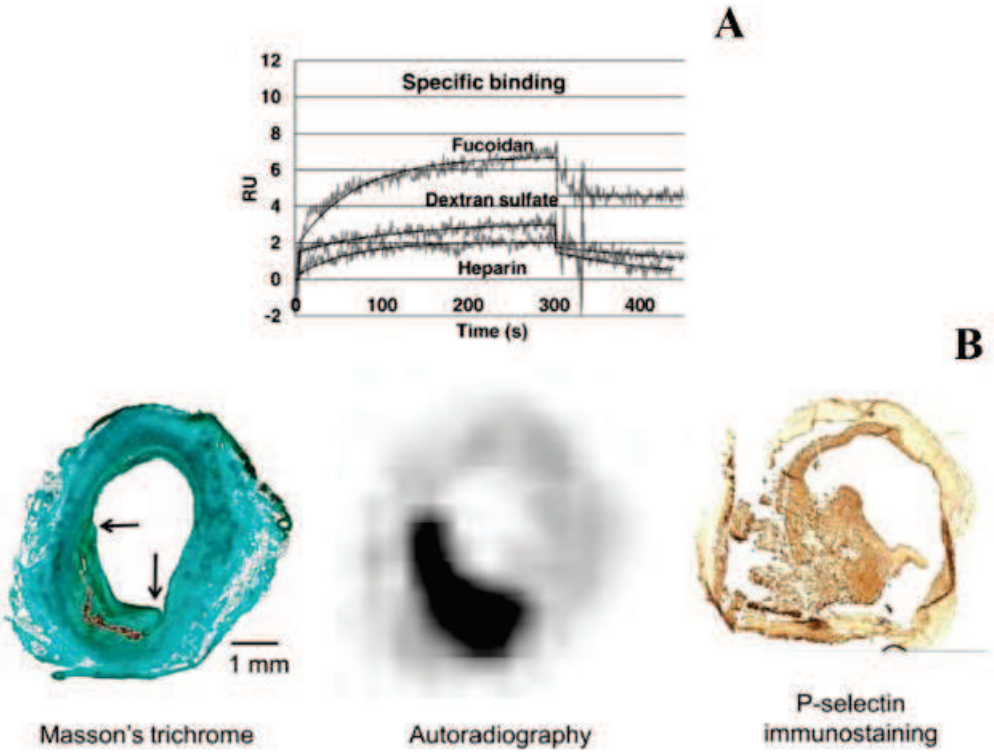

Figure 10. Targeting P-selectin by ^{99m}Tc-Fucoidan. (A) Dissociation constants were calculated using a 1:1 Langmuir binding model plot for the specific binding on P-selectin of fucoidan (upper curve), heparin (lower curve) or dextran sulfate (middle curve);[45] (B) Intraluminal thrombus in AAA in rat. Compared analysis of histology (Masson trichrome) and autoradiography on same slice, P-selectin immunostaining with nuclear counterstaining (different sample). Mural thrombus on Masson trichrome staining (arrows) matched 99mTc- fucoidan uptake on autoradiography.[46]

2.3 Molecular imaging platforms

Molecular imaging depends on various imaging modalities, as reviewed in **Table 1**. Each approach exhibits advantages and weaknesses.[47] Among those, X-ray and CT offer high spatial resolution and rapidity, but they are limited by sensitivity and require exposure to radiation. Positron Emission Tomography (PET)/Single Photon Emission Computed Tomography (SPECT) imaging provide high sensitivity, whereas

they rely on radioactivity and are very expensive. MRI also exhibits high sensitivity and resolution but lacks contraindication for certain metallic implants and cost. Ultrasound keeps promise for imaging because of its relative low cost, wide availability, and high spatial resolution. The challenges of echography include restricted depth penetration and sensitivity. Combined with respective molecular imaging probes, these imaging technologies could provide new perspective to review vascular disease.

Table 1. Summary of imaging technologies for imaging arterial pathology. (adapted from [48])

Modality	Capabilities		Application		Contrast Agents/ Radionuclide Tracers
	Anatomical	Molecular/Functional	Benefits	Limitations	
Ultrasound	X	X	Rapid, accurate, low cost, reproducibility, widely available	Limited resolution, Image interpretation difficult, artifacts common	Microbubbles
CT	X	X	Rapid, high resolution, useful for early clinical followup	Ionizing radiation, requires contrast agent	Iodine or Barium
MRI	X		Soft tissue contrast, high resolution	High cost, large equipment required	Gadolinium chelates
		X	Customizable molecular targeting, cell tracking	Limited sensitivity, requires contrast agent	USPIO or gadolinium chelates
Bio-lumine scence		X	High sensitivity, high specificity	Shallow tissue penetration, requires transgenic modification	Exotic transgenic cells combined with luciferin
SPECT		X	3D imaging, widely available, highly sensitive, simultaneous imaging of multiple processes	Limited temporal resolution, few radionuclide tracers	^{99}TC, ^{111}In, ^{201}Tl, ^{123}I, ^{131}I
PET		X	Quantification of metabolism and blood flow, high sensitivity, many radionuclide tracers	High cost, limited availability, large equipment required, short tracer half-life, single process evaluation	^{18}F, ^{11}C, ^{13}N, ^{15}O, ^{82}RB

2.4 Micro-/Nanoparticles for molecular imaging of biomarkers

2.4.1 What is so special about the micro-/nanoscale?

Recently, many peptides, antibodies or other small molecules have been conjugated directly to contrast agents for imaging of cardiovascular inflammatory events. Their

promising results makes molecule imaging promising in revolutionizing diagnostic modalities for vascular disease. In addition, their small size is conducive to injection into the body without causing complication or vascular occlusion, but they also have many shortcoming such as poor relaxation enhancement efficiency, the rapid elimination and extravasation out of the vasculature.[49] Due to their larger size, nano-/macromolecular combines contrast agent and targeting agents are being developed for overcoming these limitations. This approach has many advantages in early diagnostic accuracy of the diseases:[50]

- Long-circulating formulation and tunable biodistribution can be imparted by ease of surface modification;[51]

- Hypothetical biocompatibility and imaging properties can be adjusted by their chemical composition, structures and sizes;

- Desired targeting property can be engineered by conjugation with specific molecules interactions, such as antibodies, nucleic acids, peptides and polysaccharide ligands;

- Large surface area-to volume ratio which enables high conjugation of ligand leading to a higher affinity with target molecules.

2.4.2 Micro-/Nanoparticles service for molecular imaging

This part focuses on the development of an array of micro-/nanoparticles contrast agents already being evaluated or with promise for future applications in cardiovascular disease imaging (**Table 2**). Among them, three type of nanoparticles: lipid-based, inorganic nanoparticles and polymer-based have been developed for molecular imaging of cardiovascular pathologies.

Lipid-based nanoparticles, such as liposomes, micelle or microemulsions are closed spherical vesicles composed of lipid and/or amphiphilic components, which have both hydrophobic and hydrophilic parts that spontaneously assemble into aggregates under

aqueous conditions. Micelles are made of a monolayer of lipids surrounding a hydrophobic core with diameter 50 nm. Similar to micelles, liposomes are created from hydrophilic core enclosed by the bilayer-forming lipids, which are usually composed of a polar headgroup and two fatty acyl chains, their size stands around 150 nm.[52] High density lipoproteins (HDL)-like nanoparticles have been demonstrated to selectively targets atherosclerotic plaques *in vivo* and substantially enhance the MRI image.[53] Therefore, according to their biocompatibility and their versatility, modified lipid-based nanosystems are valuable formulations for probing preclinical cardiovascular diseases.[54]

Table 2. Summary of select micro-/nanoparticle applications in cardiovascular imaging.

Modality	Contrast agent	Particle type	Mean diameter	Targeting strategy	Targets	Animal model	Ref.
MRI	USPIO	Micro	2.3 um	Fucoidan	P-selectin	AAA	[55]
		Nano	47.5 nm	-	-	AAA	[56]
	MPIO	Micro	1.0 um	Antibodies	P-selectin VCAM-1	apoE$^{-/-}$ mice	[57]
SPET	^{99m}Tc	Nano	350 nm	Fucoidan	P-selectin	AAA	[58]
CT	Au	Nano	100 nm	-	-	Thrombus in mouse carotid arteries	**[59]**
PET	^{64}Cu	Nano	15 nm	Antibody	CCR8 receptor	apoE$^{-/-}$ mice	[60]
Ultrasound	Perfluoropropane	Microbubble	1 um	Peptides	glycoprotein IIb/IIIa	Acute thrombotic occlusion in rabbit	[61]
	gas	Microbubble	2 um	Antibodies	glycoprotein IIb/IIIa	Thrombus in mouse carotid arteries	[62]

Inorganic nanoparticles (NPs), such as semiconductor quantum dots (QDs), iron oxide NPs and gold NPs, have been exploited as contrast agents for diagnostics by molecular imaging.[63] QDs have been especially useful for multiplexed and long term optical imaging of biological processes; Magnetic nanoparticles are particularly important for MRI and drug delivery; Metallic gold nanoparticles are important in imaging, as drug carriers, and also for thermotherapy of biological targets. Small molecules, as bisphosphonates, phospholipids and polymer have been widely used as a coating in order to improve stability and biocompatibility.

Synthetic and natural polymers nanoparticles have been studied by many research

groups and play a pivotal role in a wide range of files in the past decades.[64] Various techniques such as: solvent evaporation, emulsion polymerization, interfacial polymerization are employed for their preparation. The properties of polymer nanoparticles such as size, porosity and hydrophobicity, is adjustable due to the polymer nature and the synthesis parameters. Polymer nanoparticles with specific biomarkers have been highly investigated in medical imaging for diagnosis and treatment of cardiovascular diseases. Poly(alkyl cyanoacrylates) (PACA) are biodegradable and biocompatible polymers widely employed for nanobiologic research.[65] Polysaccharide-based nanosystems have received a lot of attention in atherothrombosis management.[66] In particular, heparin or fucoidan-based nanoparticles present a high affinity to P-selectin, respectively.[67]

Unfortunately, of many molecular imaging agents that have been introduced for detection of inflammation and matrix remodeling in cardiovascular pathology, only a small subset has been evaluated in clinical studies and preclinical models of aneurysm.

3. Ultrasound molecular imaging

3.1 Echography

Echography, also called ultrasound imaging or sonography, is an imaging method which uses high-frequency sound waves to create an image of a part of body in real time; that is, not only do they show the structure of body tissues and organs, but also show movement of the body's internal organs as well as blood flowing through vessels. A computer program could analyze the echoes of sound waves sent into body and generate an image on screen. It is a widely available, portable non-invasive and cost-effective diagnostic modality comparable to other imaging modalities, which is employed for many different therapeutic and diagnostic spanning cardiology, peripheral vascular disease and obstetrics.

3.2 Principal theory behind ultrasound

Ultrasound works on acoustic signals produced by reflection or backscattering of acoustic waves with frequencies. An ultrasound transducer sends wave pulses consisting of alternating high and low pressure, which are partially reflected by surfaces between different tissues and various structures within the body. Backscattered ultrasound waves generate echoes that can be detected by the ultrasound probe, then can be converted into electrical pulses and digitized by imaging system. Owing to the time intervals between pulse transmission and reception, as well as the speed of sound in the tissue, an image can be generated depending on scattered sound signals.[68]

Medical ultrasound devices frequencies range from 1 MHz to 20 MHz. Proper selection of transducer frequency is an important concept for providing optimal image resolution in diagnostic and procedural ultrasound (**Figure 11**). Normally, compared with low frequency waves (long wavelength), the high frequency waves (short wavelength) generate higher axial resolution images, but the lower depth of ultrasound penetration. Therefore, they are suitable for imaging mainly superficial structures.[69] On the contrary, low frequency waves offer images of poorer resolution but can penetrate to deeper structures.[70]

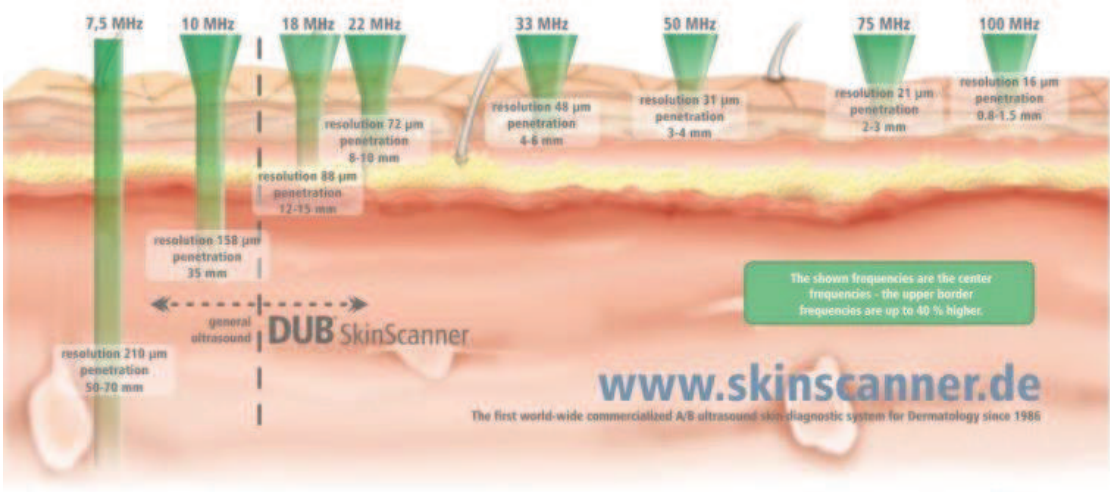

Figure 11. Different frequencies of ultrasound.

Current technologies based on simple reflection and reading of sound echoes, called brightness-mode, or "B-Mode", can produce an image at resolutions down to the millimeter scale. B-Mode imaging is frequently used to detect abnormalities within major organs, arteries, and veins in the cardiovascular system, or to image a growing fetus. In all of these cases, there is a significant acoustic mismatch between the surrounding media, blood or amniotic fluid, respectively, and the targeted tissues, allowing them to show up as bright outlines. However, features such as thrombus or cancers are similarities in tissue compressibility, making them difficult to distinguish from background noise. Additionally, B-mode can be insufficient to early diagnose and identify tissue diseases such as arterial wall dilatation because of the resolution limit.

Contrast agents, or small particles that can be injected and have a high echogenicity in comparison to the surrounding tissue, have been developed to overcome these limitations. The addition of a contrast agent allows for much easier viewing of tissue contours, enabling the clinician to find any physical abnormalities quickly.

3.3 Microbubbles

The majority of ultrasound contrast agents being used are microbubbles. As their name implies, their size range between 1 and 10 μm (**Figure 12**). Extravasation of microbubbles (MB) to surrounding tissue is inhibited, preventing unspecific accumulation in the interstitial space and unwanted background signals.

Micron-sized bubbles were found to cause proper backscattering of applied ultrasound pulses, not only with linear oscillations, but also with non-linear ones, which are not strongly present in most tissues (**Figure 12**). Thus, MBs can be detected with high sensitivity and a good contrast. With the introduction of microbubble contrast agents, diagnostic ultrasound has entered a new area that allows the dynamic detection of tissue flow of both the macro and microvasculature.

The major factor that affects the properties of MBs includes the type of gas and shells. The choice of gas is the most important factor that considered first.

The first-generation MBs (e.g. Albunex@) were filled with air, which disappeared from the bloodstream within a few seconds after administration, due to the high solubility of air in blood and a thin (10-15 nm) protein shell coat that was insufficient against gas diffusion.[71] In the currently-MBs, biocompatibility, inert and high molecular weight gases like perfluorocarbon or sulfur hexafluoride were used (**Figure 12**). They prolong the lifespan of MBs with the circulation due to their decreased solubility and low diffusion coefficient in water/blood.

Even though the included gas is responsible for the majority of the bubbles' acoustic properties, the shell adds a mechanical stiffness and reduces the compressibility of the gas (**Figure 12**). Therefore, the shell material provides multiple possibilities to tailor the MBs to their specific application by changing surface properties.[72] Meanwhile, encapsulation improves stability against gas loss, dissolution, and microbubble coalescence, and it produces a more standard size distribution.

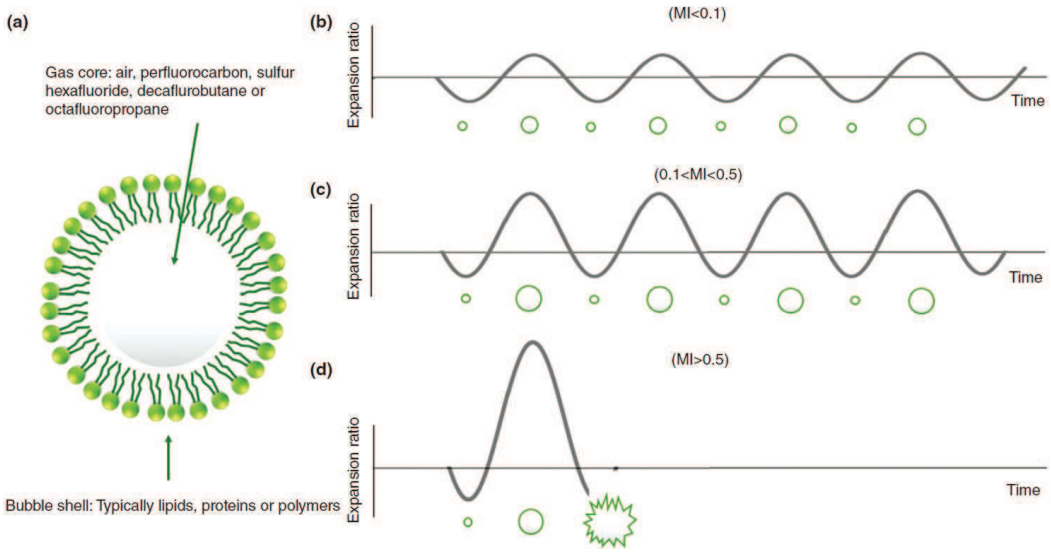

Figure 12. Microbubble ultrasound contrast agents. (a) Structure of a microbubble; (b) Microbubble linear oscillation under low acoustic power; (c) Microbubble nonlinear oscillation under medium acoustic power; (d) Microbubble destruction under high acoustic power (MI>0.5).[73]

3.3.1 Hard-shell microbubbles

Hard-shell microbubbles commonly have a more rigid shell made of polymers or denatured proteins which have lower elastical properties and can increase their stability to certain degree. Generally, hard-shell microbubbles offer the advantage of being more stable and increasing circulation time *in vivo*. Though the rigidity of shell has been shown to significantly hamper oscillations of the gas core and impair echogenicity of microbubbles, it does not change the fact that hard-shell microbubbles is considered as the first choice of contrast agent for higher-intensity ultrasound application where they provide a higher echogenicity than soft-shell microbubbles which might be destroyed.[74]

- Polymer-shelled microbubbles

In addition to improving the stability, the thick polymer shell may allow microbubbles loading a large number of drugs and offer higher ligands density for the efficient targeting of tissues. To date, many kinds of biocompatible synthetic polymer were used as shell materials.[75]

In recent years, poly (D, L-lactide-co-glycolide) (PLGA) with varying lactic and glycolic acid ratios has become one of the most studied diblock copolymer biomaterials and attracted widely attention. PLGA microbubbles are produced from a double emulsion-solvent evaporation method. Changing the reaction conditions such as the emulsification speed and sodium cholate concentration will result in microbubbles with diameters of several hundred nanometers to several micrometers. The shell of PLGA-MBs could also be adjusted by varying factors like the molecular weight, adding phospholipids or capping structures to polymers' ends.[76] A recent study has shown PEGylated and biotinylated could be incorporated PLGA microcapsules shells.[77] These structures could be attractive molecular target contrast agents via link specific ligand. However, there is currently no Food and Drug (FDA)-approved PLGA-MB for clinical applications.

Cyanoacrylate is another commonly used as membrane material for polymer microbubbles synthesis. Sonovist® (Schering AG, Germany) is a contrast agent made of air bubbles encapsulated in a poly(cyanoacrylate) shell.[78] These compounds were shown to last more than 10 min circulation *in vivo* and to be taken up by the reticuloendothelial system effectively. This microbubble can be synthesized in a simple one-step synthesis by vigorously stirring during polymerization in presence of surfactant and cyanoacrylate. Since Sonovist®, other cyanoacrylates are investigated for preparation microbubbles as well. poly(n-butyl cyanoacrylate) (PBCA) is characterized by a good biocompatible polymer and considered as a membrane material for MB synthesis. Similar to Sonovist®, PBCA-MB are synthesized during intensive stirring and in presence of surfactant and hydrochloric acid.[79] PBCA-MB has been tested for various diagnostic or therapeutic ultrasound-supporting applications. Olbrich *et al.* compared one-and two-step synthesis protocols as well as the stirring intensity to evaluate the variation of the size, the shell thickness, the resulting properties of MB under acoustic pressure, and finally the MB survival time in plasma and serum.[80] Palmowski *et al.* synthesized streptavidin-coated PBCA-MB, which can target specific area by conjugating specific ligands, antibodies.[81] After labeled by fluorophores or iron nanoparticles, PBCA-MB is able to be a useful tool for multimodal imaging with ultrasound and 2-photon-/fluorescence microscopy or MRI.[75]

- Protein-shelled microbubbles

Despite protein-shelled microbubble are less resistant to ultrasound waves than polymer-coated MB, it has longer history of use and development. Albunex® (Molecular Biosystems, San Diego, CA, USA, and Mallinckrodt, St. Louis, MO, USA) was the first generation commercially available ultrasound contrast agent for cardiac echography approved by USA and Japan. It consists of air encapsulated by a thermally denatured serum albumin shell. However, the bubbles had a very limited lifetime (< 1 min) *in vivo* due to its air-filled core. The second generation USCA, such as Optison® (GE Healthcare, Bucking hamshire, UK), was the improved.

Perfluoropropane gas was used instead of air, since this is stable and results in a longer persistence time, their diameter ranged from 2 to 5 μm. Optison® is FDA-approved for cardiac applications such as left ventricular opacification and endocardial border definition. Albumin-based MBs combined with dextrose were used for molecular targeting.[82]

3.3.2 Soft-shell microbubbles

Soft-shell microbubbles commonly covered by a monolayer of surfactant molecules or phospholipids and readily expand and contract during the ultrasound pulse, making them are sensitively detectable by their non-linear oscillations.[83] The better echogenicity of soft-shell MBs compared with hard-shell MBs are mainly due to the thinner, more flexible shells, which are held together through hydrophobic interactions (i.e., intermolecular dispersion and electrostatic forces) rather than covalent bonding or chain entanglement. Recent experimental evidence has shown soft-shell microbubbles are able to split into several smaller bubbles at high acoustic pressures instead of destruction like hard-shell MBs.[84] Sonazoid™ (GE-Healthcare) is surfactant stabilized contrast agent containing perfluorocarbon gas for heart and liver imaging. BR14® Bracco (Geneva, Switzerland) is a novel ultrasound agent with a shell of a phospholipid monolayer. Perfluoropropane gas core is used as the gaseous core and is currently undergoing Phase II studies in humans.

3.4 Nanobubbles

The relatively large sizes of microbubbles normally do not allow effective extravasation from the vasculature and limit their application to the extravascular. Targeting of tissues outside the bloodstream, such as solid tumors, requires the diameters of bubbles less than 400-800 nm, therefor referred to as nanobubbles (**Figure 13**). Oeffinger's work proved that nanobubbles of this dimension were able to produce an enhanced backscatter.[85] PLGA have been used to develop nanobubbles that have been labeled with antibodies that specifically bind to tumors.[86]

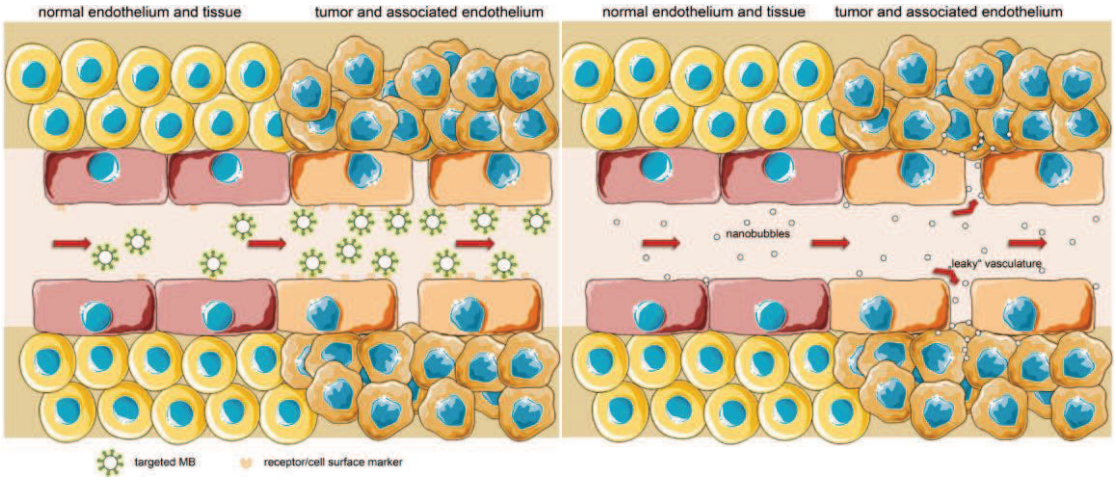

Figure 13. Micro-/nanobubbles targeting.[74]

3.5 Liquid perfluorocarbons as contrast agents

Recently, liquid perfluorinated chemicals (PFCs) contrast agents have been used instead of gaseous bubbles because they lead to ultrasound contrast agents that are more resistant to pressure changes and mechanical stresses (**Figure 14**).[87] Liquid PFCs present minimal toxicological risk compared to gaseous ones.[88] Their safety and biocompatibility have been well-documented, mostly pertaining to their development and their use as artificial blood substitutes.[89] The length of the fluorinated carbon chain determines the perfluorocarbon physical properties: small chains PFCs, such as perfluorocarbon, are gases, and larger chain PFCs, such as perfluorooctane and PFOB are liquids denser than water. Liquid PFCs have been tested as contrast agents for ultrasonography and Magnetic Resonance Imaging since the end of the 1970s.[88] Nano-/micro-system encapsulating liquid PFC as contrast agents are more stable and are able to load larger amount of drug as compared to nano-/microbubbles. However, they tend to be less echogenic than gaseous bubbles, in particular when particle size reduce to nano-scale, because they are incompressible and do not oscillate strongly with the passing acoustic wave.

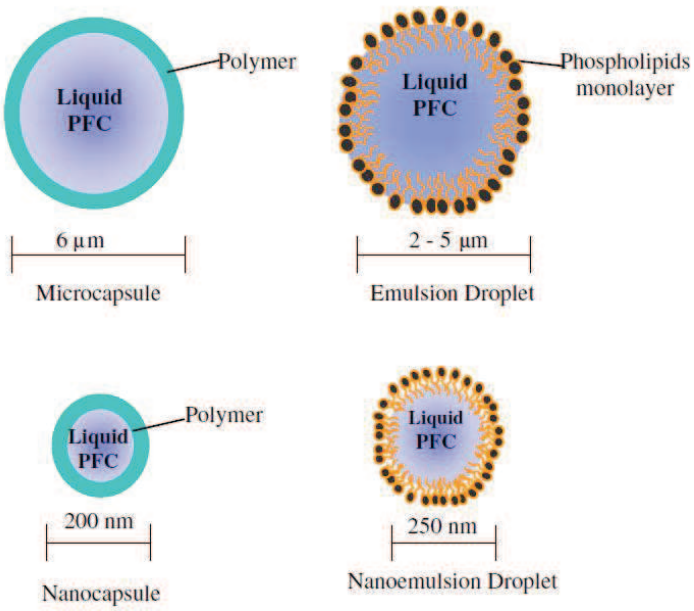

Figure 14. Scheme of systems of contrast agent with liquid PFCs.[87]

4. Design considerations for P-selectin targeting ultrasound contrast agents

4.1 Construct a simple "skeleton"

Alkyl cyanoacrylates are widely known monomers, extremely appreciated for their very high reactivity and excellent adhesive properties of the resulting polymers. They have been widely applied in the biomedical materials due to their excellent biodegradability and biocompatibility, PACA nanoparticles also have recently been considered as a kind of low-toxic drug carrier in clinical development for cancer therapy.[90] The structure of some alkyl cyanoacrylates, which are used for the preparation of nanoparticles, as shown in **Figure 15**.[91]

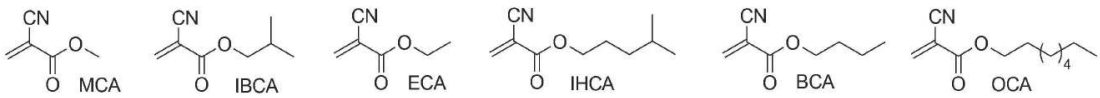

Figure 15. Chemical structures of alkyl cyanoacrylates monomers used for the preparation nanoparticles.[91]

4.2 Methods of preparation of PACA nanoparticles

Alkyl cyanoacrylate monomers are highly reactive because the two electron-withdrawing groups localize on the same carbon atom, which leads to polarization of the C=C bond and hence it could be easily by anions, compounds with nucleophilic groups (such as amines) and radical ions (**Figure 16**).[91] And the polymerization reaction proceeds quite rapidly. Because of this character, there are two main techniques used for the preparation of PACA nanoparticles: polymerization-based and nanoprecipitation-based methods, resulting in the two main types of nanoparticles, namely, nanospheres and nanocapsules, respectively. Nanospheres are matrix systems constituted by a polymer, whereas nanocapsules are vesicular systems containing a liquid or oil core, surrounded by a polymer shell.

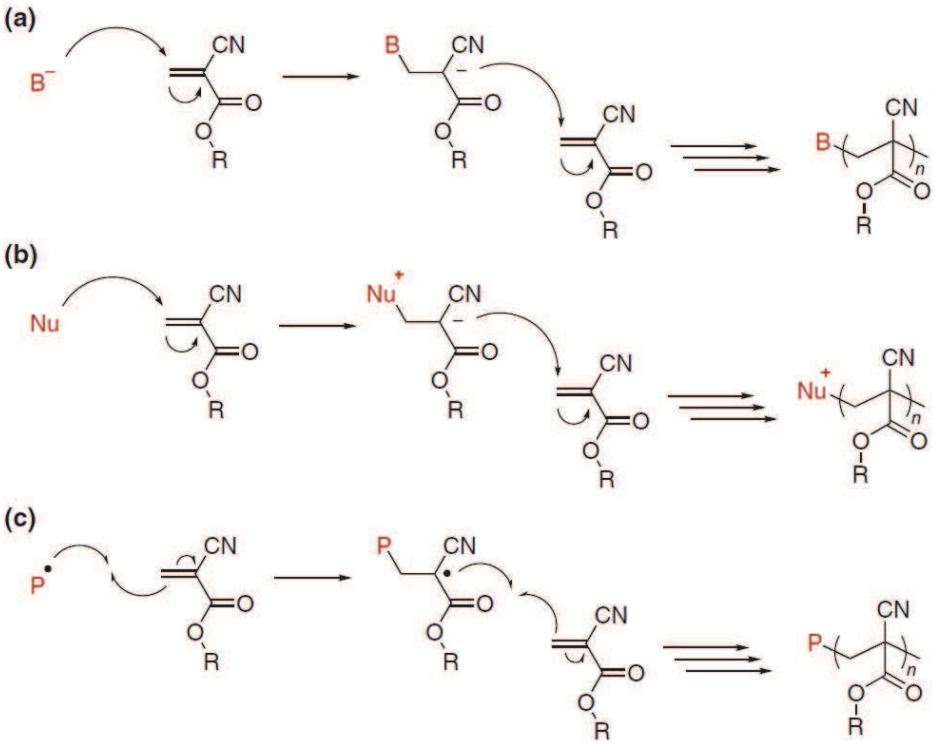

Figure 16. The polymerization mechanisms of alkyl cyanoacrylates used in emulsion polymerization method. (A) anionic; (B) zwitterionic and (C) radical.[65]

4.2.1 Polymerization-based methods

The polymerization of alkyl cyanoacrylate monomers can theoretically be triggered by two different initiators, free radical (radical polymerization) and anion (anionic polymerization), including emulsion polymerization,[92] interfacial polymerization[93] and miniemulsion polymerization methods[94]

- Emulsion polymerization

Emulsion polymerization method is a classical method for preparing polymer colloids with a matrix structure (nanospheres) in aqueous medium. In this system, the polymerization of alkyl cyanoacrylate monomers is initiated by an anion (OH^-) in an acidic aqueous medium (generally pH 2.0–3.0) containing the suitable amount of a surfactant (e.g. poloxamer 188, pluronic F127) or a stabilizing agent (e.g. dextran, heparin, chitosan). Afterwards, the mixture is stirred for several hours to prolong the polymer chains and produce PACA nanospheres.

Polysaccharide-decorated PACA nanoparticles have been prepared in nitric acid dissolved various polysaccharides via redox radical emulsion polymerization mechanism, thanks to the polysaccharide/cerium IV (Ce^{4+}) ions redox couple as the initiator.[95] In this polymerization process, the free-radical chain growth benefited from radical initiation rate much faster than anionic polymerization.

The polysaccharide chains at the surface of the nanospheres are in direct relation with the structure of the copolymer, anionic emulsion polymerization led to grafted copolymers and form compact loops, whereas linear block copolymers were achieved under redox radical initiation lead to hairy polysaccharide chains (**Figure 17**).

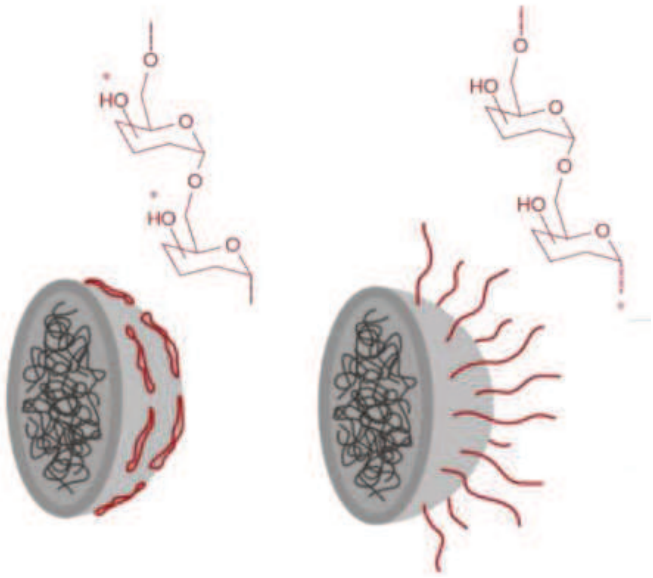

Figure 17. Schematic representation of poly (alkyl cyanoacrylate)-based nanospheres using (a) polysaccharide chains under anionic initiation, (b) polysaccharide chains under redox radical initiation.[65]

- Interfacial polymerization method

Interfacial polymerization takes place at the interface between oil phase and aqueous phase by hydroxide anions present in the water. Therefore, the reactions are prepared either in water-in-oil or oil-in-water emulsion systems, leading to PACA nanocapsules consisting of oil or an aqueous core, surrounded by a thin polymer membrane, respectively.[96] Briefly, the oil phase is slowly added to the aqueous solution of colloidal stabilizer or the aqueous phase is slowly added to the oil phase under vigorous stirring, leading to small oil/water or water/oil droplets and accomplishing the interfacial polymerization process. In addition, PACA nanocapsules also could be obtained through added monomer into reaction system after forming the emulsion. The main problem in these protocols is that nanospheres are obtained together with the nanocapsules, in order to minimize the formation of nanospheres, it is desirable to optimize the solvent/oil ration.

- Miniemulsion polymerization methods

Miniemulsion polymerization method was first used by Limouzin *et al.* to prepare PBCA nanoparticles.[97] It is similar to emulsion polymerization or interfacial polymerization, and additionally has ultrasonication process. In miniemulsion polymerization process, an appropriate amount of oil is added to an acidic aqueous solution containing surfactant and colloidal stabilizer, and then sonicated or rapidly stirred to yield a pre-emulsion. Afterward, monomer is added and the mixture is sonicated to produce a miniemulsion, with the polymerization of cyanoacrylate taking place at the interface between aqueous phase and oil phase to form nanocapsules.

4.2.2 Nanoprecipitation-based methods

Nanoprecipitation-based method is another approach for the preparation of poly(n-butyl cyanoacrylate) (PBCA) nanoparticles, beginning with pre-synthesized polymer.[90] Briefly, water phase is obtained by dissolving an appropriate amount of stabilizer (dextran, poloxamer 188 or polysorbate 80) in the water or PBS, and then the acetone solution containing dissolved pre-synthesized PBCA is added drop wise to the water phase, the mixture is stirred continuously, and the resulting nanoparticles are usually 200-300 nm in size.[98] This technique could be used to entrap desired drugs by adding them to either the water phase or the acetone solution due to their solubility.[99]

Compared to the polymerization-based method, the nanoprecipitation-based method has the advantage that nanocarriers' characteristics need to be independent of the preparation conditions of the nanoparticle formation due to the use of pre-synthesized polymers. Moreover, no chemical reaction happens between drug molecules and n-butyl cyanoacrylate monomers during the formation of nanoparticles prepared by nanoprecipitation. This method is used to load highly reactive and/or biologically active drugs because these compounds could initiate the polymerization of monomers during the classical emulsion method.

References

[1] I. Manduteanu, M. Simionescu, *J. Cell. Mol. Med.* **2012**, 16, 1978.

[2] G. Lippi, M. Franchini, G. Targher, *Nat Rev Cardiol* **2011**, 8, 502.

[3] S. P. Jackson, *Nat. Med.* **2011**, 17, 1423.

[4] K. W. Johnston, R. B. Rutherford, M. D. Tilson, D. M. Shah, L. Hollier, J. C. Stanley, *J Vasc Surg* **1991**, 13, 452.

[5] N. L. Weintraub, *The New England journal of medicine* **2009**, 361, 1114.

[6] M. L. McCormick, D. Gavrila, N. L. Weintraub, *Arterioscler Thromb Vasc Biol* **2007**, 27, 461.

[7] K. C. Kent, *New Engl. J. Med.* **2014**, 371, 2101.

[8] E. Choke, M. M. Thompson, J. Dawson, W. R. Wilson, S. Sayed, I. M. Loftus, G. W. Cockerill, *Arterioscler Thromb Vasc Biol* **2006**, 26, 2077.

[9] F. A. Hellenthal, W. A. Buurman, W. K. Wodzig, G. W. Schurink, *Nat Rev Cardiol* **2009**, 6, 543.

[10] L. Fernández-Friera, A. García-Álvarez, B. Ibáñez, *Revista Española de Cardiología (English Edition)* **2013**, 66, 134.

[11] O. Lairez, Z. A. Fayad, *Arch Cardiovasc Dis* **2013**, 106, 551.

[12] J. M. Tarkin, M. R. Dweck, N. R. Evans, R. A. P. Takx, A. J. Brown, A. Tawakol, Z. A. Fayad, J. H. F. Rudd, *Circul. Res.* **2016**, 118, 750.

[13] J. Sanz, Z. A. Fayad, *Nature* **2008**, 451, 953.

[14] V. Fuster, F. Lois, M. Franco, *Nat Rev Cardiol* **2010**, 7, 327.

[15] H. Hong, Y. Yang, B. Liu, W. Cai, *Curr Vasc Pharmacol* **2010**, 8, 808.

[16] U. Y. Ryo, S. M. Pinsky, *CRC Crit Rev Clin Radiol Nucl Med* **1976**, 8, 107; S. W. Stavropoulos, M. Itkin, P. Lakhani, J. P. Carpenter, R. M. Fairman, A. Alavi, *Journal of vascular and interventional radiology : JVIR* **2006**, 17, 1739.

[17] A. M. Lees, R. S. Lees, F. J. Schoen, J. L. Isaacsohn, A. J. Fischman, K. A. McKusick, H. W. Strauss, *Arteriosclerosis* **1988**, 8, 461.

[18] H. Sinzinger, J. O'Grady, P. Fitscha, K. Silberbauer, R. Hofer, *Lancet* **1984**, 2, 1365; L. Forstrom, P. Thorpe, E. K. Weir, T. Johnson, *Clin Nucl Med* **1985**, 10, 683; E.

C. Bourekas, R. H. Tupler, E. H. Turbiner, *J Nucl Med* **1992**, 33, 1553.

[19] B. P. Mandalapu, M. Amato, H. G. Stratmann, *Chest* **1999**, 115, 1684.

[20] H. Iida, S. Eberl, *J Nucl Cardiol* **1998**, 5, 313.

[21] D. A. Mankoff, *J Nucl Med* **2007**, 48, 18N.

[22] J. Toczek, J. L. Meadows, M. M. Sadeghi, *Circ Cardiovasc Imaging* **2016**, 9, e003023.

[23] G. K. Hansson, *N Engl J Med* **2005**, 352, 1685.

[24] K. A. Paschos, D. Canovas, N. C. Bird, *Cell. Signal.* **2009**, 21, 665.

[25] G. S. Kansas, *Blood* **1996**, 88, 3259.

[26] K. Ley, *Trends Mol. Med.* **2003**, 9, 263.

[27] S. D. Rosen, *Annu. Rev. Immunol.* **2004**, 22, 129.

[28] J. F. Leeuwenberg, E. F. Smeets, J. J. Neefjes, M. A. Shaffer, T. Cinek, T. M. Jeunhomme, T. J. Ahern, W. A. Buurman, *Immunology* **1992**, 77, 543.

[29] R. P. McEver, *Agents Actions Suppl* **1995**, 47, 117; R. J. Ludwig, M. P. Schon, W. H. Boehncke, *Expert Opin Ther Targets* **2007**, 11, 1103.

[30] K. E. Foreman, A. A. Vaporciyan, B. K. Bonish, M. L. Jones, K. J. Johnson, M. M. Glovsky, S. M. Eddy, P. A. Ward, *J. Clin. Invest.* **1994**, 94, 1147.

[31] J. W. Kevin, C.-D. Jaye, *Inflammation & Allergy-Drug Targets (Discontinued)* **2007**, 6, 69.

[32] F. Alfonso, D. J. Angiolillo, *J. Am. Coll. Cardiol.* **2013**, 61, 2056.

[33] J. R. Lindner, J. Song, J. Christiansen, A. L. Klibanov, F. Xu, K. Ley, *Circulation* **2001**, 104, 2107; M. A. McAteer, J. E. Schneider, Z. A. Ali, N. Warrick, C. A. Bursill, C. von zur Muhlen, D. R. Greaves, S. Neubauer, K. M. Channon, R. P. Choudhury, *Arterioscler Thromb Vasc Biol* **2008**, 28, 77.

[34] R. P. Choudhury, E. A. Fisher, *Arterioscler Thromb Vasc Biol* **2009**, 29, 983.

[35] Y. Hiramatsu, H. Tsujishita, H. Kondo, *J. Med. Chem.* **1996**, 39, 4547.

[36] O. Berteau, B. Mulloy, *Glycobiology* **2003**, 13, 29R.

[37] L. Cunha, A. Grenha, *Mar. Drugs* **2016**, 14, 42.

[38] B. Li, F. Lu, X. Wei, R. Zhao, *Molecules* **2008**, 13, 1671.

[39] N. E. Ustyuzhanina, M. I. Bilan, N. A. Ushakova, A. I. Usov, M. V. Kiselevskiy,

N. E. Nifantiev, *Glycobiology* **2014**, 24, 1265.

[40] I. D. Makarenkova, P. G. Deriabin, K. L'Vov D, T. N. Zviagintseva, N. N. Besednova, *Vopr. Virusol.* **2010**, 55, 41.

[41] Z. Zhu, Q. Zhang, L. Chen, S. Ren, P. Xu, Y. Tang, D. Luo, *Thrombosis Research*, 125, 419.

[42] K. Senthilkumar, P. Manivasagan, J. Venkatesan, S. K. Kim, *Int J Biol Macromol* **2013**, 60, 366.

[43] A. Cumashi, N. A. Ushakova, M. E. Preobrazhenskaya, A. D'Incecco, A. Piccoli, L. Totani, N. Tinari, G. E. Morozevich, A. E. Berman, M. I. Bilan, A. I. Usov, N. E. Ustyuzhanina, A. A. Grachev, C. J. Sanderson, M. Kelly, G. A. Rabinovich, S. Iacobelli, N. E. Nifantiev, *Glycobiology* **2007**, 17, 541.

[44] Z. Zhu, Q. Zhang, L. Chen, S. Ren, P. Xu, Y. Tang, D. Luo, *Thromb Res* **2010**, 125, 419.

[45] L. Bachelet, I. Bertholon, D. Lavigne, R. Vassy, M. Jandrot-Perrus, F. Chaubet, D. Letourneur, *Biochim. Biophys. Acta* **2009**, 1790, 141.

[46] F. Rouzet, L. Bachelet-Violette, J. M. Alsac, M. Suzuki, A. Meulemans, L. Louedec, A. Petiet, M. Jandrot-Perrus, F. Chaubet, J. B. Michel, D. Le Guludec, D. Letourneur, *J Nucl Med* **2011**, 52, 1433.

[47] T. Quillard, P. Libby, *Circ Res* **2012**, 111, 231.

[48] A. K. Ramaswamy, M. Hamilton, R. V. Joshi, B. P. Kline, R. Li, P. Wang, C. J. Goergen, *The Scientific World Journal* **2013**, 2013, 18.

[49] A. M. Mohs, Z.-R. Lu, *Expert Opinion on Drug Delivery* **2007**, 4, 149.

[50] D. Zhu, F. Liu, L. Ma, D. Liu, Z. Wang, *Int J Mol Sci* **2013**, 14, 10591.

[51] T. M. Allen, C. Hansen, F. Martin, C. Redemann, A. Yau-Young, *Biochim. Biophys. Acta* **1991**, 1066, 29.

[52] W. J. Mulder, G. J. Strijkers, G. A. van Tilborg, A. W. Griffioen, K. Nicolay, *NMR Biomed.* **2006**, 19, 142.

[53] J. C. Frias, K. J. Williams, E. A. Fisher, Z. A. Fayad, *J. Am. Chem. Soc.* **2004**, 126, 16316.

[54] S. Geninatti Crich, D. Alberti, L. Orio, R. Stefania, D. Longo, S. Aime, *Current*

Cardiovascular Imaging Reports **2013**, 6, 69; J. C. Frias, M. J. Lipinski, S. E. Lipinski, M. T. Albelda, *Contrast Media Mol Imaging* **2007**, 2, 16.

[55] T. Bonnard, J. M. Serfaty, C. Journe, B. Ho Tin Noe, D. Arnaud, L. Louedec, S. M. Derkaoui, D. Letourneur, C. Chauvierre, C. Le Visage, *Acta Biomater.* **2014**, 10, 3535.

[56] L. Bachelet-Violette, A. K. A. Silva, M. Maire, A. Michel, O. Brinza, P. Ou, V. Ollivier, A. Nicoletti, C. Wilhelm, D. Letourneur, C. Menager, F. Chaubet, *RSC Advances* **2014**, 4, 4864.

[57] M. A. McAteer, K. Mankia, N. Ruparelia, A. Jefferson, H. B. Nugent, L. A. Stork, K. M. Channon, J. E. Schneider, R. P. Choudhury, *Arterioscler Thromb Vasc Biol* **2012**, 32, 1427.

[58] T. Bonnard, G. Yang, A. Petiet, V. Ollivier, O. Haddad, D. Arnaud, L. Louedec, L. Bachelet-Violette, S. M. Derkaoui, D. Letourneur, C. Chauvierre, C. Le Visage, *Theranostics* **2014**, 4, 592.

[59] D.-E. Kim, J.-Y. Kim, I.-C. Sun, D. Schellingerhout, S.-K. Lee, C.-H. Ahn, I. C. Kwon, K. Kim, *Ann. Neurol.* **2013**, 73, 617.

[60] H. P. Luehmann, E. D. Pressly, L. Detering, C. Wang, R. Pierce, P. K. Woodard, R. J. Gropler, C. J. Hawker, Y. Liu, *J Nucl Med* **2014**, 55, 629.

[61] K. Hagisawa, T. Nishioka, R. Suzuki, T. Takizawa, K. Maruyama, B. Takase, M. Ishihara, A. Kurita, N. Yoshimoto, F. Ohsuzu, M. Kikuchi, *Int J Cardiol* **2011**, 152, 202.

[62] X. Wang, C. E. Hagemeyer, J. D. Hohmann, E. Leitner, P. C. Armstrong, F. Jia, M. Olschewski, A. Needles, K. Peter, I. Ahrens, *Circulation* **2012**, 125, 3117.

[63] E. C. Cho, C. Glaus, J. Chen, M. J. Welch, Y. Xia, *Trends Mol. Med.* **2010**, 16, 561.

[64] J. P. Rao, K. E. Geckeler, *Progress in Polymer Science* **2011**, 36, 887.

[65] J. Nicolas, P. Couvreur, *Wiley interdisciplinary reviews. Nanomedicine and nanobiotechnology* **2009**, 1, 111.

[66] D. G. You, G. Saravanakumar, S. Son, H. S. Han, R. Heo, K. Kim, I. C. Kwon, J. Y. Lee, J. H. Park, *Carbohydr. Polym.* **2014**, 101, 1225.

[67] A. K. Silva, D. Letourneur, C. Chauvierre, *Theranostics* **2014**, 4, 579.

[68] S. Hernot, A. L. Klibanov, *Adv Drug Deliv Rev* **2008**, 60, 1153.

[69] J. P. Lawrence, *Crit Care Med* **2007**, 35, S314.

[70] S. C. Manion, J. P. Rathmell, Ed.^Eds. LWW, **2011**.

[71] A. Kabalnov, D. Klein, T. Pelura, E. Schutt, J. Weers, *Ultrasound Med. Biol.* **1998**, 24, 739.

[72] L. Hoff, P. C. Sontum, B. Hoff, "Acoustic properties of shell-encapsulated, gas-filled ultrasound contrast agents", presented at *Ultrasonics Symposium, 1996. Proceedings., 1996 IEEE*, 3-6 Nov 1996, **1996**; F. Kiessling, M. E. Mertens, J. Grimm, T. Lammers, *Radiology* **2014**, 273, 10.

[73] R. H. Perera, C. Hernandez, H. Zhou, P. Kota, A. Burke, A. A. Exner, *Wiley Interdisciplinary Reviews: Nanomedicine and Nanobiotechnology* **2015**, n/a.

[74] V. Paefgen, D. Doleschel, F. Kiessling, *Front Pharmacol* **2015**, 6, 197.

[75] X. Xiong, F. Zhao, M. Shi, H. Yang, Y. Liu, *Journal of biomaterials science. Polymer edition* **2011**, 22, 417.

[76] J. R. Eisenbrey, O. M. Burstein, M. A. Wheatley, *Polymer Engineering & Science* **2008**, 48, 1785.

[77] R. Diaz-Lopez, N. Tsapis, D. Libong, P. Chaminade, C. Connan, M. M. Chehimi, R. Berti, N. Taulier, W. Urbach, V. Nicolas, E. Fattal, *Biomaterials* **2009**, 30, 1462.

[78] F. Kiessling, J. Huppert, M. Palmowski, *Curr. Med. Chem.* **2009**, 16, 627.

[79] J. R. Harris, F. Depoix, K. Urich, *Micron* **1995**, 26, 103.

[80] C. Olbrich, P. Hauff, F. Scholle, W. Schmidt, U. Bakowsky, A. Briel, M. Schirner, *Biomaterials* **2006**, 27, 3549.

[81] M. Palmowski, J. Huppert, G. Ladewig, P. Hauff, M. Reinhardt, M. M. Mueller, E. C. Woenne, J. W. Jenne, M. Maurer, G. W. Kauffmann, W. Semmler, F. Kiessling, *Mol. Cancer Ther.* **2008**, 7, 101; M. Palmowski, B. Morgenstern, P. Hauff, M. Reinhardt, J. Huppert, M. Maurer, E. C. Woenne, S. Doerk, G. Ladewig, J. W. Jenne, S. Delorme, L. Grenacher, P. Hallscheidt, G. W. Kauffmann, W. Semmler, F. Kiessling, *Invest Radiol* **2008**, 43, 162.

[82] G. Korpanty, P. A. Grayburn, R. V. Shohet, R. A. Brekken, *Ultrasound Med. Biol.*

2005, 31, 1279.

[83]M. A. Borden, D. E. Kruse, C. F. Caskey, S. Zhao, P. A. Dayton, K. W. Ferrara, *IEEE Trans Ultrason Ferroelectr Freq Control* **2005**, 52, 1992.

[84]F. Cavalieri, M. Zhou, M. Tortora, B. Lucilla, M. Ashokkumar, *Curr. Pharm. Des.* **2012**, 18, 2135.

[85]B. E. Oeffinger, M. A. Wheatley, *Ultrasonics* **2004**, 42, 343.

[86]J. S. Xu, J. Huang, R. Qin, G. H. Hinkle, S. P. Povoski, E. W. Martin, R. X. Xu, *Biomaterials* **2010**, 31, 1716; X. Zhang, Y. Zheng, Z. Wang, S. Huang, Y. Chen, W. Jiang, H. Zhang, M. Ding, Q. Li, X. Xiao, X. Luo, Z. Wang, H. Qi, *Biomaterials* **2014**, 35, 5148.

[87]R. Díaz-López, N. Tsapis, E. Fattal, *Pharmaceutical Research* **2010**, 27, 1.

[88]M. S. Liu, D. M. Long, *Radiology* **1977**, 122, 71.

[89]P. T. Leese, R. J. Noveck, J. S. Shorr, C. M. Woods, K. E. Flaim, P. E. Keipert, *Anesth. Analg.* **2000**, 91, 804; R. J. Noveck, E. J. Shannon, P. T. Leese, J. S. Shorr, K. E. Flaim, P. E. Keipert, C. M. Woods, *Anesth. Analg.* **2000**, 91, 812.

[90]S. Gao, Y. Xu, S. Asghar, M. Chen, L. Zou, S. Eltayeb, M. Huo, Q. Ping, Y. Xiao, *J Drug Target* **2015**, 23, 481.

[91]G. Yordanov, *Bulgarian Journal of Chemistry* **2012**, 1.

[92]R. Tan, M. Niu, J. Zhao, Y. Liu, N. Feng, *J Drug Target* **2014**, 22, 509; C. X. Wang, L. S. Huang, L. B. Hou, L. Jiang, Z. T. Yan, Y. L. Wang, Z. L. Chen, *Brain Res.* **2009**, 1261, 91.

[93]M. Wohlgemuth, C. Mayer, *J. Colloid Interface Sci.* **2003**, 260, 324; H. Gao, J. Y. Wang, X. Z. Shen, Y. H. Deng, W. Zhang, *World J Gastroenterol* **2004**, 10, 2010.

[94]N. Behan, C. Birkinshaw, N. Clarke, *Biomaterials* **2001**, 22, 1335; F. Hansali, G. Poisson, M. Wu, D. Bendedouch, E. Marie, *Colloids Surf. B. Biointerfaces* **2011**, 88, 332.

[95]C. Chauvierre, D. Labarre, P. Couvreur, C. Vauthier, *Macromolecules* **2003**, 36, 6018; C. Chauvierre, D. Labarre, P. Couvreur, C. Vauthier, *Pharmaceutical Research* **2003**, 20, 1786; C. Chauvierre, D. Labarre, P. Couvreur, C. Vauthier, *Colloid and Polymer Science* **2004**, 282, 1097; C. Chauvierre, M. C. Marden, C. Vauthier, D.

Labarre, P. Couvreur, L. Leclerc, *Biomaterials* **2004**, 25, 3081.

[96] M. Gallardo, G. Couarraze, B. Denizot, L. Treupel, P. Couvreur, F. Puisieux, *Int. J. Pharm.* **1993**, 100, 55; G. Puglisi, M. Fresta, G. Giammona, C. A. Ventura, *Int. J. Pharm.* **1995**, 125, 283; G. Lambert, E. Fattal, H. Pinto-Alphandary, A. Gulik, P. Couvreur, *Pharmaceutical Research* **2000**, 17, 707; H. Hillaireau, T. Le Doan, H. Chacun, J. Janin, P. Couvreur, *Int. J. Pharm.* **2007**, 331, 148.

[97] C. Limouzin, A. Caviggia, F. Ganachaud, P. Hémery, *Macromolecules* **2003**, 36, 667.

[98] G. G. Yordanov, C. D. Dushkin, *Colloid and Polymer Science* **2010**, 288, 1019.

[99] G. Yordanov, R. Skrobanska, A. Evangelatov, *Colloids Surf. B. Biointerfaces* **2012**, 92, 98; W. He, X. Jiang, Z. R. Zhang, *J. Pharm. Sci.* **2008**, 97, 2250.

EXPERIMENTAL WORK

CHAPTER I

Polysaccharides-coated poly (isobutyl cyanoacrylate) perfluorooctyl bromide nanoparticles dedicated to contrast agents for ultrasound molecular imaging of atherothrombosis

ABSTRACT

Non-invasive diagnostic imaging methods in clinical examination are important for understanding disease process and risk in cardiovascular pathology. Here we report a new potential contrast agent based on polysaccharides-coated poly (isobutyl cyanoacrylate) nanoparticles loaded with perfluorooctyl bromide (PFOB) designed for ultrasound imaging. PFOB was embedded in the surface of nanoparticles with the help of Tween 80, and these nanoparticles could be functionalized with fucoidan easily. In addition, the physico-chemical characterizations of the obtained nanoparticles were carried out in order to evaluate the contents of fucoidan and PFOB. Flow cytometry analysis showed a stronger interaction between activated platelets and fucoidan functionalized PFOB nanoparticles (Fuco-TNPs-PFOB) than non-functionalized PFOB nanoparticles. Moreover, *in vivo* ultrasound imaging experiments showed an accumulation of Fuco-TNPs-PFOB in the thrombotic abdominal aortic aneurysm wall, where P-selectin is expressed. This study revealed that Fuco-TNPs-PFOB have the potential to track vascular diseases characterized by P-selectin overexpression *in vivo*.

Graphical Abstract

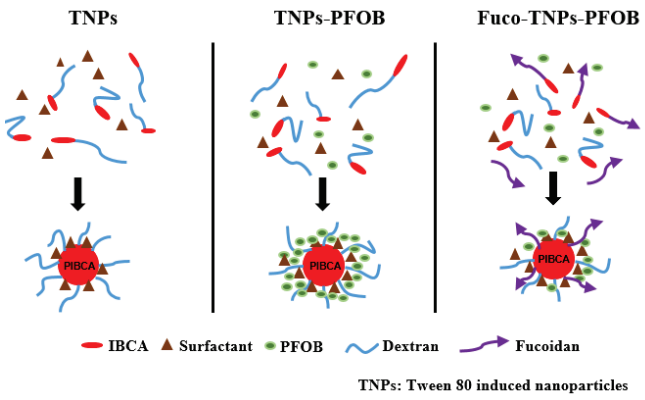

1. Introduction

Cardiovascular diseases due to atherosclerosis remain the leading cause of mortality in developed countries.[1] During the past decade, molecular imaging techniques have improved our understanding and shown promise in identifying the steps of atherosclerotic disease based on ligand-modified contrast agents that bind selectively to a target site contained specific biomarkers.[2] Among the many imaging modalities, ultrasonic imaging is considered to be one of the best candidates because it is widely available, non-invasive and cost-effective.[3] The main limitation of clinical ultrasound imaging is the poor resolution of the results, which are generally in the millimeter range. Ultrasound contrast agents are considered to address this problem.[4]

Polymer ultrasound contrast agents have been developed in the current study, they were different from the first-generation microbubbles contrast agent because they consist of nano-/microcapsules of poly(lactide-co-glycolide) (PLGA) encapsulating a liquid core of perfluorooctyl bromide (PFOB).[5] They have shown promise for blood pool contrast and the polymer shell improved the stability of the capsules as compared to traditional ultrasound contrast agents. However, due to their rather hydrophobic surface, these contrast agents are quickly eliminated by the mononuclear phagocyte system and they end up in the liver.

To avoid a rapid clearance from the systemic circulation, surface modification of these polymer contrast agents has been considered to provide them stealth.[6] Poly(alkyl cyanoacrylate) (PACA) were employed as materials for biomedical applications science the early 1980s.[7] PACA nanoparticles are already in clinical development for cancer therapy.[8] Particularly, polysaccharides coated poly(isobutyl cyanoacrylate) (PIBCA) nanoparticles could effectively prevent blood proteins adsorption and observably reduce the uptake by the mononuclear phagocyte system.[9]

P-selectin belongs to the family of selectin adhesion molecules and is expressed at the surface of activated platelets and pathological vascular endothelium.[10] This pattern of

expression is considered to be involved in inflammation and coagulation, which are key processes in the early pathogenesis of atherosclerotic cardiovascular diseases.[11] Therefore, revealing the expression of P-selectin with a molecular imaging tool is a promising clinically relevant strategy for the diagnosis of vascular diseases such as atherosclerosis.[12]

Some authors have developed contrast agents for targeting P-selectin, most of them are functionalized with P-selectin antibodies or synthetic mimics of sialyl lewis^X (SLe^X), which is the natural ligand of P-selectin.[13] New non-invasive carrier systems with strong P-selectin binding specificity are still needed for vascular-targeted imaging or drug delivery.

Recently, fucoidan, a type of sulfated and fucosylated polysaccharide mainly derived from brown seaweed, has attracted much attention.[14] Fucoidan exhibited *in vitro* a high affinity for immobilized P-selectin.[15] Our group recently demonstrated that Technetium (^{99m}Tc) radiolabeled fucoidan enabled detection by activated endothelium and thrombosis with P-selectin expression in rats.[16] Moreover, we have designed Ultrasmall Superparamagnetic Iron Oxide (USPIO) nanoparticles associated with fucoidan (USPIO-FUCO) as a new contrast agent.[17] 15 min after injection, USPIO-FUCO start to localize in platelet-rich thrombus area in a rat model, the signal enhancement could be detected by MRI.[18]

In the present study, we propose a novel ultrasound contrast agent for molecular imaging of abdominal aortic aneurysm (AAA). As a first step, we explored a simple method to synthesize dextran-coated PIBCA nanoparticles loaded with perfluorooctyl bromide (PFOB) and functionalized with fucoidan. Next, the physicochemical characterization of the obtained product was carried out in order to evaluate the contents of fucoidan and PFOB. Then, flow cytometry was performed to assess the interaction between activated platelets and these nanoparticles. Moreover, their ability to detect active intravascular thrombi was evaluated *in vivo* in rat models by following elastase-induced vascular injury.

2. Experimental Section

Materials:

1-Bromoheptadecafluorooctane (PFOB), $CDCl_3$ (99.96 atom % D), Tween 80, nitric acid and fucoidan were provided by Sigma Aldrich (Saint Quentin Fallavier, France). Dextran 20 and FITC-Dextran 20 were obtained from TdB Consultancy (Uppsala, Sweden). Perfluoro-15-crown-5-ether (PFCE) was purchased from Fluorochem (Hadfield, UK). Isobutyl cyanoacrylate (IBCA) was provided by ORAPI (Saint Vulbas, France). TRAP (thrombin receptor-activating-peptide) was obtained from PolyPeptide laboratories (Strasbourg, France). Cerium (IV) ammonium nitrate was supplied by Merck Millipore (Fontenay-sous-Bois, France).

Synthesis of nanoparticles:

The redox radical emulsion polymerization (RREP) methods described by Chauvierre *et al.* were adapted to prepare nanoparticles.[19] A total amount of polysaccharide (137.5 mg) including a blend of fucoidan and dextran in different proportions was dissolved in 8 mL of 0.2 M nitric acid. The solution was placed under magnetic stirring at 40°C under gentle stirring and nitrogen bubbling. After 10 min, 2 mL of cerium (IV) ammonium nitrate (8×10^{-2} M) in 0.2 M nitric acid and 0.5 mL of IBCA were added successively under vigorous magnetic stirring. The reaction was maintained under magnetic stirring and nitrogen bubbling was maintained for 10 min. The system was left to continue under vigorous stirring for 40 min. After cooling down to room temperature, 1.25 mL of an aqueous solution of tri-sodium citrate dihydrate (1.02 M) was added to react with the remaining cerium ions and the pH was adjusted to 7.0 with NaOH.

To prepare PFOB loaded nanoparticles, Tween 80 was dissolved into nitric acid and desired amount of PFOB was dispersed in ultrasonic cleaner. To prepare fluorescent-labeled nanoparticles, 5% (w/w) of FITC-Dextran was blended into

polysaccharide and was dissolved into nitric acid solutions.

Nanoparticles (NPs); Fucoidan-coated nanoparticles (Fuco-NPs); Tween 80 induced nanoparticles (TNPs)

Size and zeta potential nanoparticle determinations:

The size distribution of nanoparticles was quantitatively obtained using a laser dynamic scattering particle size-measuring instrument (Nano ZS, Malvern Instruments, Orsay, France).

Zeta potential (ζ) of the nanoparticles was measured to evaluate their stability in suspension and to identify the presence of the polysaccharides onto the surface. Samples were diluted in 1 mM KCl. Measurements were performed at 25°C using quasi-elastic light scattering apparatus (Nano ZS, Malvern Instruments, Orsay, France).

All the measurements were performed in triplicate and the results were expressed as mean ± standard deviation.

Scanning Electron Microscopy (SEM) and Transmission Electron Microscopy (TEM):

The surface morphology of nanoparticles was imaged using a SEM apparatus (Philips XL 30 ESEM-FEG, Amsterdam, Netherlands) on dried samples coated with a thin gold layer. TEM was performed using a Philips EM208 apparatus (Amsterdam, Netherlands) operating at 80 kV.

Elemental Analysis:

The presence of fluorine on the surface of nanoparticles was demonstrated by energy-dispersive X-ray spectroscopy. Global S content was quantified by UV fluorescence spectroscopy (THERMO TN-TS 3000, Thermo Fisher Scientific,

Pittsburgh, PA, USA) on freeze-dried samples of fucoidan and nanoparticles. The fucoidan content in the nanoparticles was calculated from their sulfur content and the sulfur content of fucoidan as standard.

Measurement of PFOB encapsulation efficacy:

The method used for PFOB encapsulation efficacy assay was performed according to the method as described by O. Diou et al.[20] Nanoparticles were freeze-dried for 24-48 hours. Subsequently, freeze-dried nanoparticles were dissolved into $CDCl_3$ along with PFCE as an internal standard ([PFCE] = 0.76 mmol/L). The ^{19}F NMR (Nuclear Magnetic Resonance) spectra were recorded on a Bruker (400 MHz) Spectrometer (Billerica, USA). The amount of PFOB was determined by the integration of the peak at -80.7 ppm, corresponding to the CF_3 group and by the normalization of the area of the PFCE peak at -89.5 ppm. Mass fraction C_{PFOB} was calculated as follows:

$$m_{\mathrm{PFOB}}^{\mathrm{max}} = \mathrm{m}_{\mathrm{PFOB}}^{\mathrm{feed}} \times \frac{m_{\mathrm{Nanoparticles}}^{\mathrm{mass}}}{\mathrm{m}_{\mathrm{Polysaccharides}}^{\mathrm{feed}} + \mathrm{m}_{\mathrm{polymer}}^{\mathrm{feed}} + \mathrm{m}_{\mathrm{PFOB}}^{\mathrm{feed}}} \quad (1)$$

$$\eta_{\mathrm{encaps}} = \frac{m_{\mathrm{PFOB}}^{\mathrm{NMR}}}{m_{\mathrm{PFOB}}^{\mathrm{max}}} \times 100\% \quad (2)$$

Where $\mathrm{m}_{\mathrm{Polysaccharides}}^{\mathrm{feed}}$ $\mathrm{m}_{\mathrm{polymer}}^{\mathrm{feed}}$ $\mathrm{m}_{\mathrm{PFOB}}^{\mathrm{feed}}$ are the initial masses of the components introduced in the reaction solution, $m_{\mathrm{Nanoparticles}}^{\mathrm{mass}}$ is the quantity of freeze-dried nanoparticles, and $m_{\mathrm{PFOB}}^{\mathrm{NMR}}$ corresponds to the mass of PFOB recovered after freeze-drying process.

Static binding on platelets:

The interaction between two groups of PE-Cy5 labeled platelets (non-activated platelets (PRP), activated platelets (PRP + TRAP) and two groups of FITC

nanoparticles (TNPs-PFOB, Fuco-TNPs-PFOB) were measured by flow cytometry. 5 mL of blood from healthy adult volunteers were collected in sodium citrate 3.8% (w/v). Platelet-rich plasma (PRP) was obtained by centrifugation at 200 g for 15 min (5702RH centrifuge Beckman Coulter, Villepinte, France) and platelet concentration was adjusted to 2×10^8 mL^{-1} with autologous platelet-poor plasma. Activated PRP was obtained by stimulation of PRP with 20 µM TRAP. Before assessing the interaction with nanoparticles, P-selectin expression level at the platelet surface was assessed using an anti-human CD62P-FITC. An additional tube of PRP was also incubated with a mouse IgG1/FITC to verify that the FITC signal was not due to non-specific binding to the platelets. In addition, TNPs-PFOB and Fuco-TNPs-PFOB were incubated with anti-human PE-Cy5 at a similar concentration to prove that nanoparticles could not be labeled by antibody. Thus, for each test, we measured the FITC signal by flow cytometry and confirmed that P-selectin was expressed by platelets from PRP + TRAP batches and that low level of P-selectin was detected on PRP batch. To evaluate the binding ability between nanoparticles with P-selectin expressed onto platelets, 5 µL of non-activated PRP or of activated PRP + TRAP were incubated for 20 min with 5 µL of TNPs-PFOB and of Fuco-TNPs-PFOB (5 mg/mL), together with 5 µL of PE-Cy5 mouse anti-human CD41a to label platelets. Samples were analyzed on a LSRII flow cytometer (BD Biosciences, Le Pont de Claix, France), 50,000 PE-Cy5 positive platelets collected per samples, and the mean fluorescence intensity (MFI) of FITC was measured in these platelets.

In vivo arterial disease model:

Animal studies were done in accordance with principles of laboratory animal care and with approval of the animal care and use committee of the Claude Bernard Institute (N°2012-15/698-0100) (Paris, France). The elastase induced Abdominal Aortic Aneurysm (AAA) rat model was performed on 8 male adult Wistar rats (7 weeks, Janvier Labs, Le Genest-Saint-Isle, France). Animals were anesthetized with intra-peritoneal injection of pentobarbital (1 µL/g body weight, Ceva Santé Animale

SA, La Ballastiere, France). Porcine pancreatic elastase (2.7 mg/mL, Sigma Aldrich, Saint Quentin Fallavier, France) was perfused into the lumen of an isolated segment of the infrarenal abdominal aorta for 15 minutes at a rate of 2.5 mL/h. Delbosc *et al.* reported that repeated intravenous injection of *Porphyromonas gingivalis* (Pg) in a rat model of AAA led to enhanced aortic dilation associated with neutrophil retention and persistence of a non-healing luminal thrombus. In this study, *Porphyromonas gingivalis* suspension (107 CFU in 500 µL 0.9% saline), a gift from La Pitié Salpétrière Hospital, was injected to the rats once a week via the penis vein for 4 weeks. Two days after the fourth injection, rats were anaesthetized by sodium pentobarbital intra-peritoneal injection (1 µL/g,) and 200 µL of Fuco-TNPs-PFOB (50 mg/mL) were injected slowly via the carotid artery. The imaging sequence was performed in the B-mode (transducers: MS-550D, VisualSonics 2100).

Statistical Analysis:

Data are presented as mean ± SEM (n≥3). Each experiment was performed using Student t test for paired data. Flow cytometry results were analyzed statistically with a one-way ANOVA with Bonferroni post-tests to compare data obtained with TNPs-PFOB and Fuco-TNPs-PFOB. Difference of $P<0.05$ was considered significant.

3. Results

3.1 Preparation and characterization of nanoparticles

3.1.1 Nanoparticles (NPs) and fucoidan-coated nanoparticles (Fuco-NPs)

The radical emulsion polymerization of isobutyl cyanoacrylate (IBCA) was investigated to design fucoidan-coated PIBCA nanoparticles. To achieve this, fucoidan was introduced at different proportions in a blend of polysaccharide composed of dextran and fucoidan in the polymerization medium. As indicated in **Table 1**, stable formulations of nanoparticles were obtained by both percentages of fucoidan (5% and 10%) in the blend of polysaccharides. The size of nanoparticles

slightly decreased from (from 210 ± 3 nm to 197 ± 6 nm) when the preparation contained 5% and 10% fucoidan, respectively. Moreover, the fucoidan content in Fuco-NPs increased from 2.07% to 4.92% (w/w) with fucoidan increased. While, the zeta potential of the nanoparticles became more negative when the amount of fucoidan was increased (from -21 ± 3 mV to -27 ± 2 mV).

Table 1. Physical and chemical properties of NPs and Fuco-NPs.

No.	NPs	Fuco-NPs	
		5% Fuco	10% Fuco
Size (nm)	201±5	210±3	197±6
PI	0.09	0.10	0.18
Zeta potential (mV)	-16±3	-21±3	-27±2
Mass Concentration (g/L)	40	37	36
Global sulfur content (wt %)	----	0.02%	0.05%
Global fucoidan content (wt %)	----	1.61%-2.52%	3.83%-6.01%

3.1.2 NPs loaded with PFOB

To further encapsulate PFOB into NPs, Tween 80 was introduced as a surfactant to form the PFOB emulsion before initiating the polymerization of nanoparticles. As shown in **Table 2**, the size of Tween 80 induced nanoparticles (TNPs) declined sharply (from 210 ± 3 nm to 115 ± 3 nm) compared to NPs, it would increase after added PFOB (TNPs-PFOB). Moreover, in the same way as for PFOB, the size of particles decreased as the amount of Tween 80 increased, whereas the mass of the loaded PFOB reached the maximum when the amount of Tween 80 was 2 mg. Meanwhile, the results showed the mass percent of PFOB was slightly increased with the quantity of PFOB in the condition of same amount of Tween 80. Based on these results, the 2.0 mg of Tween 80 and 120 μL of PFOB were the optimum condition for the following experiments.

Table 2. Physical and chemical properties of TNPs and Fuco-TNPs-PFOB.

No.	TNPs	TNPs-PFOB						Fuco-TNPs-PFOB	
								5% Fuco	10% Fuco
TWEEN 80 (mg)	3	0.5	1	2	3	4	2	2	2
PFOB (μL)	0	30	30	30	30	30	120	120	120
Size (nm)	115±3	231±6	243±8	203±10	182±5	158±7	249±5	198±8	200±10
PI	0.12	0.12	0.17	0.06	0.08	0.05	0.19	0.12	0.15
Zeta potential (mV)	-14±3	-14±5	-16±4	-16±2	-16±3	-15±2	-17±3	-21±2	-26±3
Mass Concentration (g/L)	40	42	43	44	43	44	48	41	40
η_{encaps} (%)	----	45.13%	47.93%	69.46%	60.43%	55.74%	58.79%	20.15%	6.70%

The morphology of obtained TNPs and TNPs-PFOB was observed by SEM and TEM **Figure 1**. Spherical objects with smooth surface are observed for both types of nanoparticles. Surprisingly, SEM images showed that TNP and TNP-PFOB have different sizes, and this is consistent with the hydrodynamic diameter measured by dynamic light scattering, whereas TEM indicated that they have the similar sizes of core.

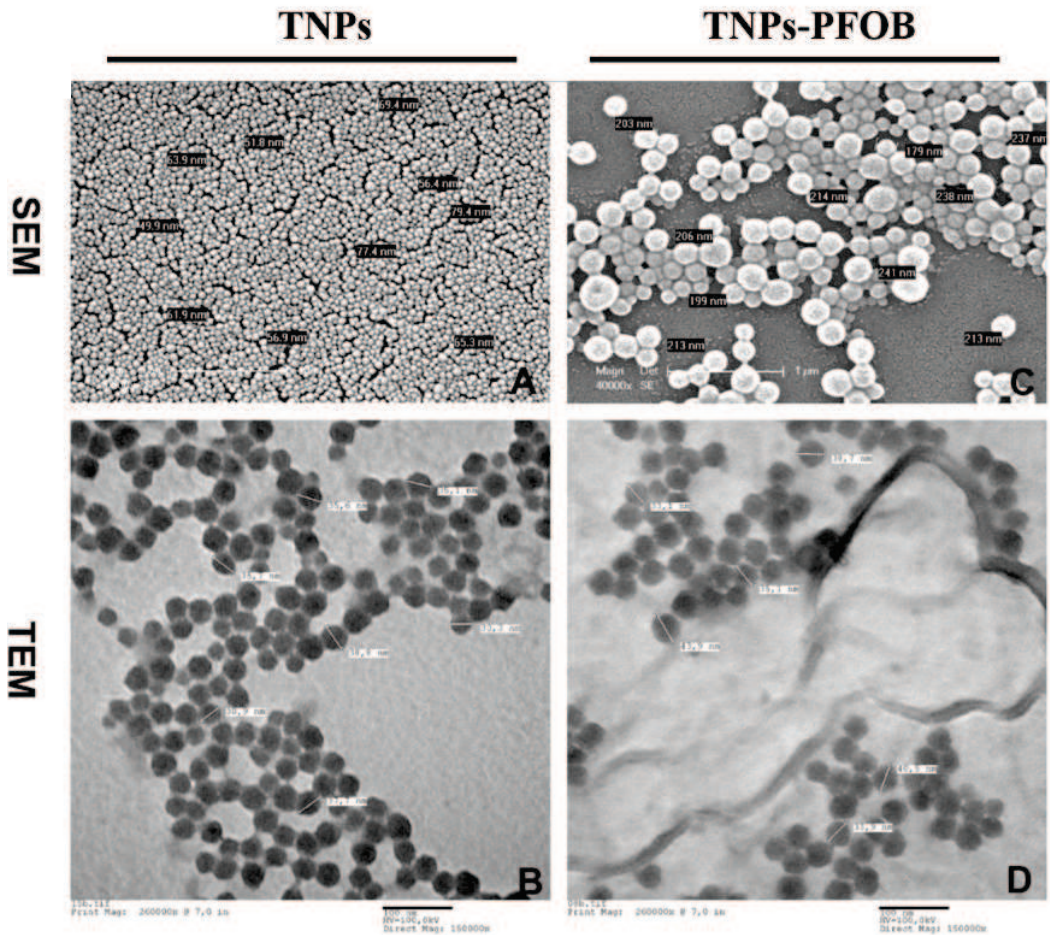

Figure 1. Scanning and transmission electron microscopy images of TNPs and TNPs-PFOB. Top: SEM images. Bottom: TEM images. Left: TNPs prepared with 2 mg Tween 80. Right: TNPs-PFOB prepare with 2 mg Tween 80 and 120 μL PFOB.

The content and distribution of PFOB in TNPs were analyzed by ^{19}F NMR (**Figure 2**) and energy-dispersive X-ray spectroscopy (EDX) experiment (**Figure 3**). The results showed the absence of CF_3 group in the control TNPs and the presence of CF_3 group in the TNPs-PFOB, meanwhile EDX indicated fluorine was located on TNPs surface.

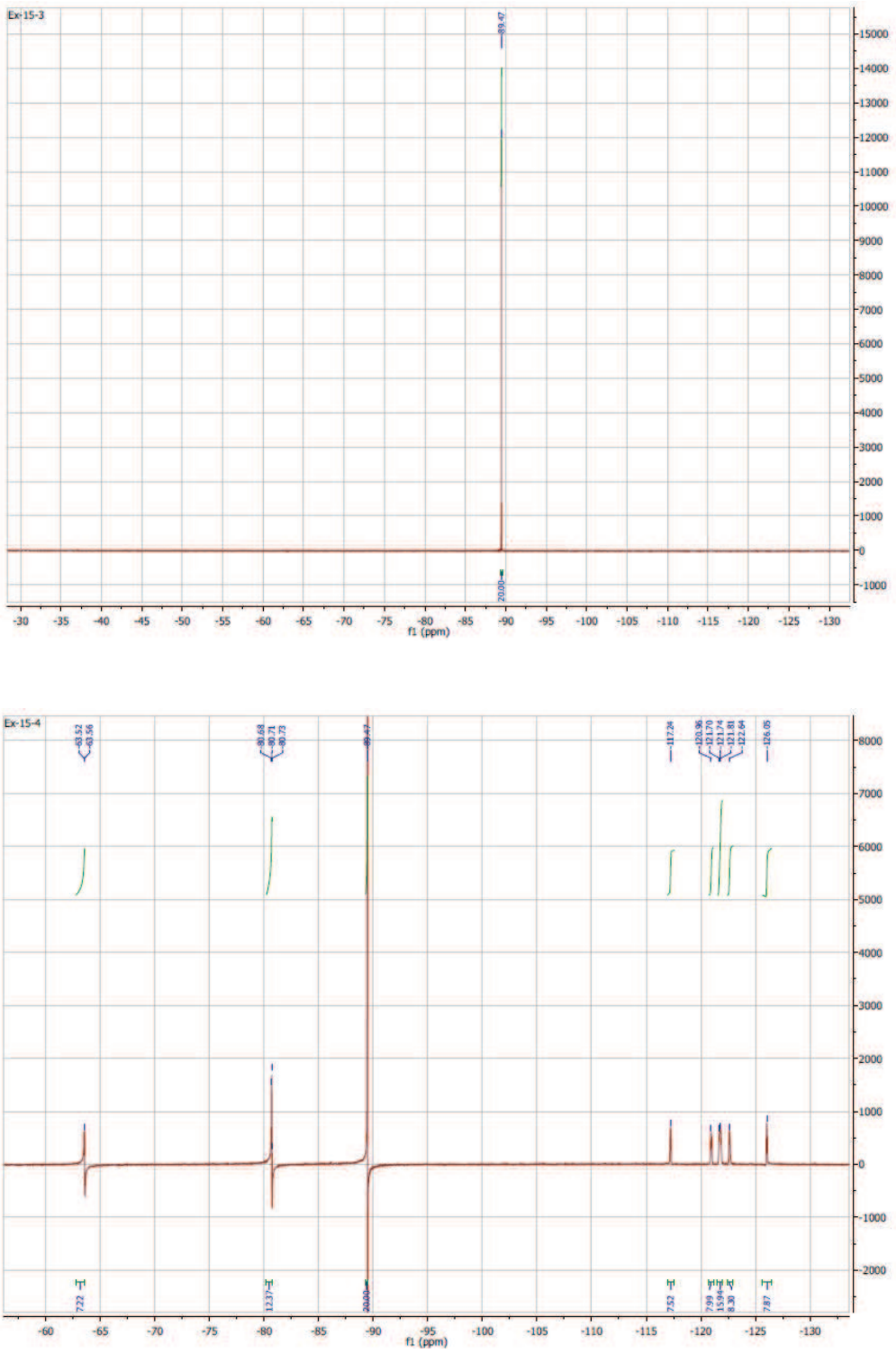

Figure 2. ^{19}F HMR spectra of TNPs (top), TNPs-PFOB (bottom) in $CDCl_3$. Perfluoro-15-crown-5-ether (PFCE) as an internal standard ([PFCE]=0.76 mmol/L) and its peak at -89.5 ppm, the amount of PFOB was determined after integration of the peak at -81 ppm corresponding to the CF_3 group.

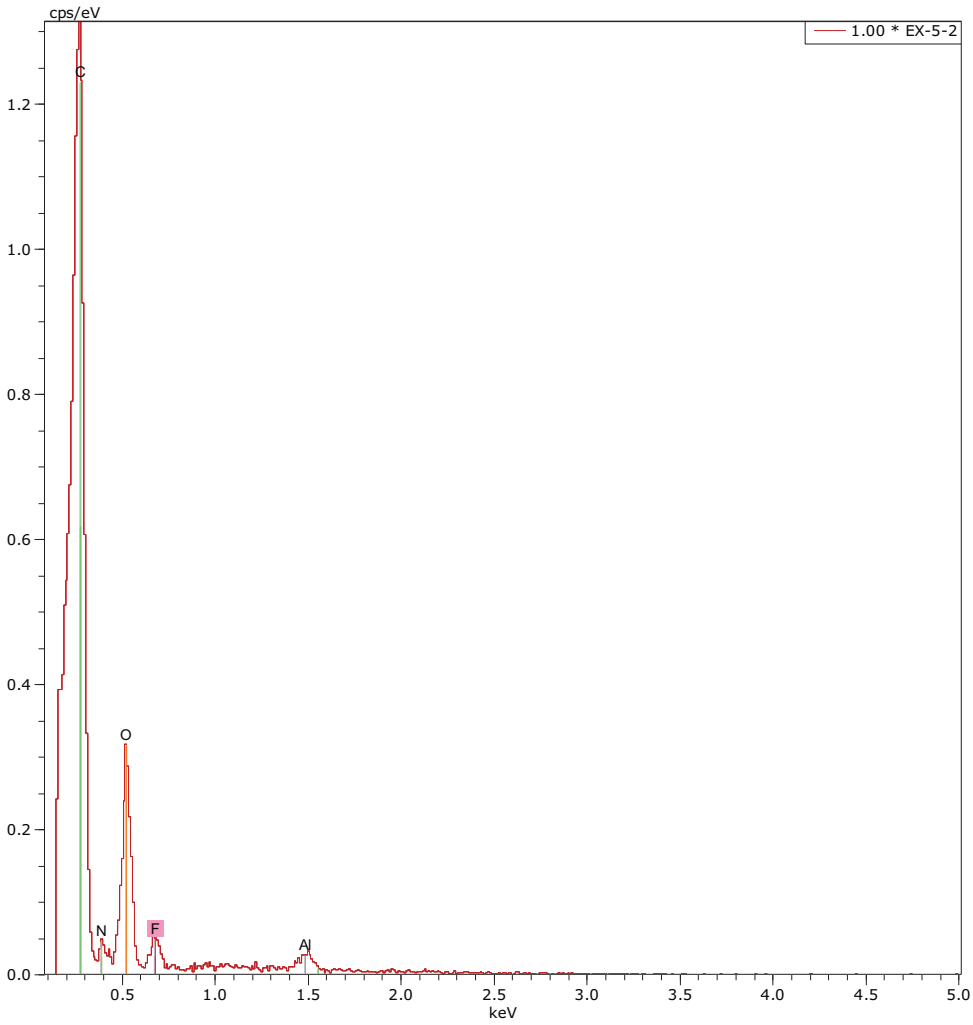

Figure 3. Determination of the chemical species present in the TNPs-PFOB by elemental analysis using energy dispersion spectroscopy.

3.1.3 TNPs-PFOB functionalized with fucoidan

To targeted TNPs-PFOB, fucoidan was introduced to the polymerization medium. As indicated in **Table 2**, stable TNPs-PFOB functionalized with fucoidan (Fuco-TNPs-PFOB) were obtained and their size slightly decreased (198 ± 8 nm for 5% Fuco-TNPs-PFOB, 200 ± 10 nm for 10% Fuco-TNPs-PFOB) compared to TNPs-PFOB (249 ± 5 nm). Meanwhile, the zeta potential of Fuco-TNPs-PFOB also decreased (-21 ± 2 mV for 5% fucoidan and -26 ± 3 mV vs -17 ± 3 mV). These results were consistent with the property of Fuco-NPs. However, the mass percentage of PFOB decreased with increasing amount of fucoidan (20.15% for 5% Fuco-TNPs-PFOB, 6.70% for 10% Fuco-TNPs-PFOB).

3.2 Static binding on platelets

To evaluate the ability of TNPs-FPOB and Fuco-TNPs-PFOB to target P-selectin expressed onto the surface of human activated platelets, flow cytometry experiments were performed. Interactions were assessed between nanoparticles and two groups from human Plasma-Rich Platelets (PRP) or activated platelets with TRAP (PRP+TRAP). As shown in **Figure 4**, TNPs-PFOB barely or only minimally bound to the two groups of platelets, as shown by low values of mean fluorescence intensity (MFI). In contrast, Fuco-TNPs-PFOB exhibited higher MFI values with activated platelets, as compared to resting platelets or activated platelets incubated with TNPs. With the increased quantity of fucoidan, the interaction of nanoparticles with activated platelets increase. Interaction with activated platelets was 2.45 times higher with 10% Fuco-TNPs-PFOB as compared to TNPs-PFOB.

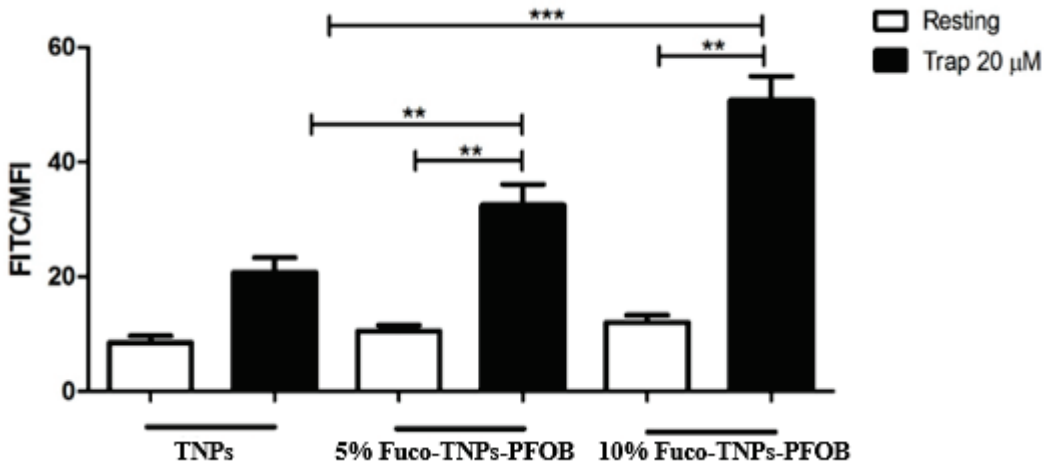

Figure 4. Flow cytometry assessment of FITC-labeled TNPs, FITC-labeled 5% Fuco-TNPs-PFOB and FITC-labeled 10% Fuco-TNPs-PFOB interaction with resting platelets and activated platelets, separately. (n=4, ** $p<0.01$, *** $p<0.001$).

3.3 Localization of Fuco-TNPs-PFOB within the abdominal aortic aneurysm wall of rats

The ability of the 10% Fuco-TNPs-PFOB to target P-selectin expression *in vivo* was evaluated in an abdominal aortic aneurysm (AAA) experimental model in rats with echography. **Figure 5** presents ultrasound images of AAA area before and after carotid injection of Fuco-TNPs-PFOB (200 μl, 50 mg/mL). Before injection, the abdominal aortic dilatation was clearly visible and the luminal blood appeared dark (**Figure 5A**) whereas after injection, the passing of Fuco-TNPs-PFOB were detected in the bloodstream immediately, and the present contrast enhancement of vascular wall in AAA area indicated some Fuco-TNPs-PFOB were uptaken by activated platelets and endothelial cells, which expressed P-selectin on their surface (**Figure 5B**). 20 min after injection the signals of Fuco-TNPs-PFOB were invisible in vessel due to dilution and clearance by circulation, whereas the contrast enhancement of vascular wall was still was observed (**Figure 5C**). In contrast, no enhanced signal intensity of arterial vascular wall was detected after the injection Fuco-TNPs-PFOB in healthy rats (Date not shown).

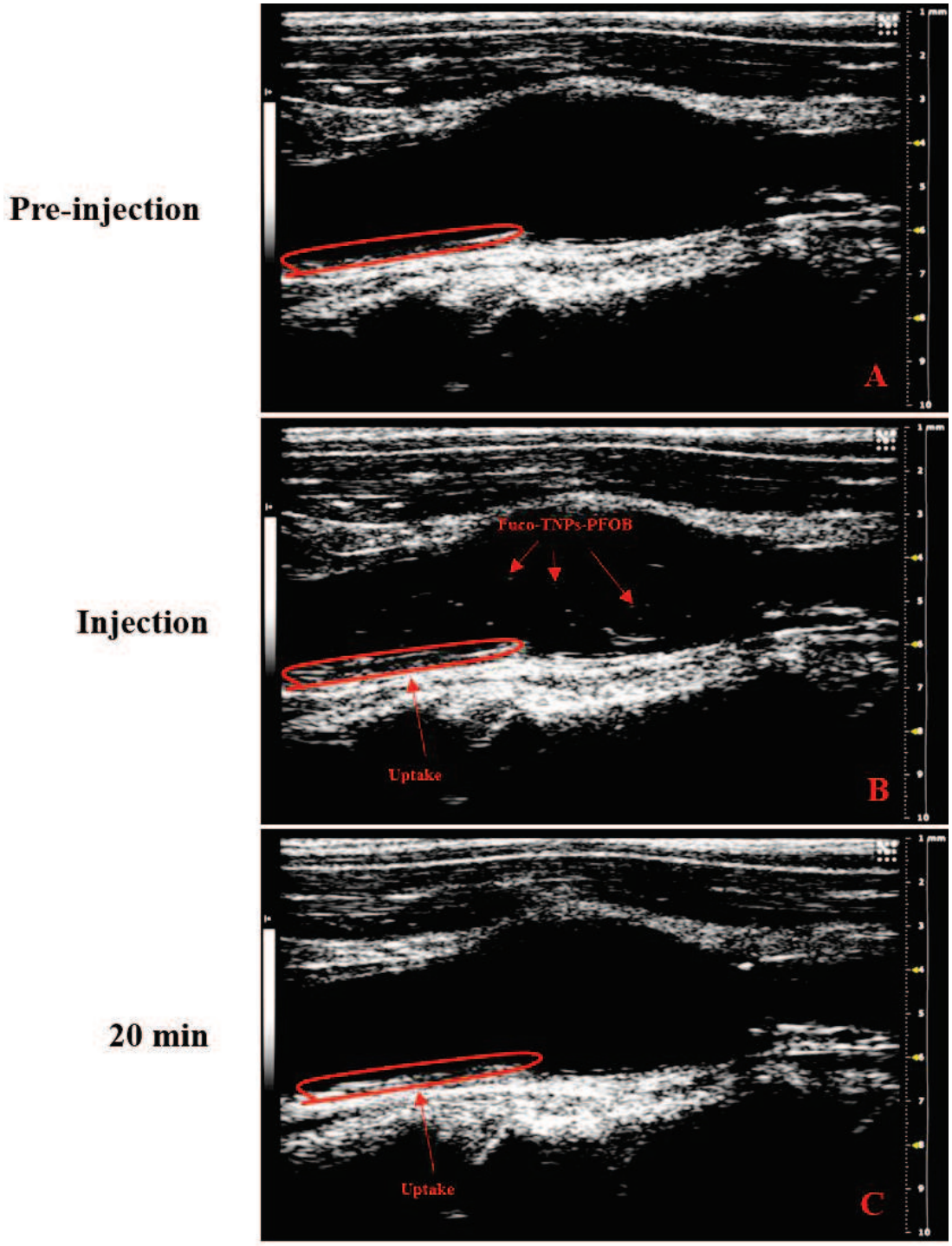

Figure 5. *In vivo* ultrasound images of the aneurysm of an AAA before and after injection into the rat carotid artery of Fuco-TNPs-PFOB (200 µL, 50 mg/mL). Passed Fuco-TNPs-PFOB and contrast uptake are indicated with red arrows. 20 mins after injections of Fuco-TNPs-PFOB are presented on the aneurysmal wall.

4. Discussion

The aim of this study was to develop nanoparticles loaded with PFOB as an ultrasound contrast agent. Subsequently they were functionalized with fucoidan, in order to target P-selectin overexpressed in cardiovascular diseases.

In a previous research, nano-/microcapsules of PLGA with a PFOB core were prepared by an emulsion-evaporation process.[5, 21] However, because of their rather hydrophobic surface, these capsules are rapidly eliminated by the mononuclear phagocyte system after intravenous administration, which obstruct their usage *in vivo*. To avoid a rapid clearance from the systemic circulation, recent strategies focus on PLGA-PEG diblock copolymer or PEGylated phospholipids instead of PLGA to formulate PFOB capsules.[20, 22] Here, PIBCA nanoparticle coated with polysaccharides are selected to load PFOB due to their biodegradability and biocompatibility.

Firstly, we demonstrated that addition of fucoidan resulted in a significant decrease of the zeta potential. These results can be explained by the presence the anionic polysaccharide at the surface of the nanoparticles. The zeta potential of nanoparticles became more negative when the amount of fucoidan was increased, it also agreed with the value of zeta potential found in previous studies.[23]

We then studied the relationship between quality of Tween 80 and mass percentage of PFOB. Results indicated 2 mg of Tween 80 is optimal for capture PFOB under the same conditions. Moreover, the mass percentage of PFOB in nanoparticles increases when added more PFOB in polymerization system.

More interestingly, dynamic light scattering results and SEM images show TNPs-PFOB have a larger diameter than TNPs. However, both of them show the similar size of core in TEM images, that may be because only polymer core seems darker and could be visible due to its higher electronic density than PFOB.[22] These

results indicated that different core-shell structure could be formed by emulsion-evaporation method. Here PFOB seemingly embedded in the surface of nanoparticles with the help of Tween 80. EDX analysis also revealed the fluorine located near the surface of TNPs-PFOB.

Furthermore, the PFOB content decreased with the addition of fucoidan. This may be interpreted with two scenarios. Firstly, fucoidan may modify the ionic strength of the polymerization system and weaken the nanoparticles stability due to its negative charge.[23] Secondly, the fucoidan chains on the nanoparticles obstruct PFOB access.

We then evidenced that the Fuco-TNPs-PFOB have a stronger affinity for human activated platelets than TNPs-PFOB by flow cytometry. Similar results had been reported by Bonnard T. *et al.* using fucoidan functionalized polysaccharide microparticles to interact with activated platelets.[24] Interestingly, with the increase of fucoidan mass fraction in initial polysaccharide, the target ability of Fuco-TNPs-PFOB to activated platelets increased significantly. This may be due to more fucoidan was distributed on the TNPs-PFOB surface, which is consistent with change of zeta potential of Fuco-NPs.

In vivo ultrasonic images analysis revealed that the contrast signals of Fuco-TNPs-PFOB were observed in vessel after injection. Some of Fuco-TNPs-PFOB accumulated in the thrombotic AAA wall and presented significant contrast enhancement even after 20 min. This observation indicates that Fuco-TNPs-PFOB efficiently are localized in the acute AAA where P-selectin is expressed.

5. Limitations

In this proof of concept study, we have developed polysaccharide coated PIBCA nanoparticles loaded with PFOB as an ultrasound contrast agent. This structure offers major advantage such as various functional chemical groups and long half-life in plasma. However, because of rapid redox radical emulsion polymerization (RREP)

process and high density of PFOB, it is very hard to form core-shell structure which encapsulates PFOB. Here, the PFOB was trapped into nanoparticles by a new method, but slightly changing the surface property of nanoparticles will directly affect PFOB loading efficiency. Our results demonstrated PFOB content significantly decreased with the increase of fucoidan dose. Actually, 10% Fuco-TNPs-PFOB contains only 6% PFOB. It is the direct cause of poor contrast signal of nanoparticles and insufficiency to identify or differentiate the contrast enhancement from tissue signal on ultrasonic imaging.

6. Conclusions

Fucoidan functionalized PIBCA nanoparticles loaded with PFOB were developed for the targeting of P-selectin expressed on the activated platelets in thrombotic abdominal aorta aneurysm. In this work, firstly, we described their elaboration with a new PFOB emulsion-RREP process, confirmed their hydrodynamic diameter distribution, the zeta potential, the nanoparticles structure and the mass percentage of fucoidan and PFOB. Subsequently, we demonstrated *in vitro* by flow cytometry that these Fuco-TNPs-PFOB could bind to the P-selectin expressed by activated human platelets. Finally, we showed *in vivo* on rats their specificity to bind to AAA and evidence their presence in the AAA wall by ultrasonic image. However, echographic signal enhancement was insufficient to clearly identify the AAA area, probably because of a poor ultrasonic signal of Fuco-TNPs-PFOB due to low content of PFOB. Results are encouraging and future work will focus on improve the signal of contrast agent to assess its ability to detect cardiovascular pathologies overexpressing P-selectins for ultrasonography.

References

[1] V. Fuster, F. Lois, M. Franco, *Nat Rev Cardiol* **2010**, 7, 327.

[2] J. M. Tarkin, M. R. Dweck, N. R. Evans, R. A. P. Takx, A. J. Brown, A. Tawakol, Z. A. Fayad, J. H. F. Rudd, *Circul. Res.* **2016**, 118, 750.

[3] M. A. Schellpfeffer, *Birth Defects Res C Embryo Today* **2013**, 99, 83.

[4] D. Cosgrove, *Eur J Radiol* **2006**, 60, 324.

[5] E. Pisani, N. Tsapis, J. Paris, V. Nicolas, L. Cattel, E. Fattal, *Langmuir* **2006**, 22, 4397.

[6] O. Diou, E. Fattal, V. Delplace, N. Mackiewicz, J. Nicolas, S. Mériaux, J. Valette, C. Robic, N. Tsapis, *European Journal of Pharmaceutics and Biopharmaceutics* **2014**, 87, 170.

[7] P. Couvreur, B. Kante, M. Roland, P. Guiot, P. Bauduin, P. Speiser, *J. Pharm. Pharmacol.* **1979**, 31, 331.

[8] I. Brigger, P. Chaminade, V. Marsaud, M. Appel, M. Besnard, R. Gurny, M. Renoir, P. Couvreur, *Int. J. Pharm.* **2001**, 214, 37; J. Kattan, J.-P. Droz, P. Couvreur, J.-P. Marino, A. Boutan-Laroze, P. Rougier, P. Brault, H. Vranckx, J.-M. Grognet, X. Morge, H. Sancho-Garnier, *Investigational New Drugs* **1992**, 10, 191.

[9] D. Labarre, C. Vauthier, C. Chauvierre, B. Petri, R. Müller, M. M. Chehimi, *Biomaterials* **2005**, 26, 5075.

[10] A. Varki, *Proceedings of the National Academy of Sciences of the United States of America* **1994**, 91, 7390.

[11] K. Ley, *Trends Mol. Med.* **2003**, 9, 263.

[12] H. H. Boersma, H. J. de Haas, C. P. Reutelingsperger, R. H. Slart, *J Nucl Med* **2011**, 52, 1337.

[13] J. J. Rychak, J. R. Lindner, K. Ley, A. L. Klibanov, *J Control Release* **2006**, 114, 288; F. Guenther, C. von zur Muhlen, E. A. Ferrante, S. Grundmann, C. Bode, A. L. Klibanov, *Invest Radiol* **2010**, 45, 586; T. Bettinger, P. Bussat, I. Tardy, S. Pochon, J. M. Hyvelin, P. Emmel, S. Henrioud, N. Biolluz, J. K. Willmann, M. Schneider, F. Tranquart, *Invest Radiol* **2012**, 47, 516; I. Nakamura, K. Hasegawa, Y. Wada, T.

Hirase, K. Node, Y. Watanabe, *Biochem. Biophys. Res. Commun.* **2013**, 433, 47; E. A. Ferrante, J. E. Pickard, J. Rychak, A. Klibanov, K. Ley, *J. Controlled Release* **2009**, 140, 100.

[14] L. Chollet, P. Saboural, C. Chauvierre, J. N. Villemin, D. Letourneur, F. Chaubet, *Mar. Drugs* **2016**, 14.

[15] L. Bachelet, I. Bertholon, D. Lavigne, R. Vassy, M. Jandrot-Perrus, F. Chaubet, D. Letourneur, *Biochim. Biophys. Acta* **2009**, 1790, 141.

[16] F. Rouzet, L. Bachelet-Violette, J. M. Alsac, M. Suzuki, A. Meulemans, L. Louedec, A. Petiet, M. Jandrot-Perrus, F. Chaubet, J. B. Michel, D. Le Guludec, D. Letourneur, *J Nucl Med* **2011**, 52, 1433.

[17] L. Bachelet-Violette, A. K. A. Silva, M. Maire, A. Michel, O. Brinza, P. Ou, V. Ollivier, A. Nicoletti, C. Wilhelm, D. Letourneur, C. Menager, F. Chaubet, *RSC Advances* **2014**, 4, 4864.

[18] M. Suzuki, L. Bachelet-Violette, F. Rouzet, A. Beilvert, G. Autret, M. Maire, C. Menager, L. Louedec, C. Choqueux, P. Saboural, O. Haddad, C. Chauvierre, F. Chaubet, J. B. Michel, J. M. Serfaty, D. Letourneur, *Nanomedicine (Lond)* **2014**, 1.

[19] C. Chauvierre, D. Labarre, P. Couvreur, C. Vauthier, *Pharmaceutical Research* **2003**, 20, 1786; C. Chauvierre, D. Labarre, P. Couvreur, C. Vauthier, *Macromolecules* **2003**, 36, 6018.

[20] O. Diou, N. Tsapis, C. Giraudeau, J. Valette, C. Gueutin, F. Bourasset, S. Zanna, C. Vauthier, E. Fattal, *Biomaterials* **2012**, 33, 5593.

[21] E. Pisani, N. Tsapis, B. Galaz, M. Santin, R. Berti, N. Taulier, E. Kurtisovski, O. Lucidarme, M. Ourevitch, B. T. Doan, J. C. Beloeil, B. Gillet, W. Urbach, S. L. Bridal, E. Fattal, *Advanced Functional Materials* **2008**, 18, 2963.

[22] R. Díaz-López, N. Tsapis, M. Santin, S. L. Bridal, V. Nicolas, D. Jaillard, D. Libong, P. Chaminade, V. Marsaud, C. Vauthier, E. Fattal, *Biomaterials* **2010**, 31, 1723.

[23] M. C. B. Lira, N. S. Santos-Magalhães, V. Nicolas, V. Marsaud, M. P. C. Silva, G. Ponchel, C. Vauthier, *European Journal of Pharmaceutics and Biopharmaceutics* **2011**, 79, 162.

[24] T. Bonnard, G. Yang, A. Petiet, V. Ollivier, O. Haddad, D. Arnaud, L. Louedec, L. Bachelet-Violette, S. M. Derkaoui, D. Letourneur, C. Chauvierre, C. Le Visage, *Theranostics* **2014**, 4, 592; T. Bonnard, J. M. Serfaty, C. Journe, B. Ho Tin Noe, D. Arnaud, L. Louedec, S. M. Derkaoui, D. Letourneur, C. Chauvierre, C. Le Visage, *Acta Biomater.* **2014**, 10, 3535.

CHAPTER II

Development of fucoidan functionalized polymer microcapsules to target P-selectin overexpressed in cardiovascular diseases

This work was accepted for publication in

Advanced Healthcare Materials

ABSTRACT

New tools for molecular imaging and targeted therapy for cardiovascular diseases are still required. Herein, biodegradable microcapsules (MCs) made of polycyanoacrylate and polysaccharide and functionalized with fucoidan (Fuco-MCs) were designed as new carriers to target arterial thrombi overexpressing P-selectin. Physico-chemical characterizations demonstrated that the microcapsules have a core-shell structure and that fucoidan was present onto the surface of Fuco-MCs. Furthermore, their size ranged from 2 to 6 µm and they were stable on storage over 30 days at 4°C in water. Flow cytometry experiments evidenced the binding of Fuco-MCs for human activated platelets as compared to MCs (mean fluorescence intensity: 12008 vs 9.00, $P<0.001$) and its absence for non-activated platelets (432.4). An *in vitro* flow adhesion assay showed high binding of Fuco-MCs to P-selectin and to activated platelet aggregates under arterial shear stress conditions. Moreover, both types of microcapsules revealed excellent compatibility with 3T3 cells in cytotoxicity assay. One hour after intravenous injection of MCs or Fuco-MCs, histological analysis revealed that Fuco-MCs were localized in the rat Abdominal Aortic Aneurysm thrombotic wall and that the binding in the healthy aorta was low. In conclusion, these microcapsules appear as promising carriers for targeting of tissues characterized by P-selectin overexpression.

Graphical Abstract

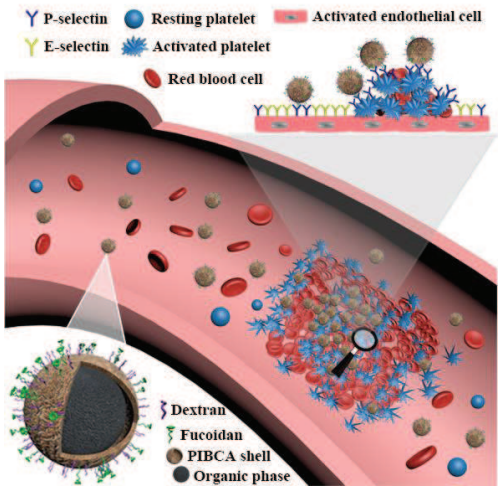

1. Introduction

P-selectin, an adhesion molecule, is expressed at the surface of activated platelets and injured vascular endothelium. Therefore, P-selectin is a marker of biologically active arterial thrombi and expansion of Abdominal Aortic Aneurysms (AAA).[1] In recent studies, P-selectin was described as a molecular imaging target for AAA early detection, dilatation and rupture risk assessment. Some authors have developed nano/micro-contrast agents for imaging of P-selectin using ultrasound or magnetic resonance.[2] Limitations are related to the low binding efficiency in high blood shear rate of nano/microspheres to P-selectin on the area of AAA leading to insufficient detectable contrast signals for predicting AAA rupture risk. Moreover, microspheres as compared to nanospheres showed higher margination efficiency in recirculating blood flow and thus may be advantageous for treatment of arterial thrombi.[3] New carrier systems with strong P-selectin binding are still needed for vascular-targeted imaging or drug delivery.

Fucoidan, a seaweed-derived polysaccharide with sulfated chains, was proved to be an efficient glycosidic ligand of P-selectin.[4] Our group previously demonstrated its ability to bind P-selectin and developed a radiotracer by combining Technetium (^{99m}Tc) to fucoidan to enable detection of activated endothelium and thrombosis.[5] Recently, we developed fucoidan functionalized iron oxide nanoparticles and polysaccharide microparticle and radiolabeled with ^{99m}Tc, for MRI or SPECT imaging respectively.[6]

The aim of the present study was to produce in an easy way injectable polymer microcapsules able to target P-selectin. The first design of biodegradable poly(alkyl cyanoacrylate) (PACA) nanoparticles prepared by emulsion polymerization as *in vivo* drug delivery carrier was described in 1979.[7] The classical approach for the preparation of PACA nanoparticles is the emulsion polymerization by either anionic or redox radical mechanisms.[8-10] Different types of PACA nanosystems have been developed in the past decades such as polymer nanoparticles,[11] core-shell polymer

nanoparticles[12] and polymer nanocapsules.[13] Moreover, a great variety of bioactive compounds have been loaded on these different types of PACA nanosystems[14] compounds such as antioxidant agents,[15] anticancer drugs,[16] antibiotics,[17] proteins,[18] peptides[19] and nucleic acids.[13, 20] However, issues still exist such as the initiation of the polymerization reaction of alkyl cyanoacrylates by the chosen reactive drug instead of by the hydroxyl ions for anionic mechanism or by free radicals for redox radical mechanism. To overcome these limitations, Yordanov G. *et al.* recently reported the preparation of poly (butyl cyanoacrylate) (PBCA) homopolymer nanospheres by the nanoprecipitation method using a pre-synthesized polymer and colloidal stabilizers.[21] Nevertheless, this method requires multiple steps for obtaining PACA nanospheres. We report here a new process to obtain microcapsules that are assembled from polymerization of isobutyl cyanoacrylate (IBCA) in presence of perfluorooctyl bromide (PFOB), coated by polysaccharides and functionalized with fucoidan. The thickness of the microcapsules can be adjusted by simply modifying the pH value of the water phase prior to emulsification. Flow cytometry and flow chamber experiments were performed to evaluate the specificity of the interaction between activated platelets and microcapsules functionalized with fucoidan (Fuco-MCs). In addition, *in vivo* experiments performed in an elastase-induced AAA rat model showed that Fuco-MCs were located in the thrombotic abdominal aorta and not in healthy rats which confirms the ability of these microcapsules to target specifically P-selectin. These microcapsules appear as new tools for imaging at molecular level or for treating cardiovascular pathologies in which P-selectin is overexpressed.

2. Experimental Section

Materials:

Methylene chloride (CH_2Cl_2) RPE-ACS 99.5% and Acetone 99.8% were provided by Carlo Erba Reactifs (Peypin, France). 1-Bromoheptadecafluorooctane (PFOB), $CDCl_3$ (99.96 atom % D), isopropanol, MTT solution and Nile Red were provided by Sigma Aldrich (Saint Quentin Fallavier, France). Dextran 20 and FITC-Dextran 20 were obtained from TdB Consultancy (Uppsala, Sweden). Fucoidan was a gift from Algues & Mer (Ouessant, France). Perfluoro-15-crown-5-ether (PFCE) was purchased from Fluorochem (Hadfield, UK). Isobutyl cyanoacrylate (IBCA) was provided by ORAPI (Saint Vulbas, France). TRAP (thrombin receptor-activating-peptide) was obtained from PolyPeptide laboratories (Strasbourg, France). PE-Cy^{TM}5 mouse anti-human CD41a and PE-Cy^{TM}5 mouse IgG1,κ Isotype Control were provided by BD Pharmingen, (Le Pont-de-Claix, France), mouse anti-human CD62P, mouse anti-human CD62P-FITC and mouse IgG1-FITC Isotype Control were obtained from Beckman Coulter (Villepinte, France). Recombinant human E-selectin, L-selectin and P-selectin were provided by R&D Systems (Lille, France). Flow chambers (Vena8Fluoro+) were obtained from Cellix Ltd (Dublin, Ireland).

Synthesis of core-shell microcapsules:

Dextran 20 coated poly (isobutyl cyanoacrylate) (PIBCA) microcapsules (MCs) with 1-Bromoheptadecafluorooctane (PFOB) core as a reference loaded agent was prepared by modification of the emulsion-evaporation process described by Pisani.[22] Briefly, 100 µL of IBCA was dissolved into 4 mL of methylene chloride along with 60 µL of PFOB. The organic solution was mixed to ensure full miscibility of the PFOB. Subsequently, the whole organic phase was slowly injected into 20 mL of a cold aqueous solution containing 300 mg of dextran (1.5% (w/v)) adjusted to the desired pH conditions (pH 3, 7 or 10), and dispersed at 30,000 rpm for 2 min with a

homogenizer (Polytron PT 3100, dispersing aggregate PT-DA 07/2 EC-B101, Kinematica, Luzern, Switzerland). To prepare fucoidan-functionalized microcapsules (Fuco-MCs), 30 mg of fucoidan was blended into 270 mg of dextran. They were dissolved into an aqueous solution at pH 10. Emulsification was performed in a 50 mL beaker placed in ice. Methylene chloride was then evaporated by magnetic stirring for about 4 h at room temperature or 3 h in a thermostatic bath (30°C). After full evaporation of the solvents, samples were centrifuged at 600 g for 30 min (5702RH centrifuge Beckman Coulter, Villepinte, France), supernatants were discarded and precipitates were washed by deionized water. The centrifugation and washing steps were repeated three times. For fluorescent and confocal microscopy studies, 10 µL (0.57 mg/ml) of Nile red were added to the organic solution and 3 mg of FITC-dextran were added to the aqueous solution before emulsification. The fluorescence intensity of microcapsules was analyzed by Image J software. Finally, the precipitate was suspended again into 3 mL of deionized water for storage at 4°C until use or for freeze-drying.

For freeze-drying, the purified suspensions were frozen at -18°C and freeze-dried during 48-72 h without using any cryo-protecting agent (Lyovac, SRK Systemtechnik, Riedstadt, Germany).

The mass yield (%) was calculated as follows:

$$Yield = \frac{m^{mass}_{Microcapsules}}{m^{feed}_{Polysaccharides} + m^{feed}_{polymer} + m^{feed}_{PFOB}} \times 100\% \quad (1)$$

Where $m^{feed}_{Polysaccharides}$ $m^{feed}_{polymer}$ m^{feed}_{PFOB} are the initial masses of the components introduced in the reaction solution, $m^{mass}_{Microcapsules}$ corresponds to the final mass of microcapsules evaluated after the freeze-drying process.

Size and zeta potential microcapsule determination:

The size distribution of microcapsules was quantitatively obtained using a laser dynamic scattering granulometry at 25ºC (Mastersizer 3000, Malvern Instruments, Orsay, France).

Zeta potential (ζ) of the microcapsules was measured to evaluate their stability in suspension and to identify the presence of the polysaccharides onto the surface. Samples were diluted in 1 mM KCl. Measurements were performed at 25ºC using quasi-elastic light scattering apparatus (Nano ZS, Malvern Instruments, Orsay, France).

All the measurements were performed in triplicate and the results were expressed as mean ± standard deviation.

Scanning Electron Microscopy (SEM) and Transmission Electron Microscopy (TEM):

The surface morphology of microcapsules was imaged using a Scanning Electron Microscopy apparatus (Philips XL 30 ESEM-FEG, Amsterdam, Netherlands) on dried samples coated with a thin gold layer. Transmission Electron Microscopy was performed using a Philips EM208 apparatus (Amsterdam, Netherlands) operating at 80 kV.

Determination of PFOB content:

Microcapsules were freeze-dried for 24-48 hours. Subsequently, freeze-dried microcapsules were dissolved into $CDCl_3$ along with PFCE as an internal standard ([PFCE] = 0.76 mmol/L). The ^{19}F NMR (Nuclear Magnetic Resonance) spectra were recorded on a Bruker (400 MHz) Spectrometer (Billerica, USA). The amount of PFOB was obtained after integration of the peak at -80.7 ppm, corresponding to the CF_3 group and normalization by the area of the PFCE peak at -89.5 ppm. Mass

fraction C_{PFOB} was calculated as follows:

$$C_{PFOB} = \frac{m_{\mathrm{PFOB}}^{\mathrm{NMR}}}{m_{MC}} \quad (2)$$

Where m_{MC} is the quantity of freeze-dried microcapsules, and $m_{\mathrm{PFOB}}^{\mathrm{NMR}}$ corresponds to the mass of PFOB recovered after the freeze-drying process.

Sulfate and fucoidan quantification:

Sulfate quantification was conducted according to Gustaffson.[23] Briefly, a certain amount of fucoidan functionalized microcapsules was freeze-dried. Subsequently, the sample was exposed to nitrogen (100 mL/min) while being boiled in iodohydric acid for 20 min. Released hydrogen sulfur reacted with zinc acetate (0.2 M) to form zinc sulfur. Then 8 mL of ammonium iron sulfate at 16 mM and 2 mL of 3.7 mM diamine were added into the sample. Following 15 min of agitation, absorbance at 675 nm and 745 nm was measured using a spectrophotometer (PerkinElmer®). Sulfate content was calculated from a standard curve obtained with a potassium sulfate reference solution. Finally, sulfate content was measured and fucoidan content of the microcapsules was calculated.

Static binding on platelets:

The interaction between three groups of PE-Cy5 labeled platelets (non-activated platelets (PRP), activated platelets (PRP + TRAP) and P-selectin blocked activated platelets (PRP + TRAP + CD62P) and two groups of microcapsules with FITC-dextran (MCs, Fuco-MCs) were measured by flow cytometry. 5 mL of blood samples from healthy adult volunteers were collected in sodium citrate 3.8% (w/v). Platelet-rich plasma (PRP) was obtained by centrifugation at 200 g for 15 min (5702RH centrifuge Beckman Coulter, Villepinte, France) and platelet concentration was adjusted to 2×10^8 ml^{-1} with autologous platelet-poor plasma (PPP). Activated PRP was obtained by stimulation of PRP with 20 μM TRAP (thrombin

receptor-activating-peptide). In some experiments, activated then P-selectin-blocked PRP were obtained by incubation with a non-labeled anti-human CD62P at high concentration (0.04 $g.L^{-1}$). Before assessing the interaction with microcapsules, P-selectin expression level at the platelet surface was assessed using an anti-human CD62P-FITC. An additional tube of PRP was also incubated with a mouse IgG1/FITC to verify that the FITC signal was not due to non-specific binding to the platelets. In addition, MCs and Fuco-MCs were incubated with anti-human PE-Cy5 at a similar concentration to prove that microcapsules could not be labeled by antibody. Thus, for each test, we measured the FITC signal by flow cytometry and confirmed that P-selectin was expressed by platelets from PRP + TRAP batches and that low level of P-selectin was detected on PRP and PRP +TRAP + CD62P batches. To evaluate the binding ability between microcapsules with P-selectin expressed onto platelets, 5 µL of non-activated PRP, of activated PRP with TRAP or of anti P-selectin-treated activated PRP were incubated for 20 min with 5 µl of MCs and of Fuco-MCs (50 mg/ml), together with 5 µL of PE-Cy5 mouse anti-human CD41a to label platelets. In addition, each PRP sample was incubated with an isotype-matched control antibody. Samples were analyzed on a LSRII flow cytometer (BD Biosciences, Le Pont de Claix, France), 50,000 PE-Cy5 positive platelets collected per samples, and the mean fluorescence intensity (MFI) was measured in these platelets.

Flow chamber experiments:

Channels were coated either with a solution of P-selectin, L-selectin or E-selectin at 100 µg/mL (PBS). Some channels were coated with different concentrations of P-selectin (from 5 µg/mL to 100 µg/mL) to confirm that the affinity of Fuco-MCs for P-selectin was dependent on the concentration of P-selectin. The selectin solutions were left in the channels overnight at 4°C in a wet chamber. Channels were then washed with NaCl 0.9%. A suspension of fluorescent MCs or Fuco-MCs at 50 mg/mL was passed through the channels for 5 minutes at a shear rate of 1,500 s^{-1}. For competitive binding experiment, fucoidan solution (10 mg/ml) was injected at the

same rate, 5 min before microcapsules were injected. After microcapsules injection, all the channels were washed with NaCl 0.9% for 1 minute at the same flow. Images of the bottom surface were taken along each channel. Fluorescence microscopy images were further analyzed with HistoLab software (Microvision, Evry, France) to quantify the number of attached particles.

For platelet dynamic binding experiments, channels were coated with collagen at 50 µg/mL. The collagen solution was left in the channels overnight at 4°C in a wet chamber. Channels were then washed with NaCl 0.9%. Collagen fibers covering the channels wall were visualized by phase contrast microscopy. Human whole blood was passed through the channels for 3.5 minutes on average at 1,500 s^{-1}. Platelets aggregations through contact with collagen were visualized in real time with phase contrast microscopy (Axio Observer, Carl Zeiss Microscopy, Oberkochen, Germany). The channels were washed for 1 minute with NaCl 0.9%. On one channel FITC anti-CD62P antibody was infused at 20 µg/mL in NaCl 0.9% for a few minutes to confirm P-selectin expression on platelets membrane. One channel was used as a control for a control isotype-matched FITC-IgG at the same concentration. In the other channels, the platelets were labeled with Dioc6 (0.15 mM) before their injection. After their aggregation, fluorescent microcapsules (MCs or Fuco-MCs) were injected through the channels at 50 mg/mL for 5 minutes. Channels were finally washed for 1 minute with NaCl 0.9%. Images in phase contrast and in fluorescence microscopy were taken along each channel. Quantitative analysis was performed on at least three channels per type of microcapsules. The mean fluorescence intensity of the red fluorescence channel of several aggregates was measured using Zen 2012 Software (Carl Zeiss, Oberkochen, Germany). The red fluorescence background was measured on aggregates only and was subtracted from the results.

In vitro cytotoxicity:

To evaluate the cytotoxicity of the microcapsules and fucoidan functionalized microcapsules, MTT colorimetric assay was used on mouse fibroblasts 3T3 line. The cells were cultured in DMEM supplemented with 10% (v/v) fetal bovine serum (FBS), 4 mmol of L-glutamine, 100 units/mL of penicillin, and 100 µg/mL of streptomycin. The cells were kept in an incubator at 37°C in a humidified atmosphere of 5% CO2, 95% air. 3T3 cells were seeded (at the density of 10^4 cells per well) in 96-well plates (Costar) and incubated for 24 hours. After that, the cell culture medium was removed and 200 µL of series of dilution (0.625, 1.25, 2.5 and 5 g/L) of microcapsules in the medium were added to the plate. Culture media were used as the positive controls. After 24 hour of incubation, the supernatant was removed and 10 µL (5 mg/mL) of MTT solution was added to the medium in each well and the plates were incubated for 4 hours at 37ºC and 5% CO2. Then, the medium with MTT was removed and 100 µL per well of isopropanol solution was added to each well to dissolve the formazan crystals. The plates were read immediately in Tecan (Infinite@ M200 PRO) at 490 nm. The relative cell viability was expressed as Abs microcapsules/Abs control × 100%, where Abs control was obtained in the absence of the microcapsules.

In vivo arterial disease model:

Animal studies were done in accordance with principles of laboratory animal care and with approval of the animal care and use committee of the Claude Bernard Institute (N°2012-15/698-0100) (Paris, France). The ability of the functionalized microcapsules to target P-selectin expression *in vivo* was assessed in an abdominal aortic aneurysm (AAA) experimental model in rats. The elastase model was performed on 8 male adult Wistar rats (7 weeks, Janvier Labs, Le Genest-Saint-Isle, France). Animals were anesthetized with intra-peritoneal injection of pentobarbital (1 µL/g body weight, Ceva Santé Animale SA, La Ballastiere, France). Porcine pancreatic elastase (2.7 mg/mL, Sigma Aldrich, Saint Quentin Fallavier, France) was perfused into the lumen of an isolated segment of the infrarenal abdominal aorta for

15 minutes at a rate of 2.5 mL/h. Delbosc *et al.* reported that repeated intravenous injection of *Porphyromonas gingivalis* (Pg) in a rat model of AAA led to enhanced aortic dilation associated with neutrophil retention and persistence of a non-healing luminal thrombus.[24] In this study, *Porphyromonas gingivalis* suspension (107 CFU in 500 µL 0.9% saline), a gift from La Pitié Salpétrière Hospital, was injected to the rats once a week via the penis vein for 4 weeks. Two days after the fourth injection, rats were anaesthetized by sodium pentobarbital intra-peritoneal injection (1 µL/g,) and 200 µl of MCs or Fuco-MCs (50 mg/mL) were injected slowly via the carotid artery. Healthy rats served as controls.

Histology:

Animals were sacrificed with pentobarbital overdose 60 minutes after injection of MCs or Fuco-MCs. Abdominal aorta aneurysms of rats and healthy aorta of normal control rats were removed, washed in 0.9 % saline, fixed in paraformaldehyde (PFA) 4% (w/v) and then frozen. The aorta samples were cryo-sectioned at 10 µm thicknesses for standard histology evaluations. The cell nucleus of arterial vascular wall were labeled with DAPI, microcapsules expressed red fluorescence. The 20x-magnified images of region of interest (ROI) were used for semi-quantitative analysis. The red and blue fluorescence areas were measured using ImageJ image analysis software.

Biodistribution of microcapsules were studies in a similar way. Briefly, liver, spleen, lungs and kidneys were excised and washed at 1 hour or 24 hours after injection of MCs or Fuco-MCs. The samples were cryo-sectioned and the cell nuclei were labeled with DAPI, the whole area of tissue slice of samples was used for semi-quantitative analysis.

Statistical Analysis:

Data are presented as mean ± SEM ($n \geq 3$). Each experiment was performed using Student t test for paired data. Flow cytometry results were analyzed statistically with a

one-way ANOVA with Bonferroni post-tests to compare data obtained with MCs and Fuco-MCs. A difference of $P < 0.05$ was considered significant.

3. Results

3.1 Preparation and characterization of microcapsules

New polymer microcapsules coated with polysaccharides and loaded with PFOB were prepared by modification of the commonly used emulsion-evaporation polymerization process (**Figure 1**).

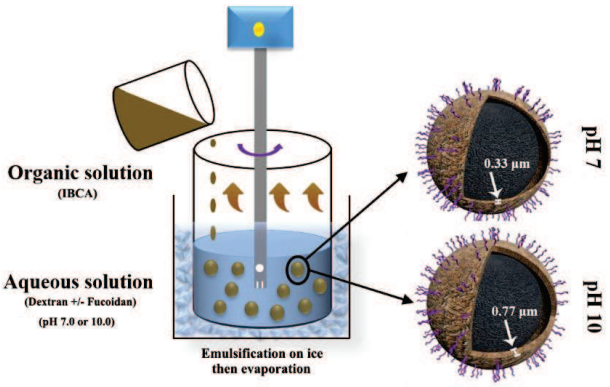

Figure 1. Overall scheme of one-step protocol for microcapsules.

According to previous studies,[4, 9, 25, 26] PACA nanoparticles are synthesized at low pH values to avoid anionic homopolymerization occurring spontaneously due to the rapid initiation by the hydroxyl groups of water. However, it was impossible to form microcapsules at a pH value lower than 3 (**Table 1**). In contrast, when the pH value was either set to 7 or 10 at 30°C, the microcapsule mass yield reached 9% or 30% respectively, whereas the weight percent fraction of PFOB (the loaded agent) represented 69% or 43% of the total microcapsule weight. The mean sizes were 41.50 ± 0.68 µm and 6.41 ± 0.02 µm respectively. The D_{90} value (90% of the particles are smaller than this diameter) was significantly lower for the microcapsules synthesized at basic pH than for the ones synthesized at neutral pH, indicating a narrower distribution of the microcapsule size. Additionally, the yield of microcapsules

decreased when reducing the temperature from 30°C to 20°C.

Table 1. Characteristics of non-functionalized microcapsules.

pH	T (°C)	Polysaccharide	Stability in water	Size distributions			Zeta potential	Yield	Loaded agent
				D_{10} (µm)	D_{50} (µm)	D_{90} (µm)	ζ (mV)	(%, w/w)	(%, w/w)
3	30	Dextran	No product	-	-	-	-	-	-
7	30	Dextran	Stable	1.57±0.01	5.68±0.04	41.50±0.68	-16.83±0.31	9.00±2.15	69.02±3.44
10	30	Dextran	Stable	2.40±0.01	4.07±0.01	6.41±0.02	-12.10±0.59	30.03±1.98	42.54±2.16
10	20	Dextran	Stable	2.31±0.04	4.03±0.05	6.50±0.10	-16.25±0.42	25.88±2.70	42.50±1.68

To further visualize the polysaccharide presence in microcapsules, a portion of dextran (1% w/w) was substituted during the emulsion process by FITC-dextran, and Nile red was added in the organic phase to stain red the hydrophobic poly (isobutyl cyanoacrylate) (PIBCA). Microcapsule suspensions were observed by confocal microscopy (**Figure 2 Left**). The core–shell structure of the microcapsules was perfectly visible; the core composed of liquid appeared in dark and the fluorescent shell was well defined. Surprisingly, polysaccharides were not preferentially localized at the polymer/water interface. In fact, the green fluorescence was homogeneously distributed in the whole shell thickness, the polysaccharides being therefore mixed with the polymer shell.

The scanning of focused equatorial slice of Nile red-labeled microcapsule shells was performed and the fluorescence intensity profiles were measured (**Figure 2 Right**). Confocal images showed that microcapsules had a thickness of 0.33 ± 0.08 µm and 0.77 ± 0.13 µm for reaction medium pH of 7 and 10 respectively.

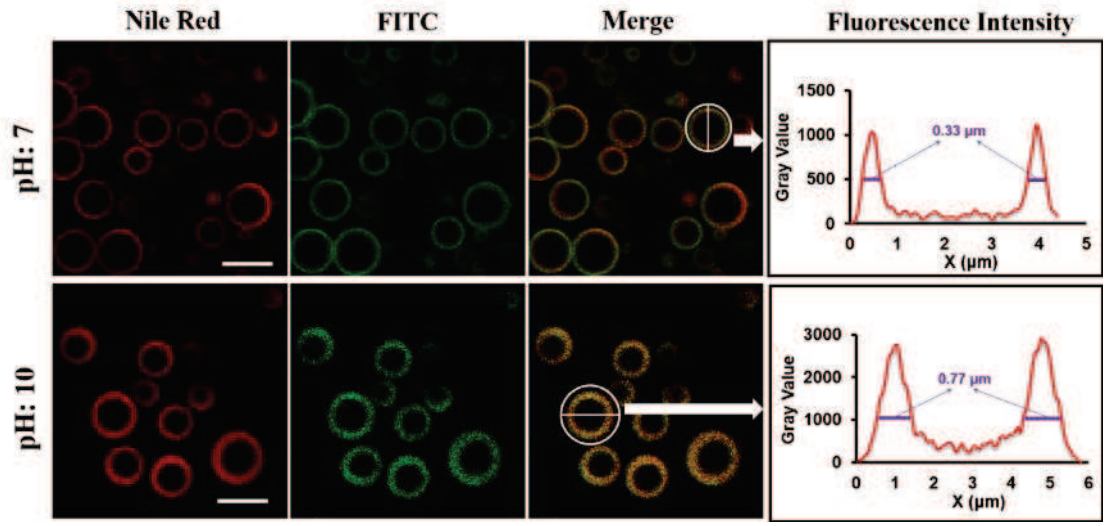

Figure 2. Confocal microscopy images of microcapsules (**Left**). Polymers appeared in color and the liquid content appeared in dark. Red fluorescence channel: PIBCA (left), green fluorescence channel: FITC-Dextran (center) and merging of both channels (right), pH 7 (top), pH 10 (bottom) (Scale bar = 5 µm). Fluorescence Intensity graph profile (X: distance measurement) (**Right**). Determination of the shell thickness, pH 7 (top) and pH 10 (bottom). (n=3)

To obtain functionalized particles, fucoidan was introduced into the polymerization medium, as 10% w/w of the total polysaccharide mass. As indicated in **Table 2**, stable microcapsules functionalized with fucoidan (Fuco-MCs) had a mean size of 7.09 ± 0.14 µm. The zeta potential of Fuco-MCs decreased compared to MCs (-50.88 ± 0.52 mV vs -12.10 ± 0.59 mV for MCs). This result indicated that at least a part of the anionic fucoidan was present at the surface of the microcapsules, a property already observed with fucoidan coated nanoparticles[26]. To further evidence/corroborate the presence of fucoidan in Fuco-MCs, FITC-fucoidan (1% w/w of the total fucoidan mass) was incorporated during their synthesis. The colocalization of FITC-fucoidan and the microcapsules was evaluated by flow cytometry. Non-fluorescent Fuco-MCs were used as a control to adjust their auto fluorescence level. A noticeable difference in the fluorescent signal was detected between FITC-Fuco-MCs and Fuco-MCs, indicating that almost all microcapsules in contact with FITC-fucoidan were functionalized by FITC-fucoidan (**Figure 3**).

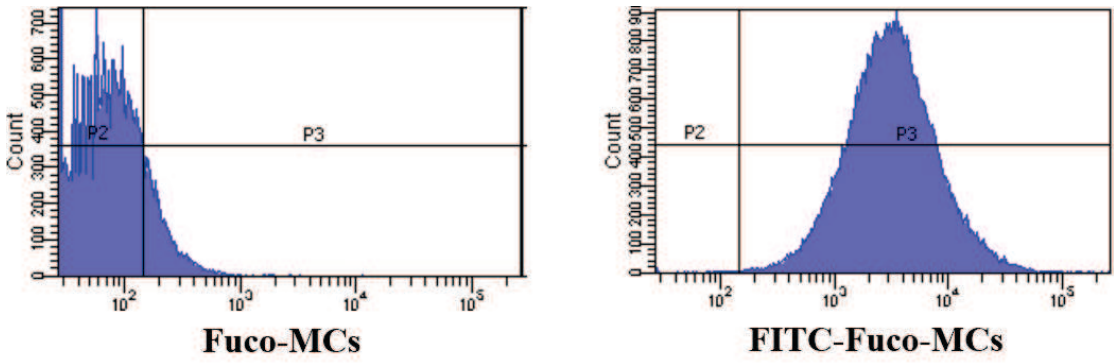

Figure 3. The flow cytometry evaluation of the efficiency with FITC-Fucoidan with microcapsules. Green fluorescence signal associated to the fucoidan functionalized microcapsules in presence or not of FITC-fucoidan.

After purification, both MCs and Fuco-MCs have similar size distribution (from 2.2 µm to 5.9 µm for MCs and from 2.2 µm to 5.8 µm for Fuco-MCs) and the mass of loaded agent was similar (42% and 41% respectively) (**Table 2**).

Table 2. Characteristics of non-functionalized and functionalized microcapsules.

Microcapsules	Stability in water		Size distributions			Zeta potential	Yield	Loaded agent
			D_{10} (µm)	D_{50} (µm)	D_{90} (µm)	ζ (mV)	(%, w/w)	(%, w/w)
Non-functionalized	Stable	After preparation	2.40±0.01	4.07±0.01	6.41±0.02	-12.10±0.59	30.03±2.12	42.54±3.05
		After purification	2.24±0.02	3.79±0.03	5.90±0.10	-8.86±0.88	29.25±3.48	42.05±2.56
(MCs)								
Functionalized with	Stable	After preparation	2.30±0.01	4.19±0.05	7.09±0.14	-50.88±0.52	28.51±2.61	45.86±1.98
fucoidan		After purification	2.19±0.02	3.69±0.02±	5.84±0.05	-51.76±1.33	24.56±3.11	41.15±2.87
(Fuco-MCs)								

The morphology of obtained microcapsules was analyzed by Scanning Electron Microscopy (SEM) and Transmission Electron Microscopy (TEM) (**Figure 4**). Both MCs and Fuco-MCs showed a typical well-defined spherical capsule structure.

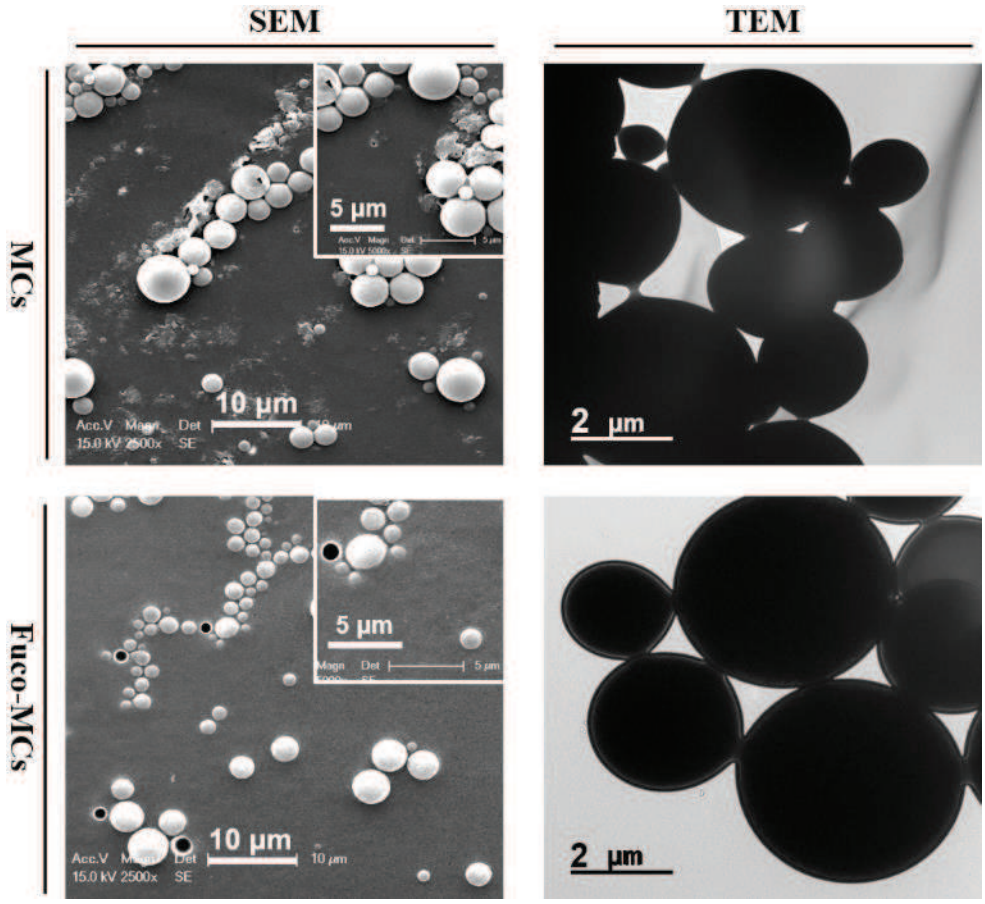

Figure 4. Scanning and Transmission Electron Microscopy images of microcapsules. Top: MCs. Bottom: Fuco-MCs. Left: SEM images with zooms. Right: TEM images.

Quantitative analysis showed that Fuco-MCs contained 0.10 µmol/g of sulfur. Since the fucoidan used in this study was determined to contain 1,550 µmol/g of sulfur, we calculated the fucoidan content of Fuco-MCs to be 0.008 % (w/w). Long-term stability in distilled water was assessed upon storage of the suspensions at 4ºC. Size and zeta potential remained stable at least for one month for both types (**Figure 5**). Moreover, the content of fucoidan in Fuco-MCs did not change greatly with time (0.006 % (w/w)).

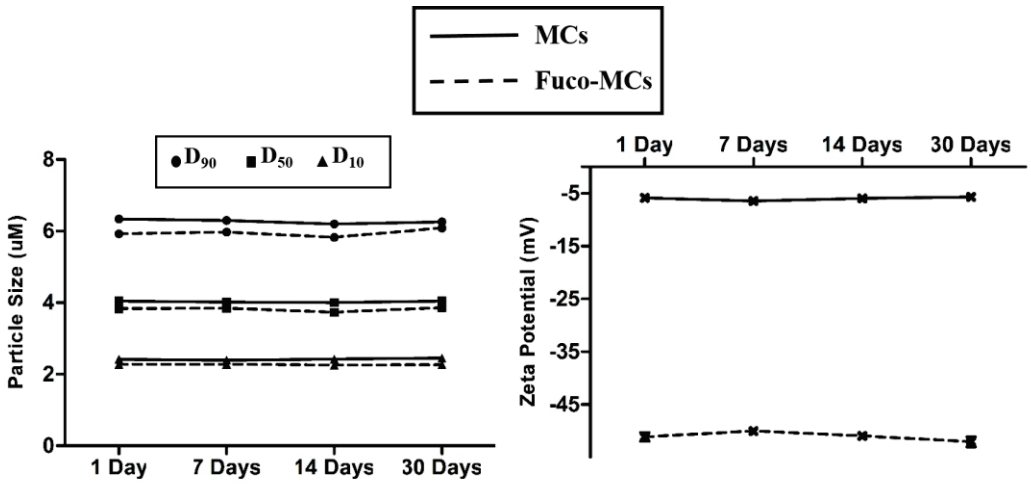

Figure 5. Stability at 4 °C in distilled water of MCs and Fuco-MCs suspensions according to size and zeta potential measurements.

3.2 Static binding on platelets

To evaluate the affinity of MCs and Fuco-MCs for P-selectin expressed onto the surface of human activated platelets, flow cytometry experiments were performed. Interactions were assessed between microcapsules and the three groups respectively composed of: human Plasma-Rich Platelets (PRP), human Plasma-Rich Platelets where platelets were activated with TRAP (PRP+TRAP), and human Plasma-Rich Platelets where platelets were activated with TRAP and P-selectin blocked by a specific blocking antibody (PRP + TRAP + anti-CD62P). As shown on **Figure 6**, non-functionalized microcapsules (MCs) barely or only minimally bound to the three groups of platelets, as shown by low values of the mean fluorescence intensity (MFI) (9.75 ± 2.11; 9.00 ± 0.87; 6.50 ± 1.77, respectively). In contrast, Fuco-MCs exhibited an enhanced binding to activated platelets (MFI = 12 008 ± 2 359) compared to PRP (MFI = 432.4 ± 212.8) or to PRP + TRAP + CD62P (MFI = 1093 ± 419.2).

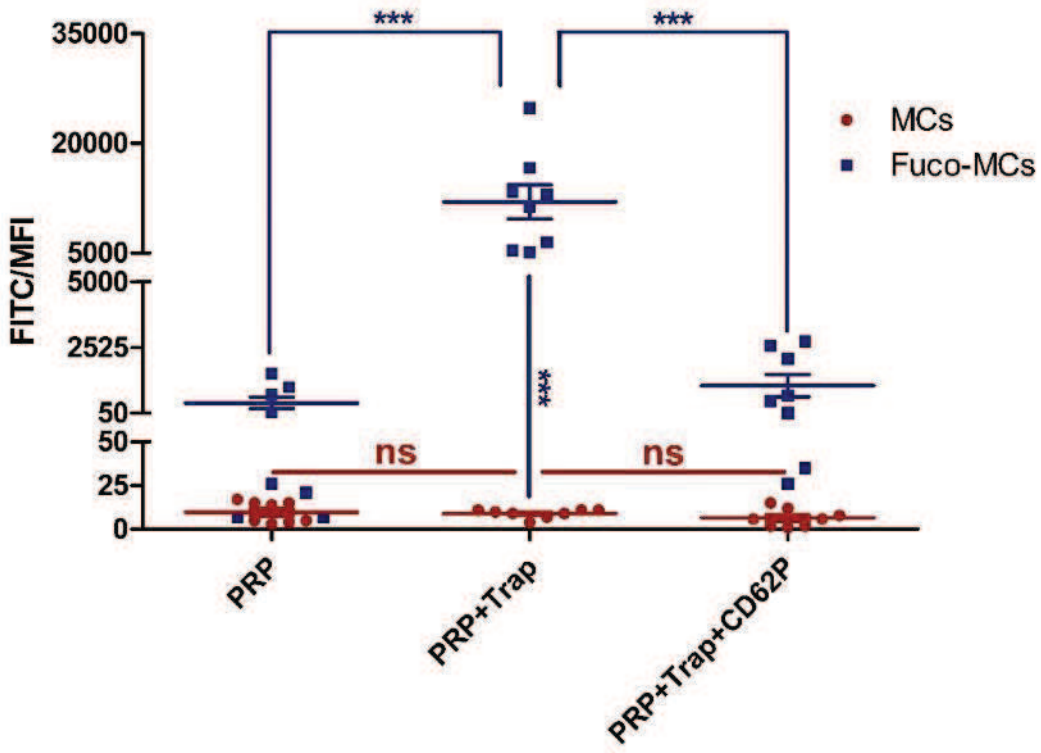

Figure 6. Flow cytometry assessment of interactions of FITC-labeled MCs and FITC-labeled Fuco-MCs with either inactivated platelet-rich plasma (PRP), platelet-rich plasma activated with TRAP (PRP + TRAP) and platelet-rich plasma activated plus P-selectin antibody. The mean fluorescence intensity (MFI) on the FITC channel was measured for 50,000 events of PE-Cy5 labeled platelets, and at a microcapsule concentration of 50 g/L (n=8; ***p<0.001).

3.3 Flow chamber experiments

To evaluate the ability of MCs and Fuco-MCs to target selectins under arterial blood flow conditions, flow chamber experiments with selectins coating were performed. Under arterial blood flow, FITC-Fuco-MCs showed a significantly higher adhesion to P-selectin than FITC-MCs (5565 ± 662 adhered Fuco-MCs versus 482 ± 113 adhered MCs, p<0.001) (**Figures 7 A&D**). Fuco-MCs adhered to the chamber immediately after their injection and remained attached for the whole duration of the experiment. On the contrary, only few MCs were seen to adhere. Washing with NaCl 0.9% at the end of the experiment did not significantly affect the adhesion of both types of microcapsules. The number of adhered Fuco-MCs after 5 min was significantly lower

to E-selectin (854 ± 502) or L-selectin (10 ± 8) than to P-selectin (5565 ± 662) (**Figure 7A**). Adhesion of Fuco-MCs was comparable to that of MCs on E-selectin or L-selectin.

The Fuco-MCs adhesion dependence on P-selectin concentration was investigated (**Figure 7B**). The number of attached Fuco-MCs was normalized over the mean number of attached microcapsules for a P-selectin concentration of 100 µg/mL. Results indicated a dose-dependent relation between the concentration of P-selectin and Fuco-MCs (r2 = 0.965) (**Figure 7B**). The competitive inhibition experiments showed that the injection of a free fucoidan solution (10 mg/ml) before the injection of Fuco-MCs suspension inhibited the binding of Fuco-MCs to P-selectin (486 ± 75 versus 3048 ± 565, respectively, $p<0.05$) (**Figure 7C**).

To mimic the interaction of microcapsules and P-selectin under physiological conditions, human platelets from whole blood were activated and aggregated on collagen at high shear stress (67.5 dyn/cm2). Aggregating platelets were visualized in real time under phase contrast microscopy and expression of P-selectin was evidenced by the green fluorescence uptake after injection of a FITC anti-CD62P antibody through the channel (**Figure 8A**). No signal was detected after injection of the FITC-IgG control (Data not shown). When passed at arterial flow on the platelets aggregates, Fuco-MCs bound to the aggregates and remained attached, whereas MCs showed almost no binding (**Figure 8A**). Quantitative analysis after 5 minutes confirmed that the mean fluorescence intensity of fluorescent microcapsules was significantly higher for Fuco-MCs than for MCs (2275 ± 188 MFI versus 305 ± 69 MFI, respectively, $P<0.001$) (**Figure 8B**).

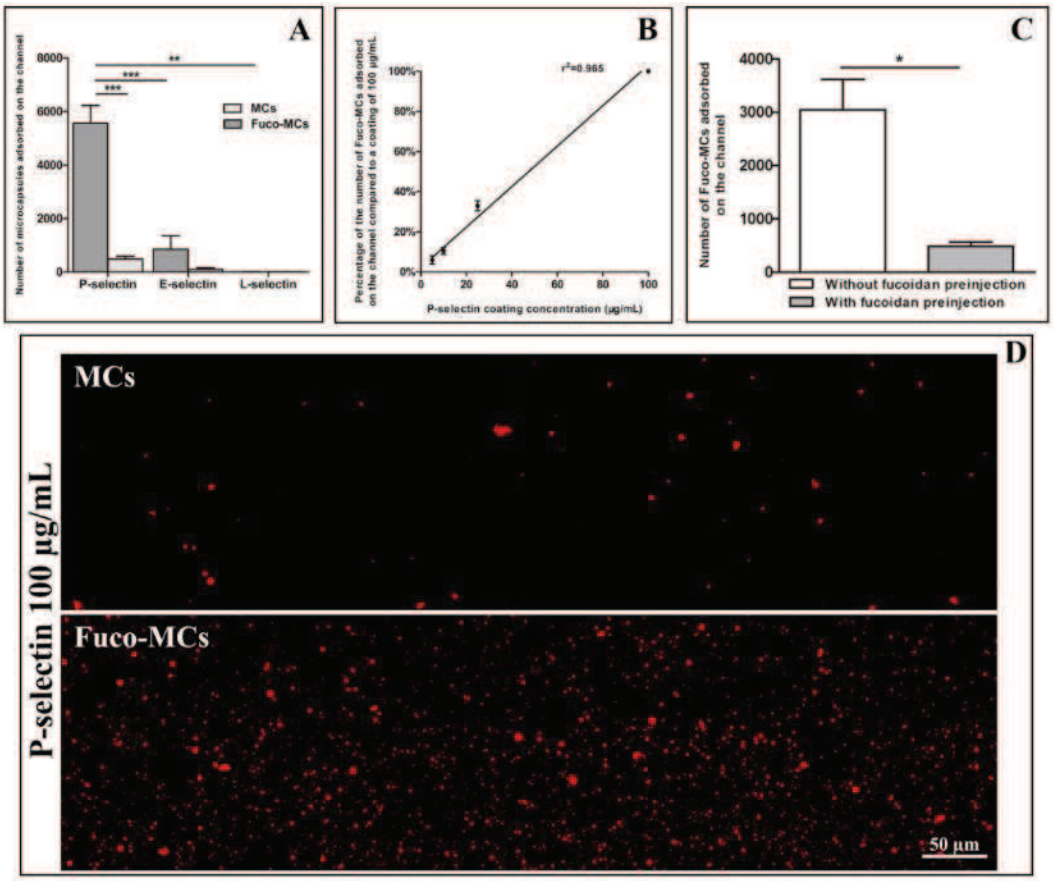

Figure 7. Evaluation of microcapsule interactions with recombinant selectins in an in vitro arterial flow assay. A) Adhesion of microcapsules on selectins. Channels were coated at an E, L, P-selectin concentration of 100 µg/mL. MCs and Fuco-MCs were injected over 5 minutes under arterial flow conditions (shear rate: 1,500 s-1). After 5 minutes, channels were washed with 0.9% NaCl. The number of fluorescent microcapsules attached along each channel was quantified with Histolab (Microvision) (n>3, **p<0.01, ***p<0.001). B) Number of attached microcapsules as a function of the P-selectin concentration from 5 µg/mL to 100 µg/mL. The number of microcapsules was normalized over the average number of microcapsules attached for a P-selectin concentration of 100 µg/mL. C) Fucoidan pre-injection inhibits Fuco-MCs binding. Channels were coated at a P-selectin concentration of 100 µg/mL. After washing with 0.9% NaCl, fucoidan solution (10 mg/ml) was injected or not over 5 min, then microcapsules were injected during 5 minutes. Channels were washed and the number of microcapsules was quantified (*p<0.05). D) Macroscopic view of MCs or Fuco-MCs adhesion over a P-selectin coating of 100 µg/mL. (n=10 for MCs and n=11 for Fuco-MCs; Scale bar = 50 µm).

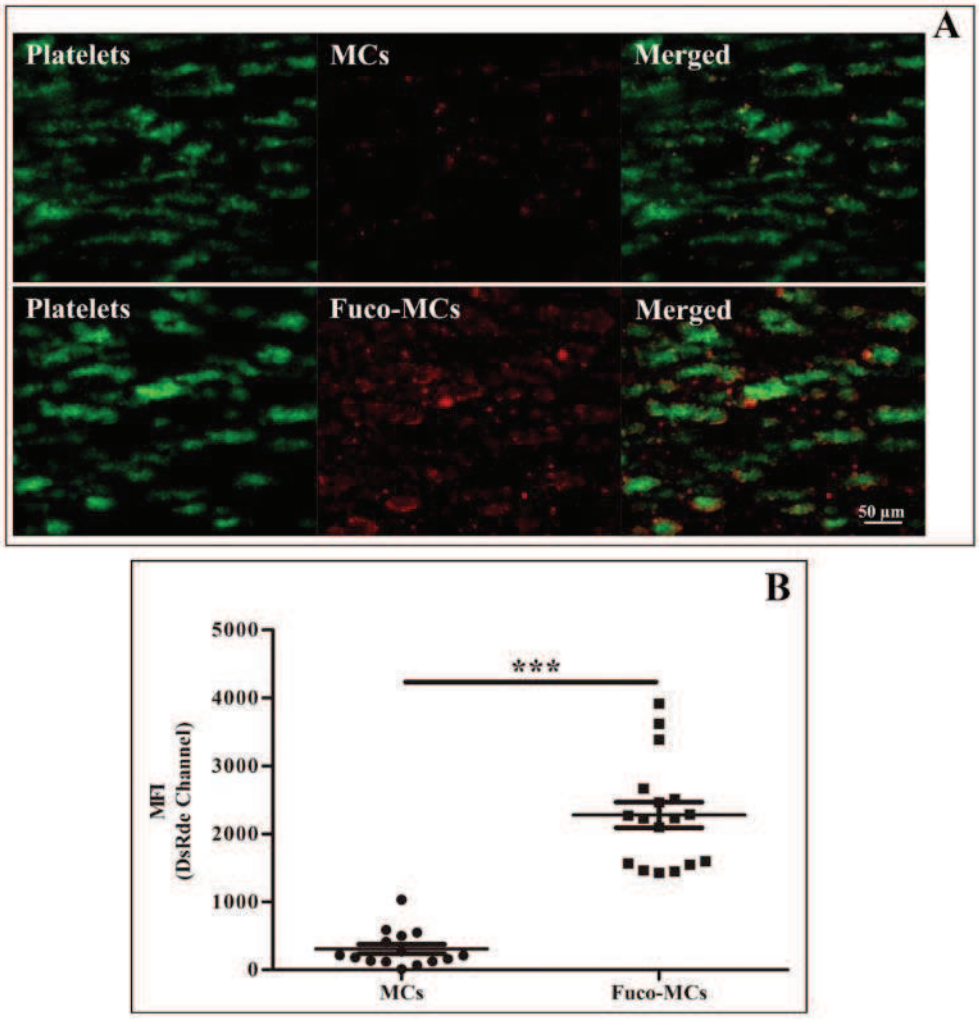

Figure 8. Microcapsule adhesion over platelet aggregates. A) Whole blood labeled with Dioc6 was injected onto channels coated with collagen at 50 µg/mL. Under arterial flow conditions, platelets adhered onto the channel wall forming aggregates expressing P-selectin (Left) and FITC-MCs or FITC-Fuco-MCs were then injected for 5 minutes (Middle panel). Channels were washed with 0.9% NaCl. Microcapsules and aggregates co-localization was assessed by merged fluorescence microscopy (Right). B) Quantitative analysis of the mean fluorescence intensity of platelet aggregates (n=15 for MCs and n=17 for Fuco-MCs; ***p<0.001).

3.4 Cell viability

The cytotoxicity of microcapsules was evaluated by MTT assay. As shown in **Figure 9**, the results demonstrated that MCs and Fuco-MCs did not significantly affect the mean viability of mouse fibroblasts 3T3 cells at concentrations of 0.625, 1.25, 2.5 and 5 g/L, there were no obvious difference between MCs and Fuco-MCs.

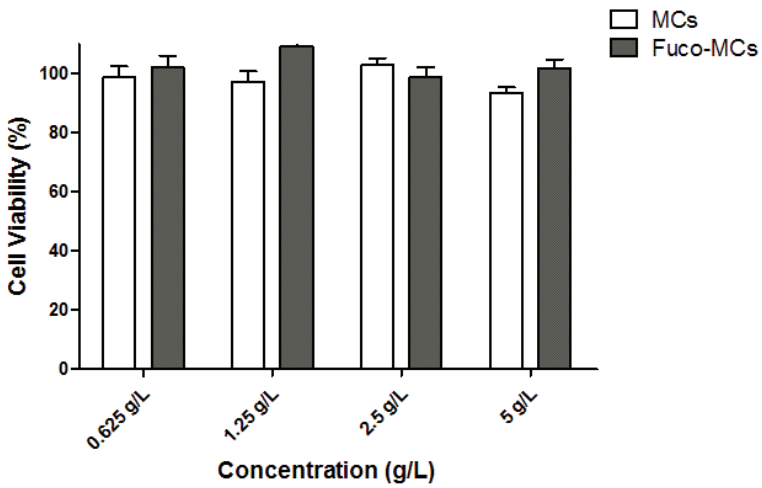

Figure 9. MTT assay performed on 3T3 cells after 24 h of incubation in the presence of MCs and Fuco-MCs at different concentrations. (n=6).

3.5 Localization of microcapsules within the thrombotic Abdominal Aortic Aneurysm wall of rats and biodistribution

To assess whether Fuco-MCs accumulated *in vivo* within an AAA, histological staining of both AAA and healthy aorta samples were performed 1 hour after the injection of FITC-MCs and FITC-Fuco-MCs. On histological stained sections, smooth muscle cells from connective tissues and several layers of the aneurysmal wall were distinguished (**Figure 10A**). Many Fuco-MCs (red spheres) were localized in the arterial wall, between the thrombus and the media layer compared to MCs (**Figure 10A**). On the other hand, only few Fuco-MCs were found in arterial wall of healthy rats (**Figure 10A**). Semi-quantitative analysis confirmed that the fluorescence in the AAA wall was higher for Fuco-MCs than for MCs, and the binding of Fuco-MCs or MCs in healthy aorta was low (**Figure 10B**).

Biodistribution of MCs and Fuco-MCs in four organs (liver, spleen, lungs and kidneys) was performed at 1 hour and 24 hours after injection. Both types of microcapsules were present in the four organs at the same range at 1 hour, while they were eliminated during 24 hours.

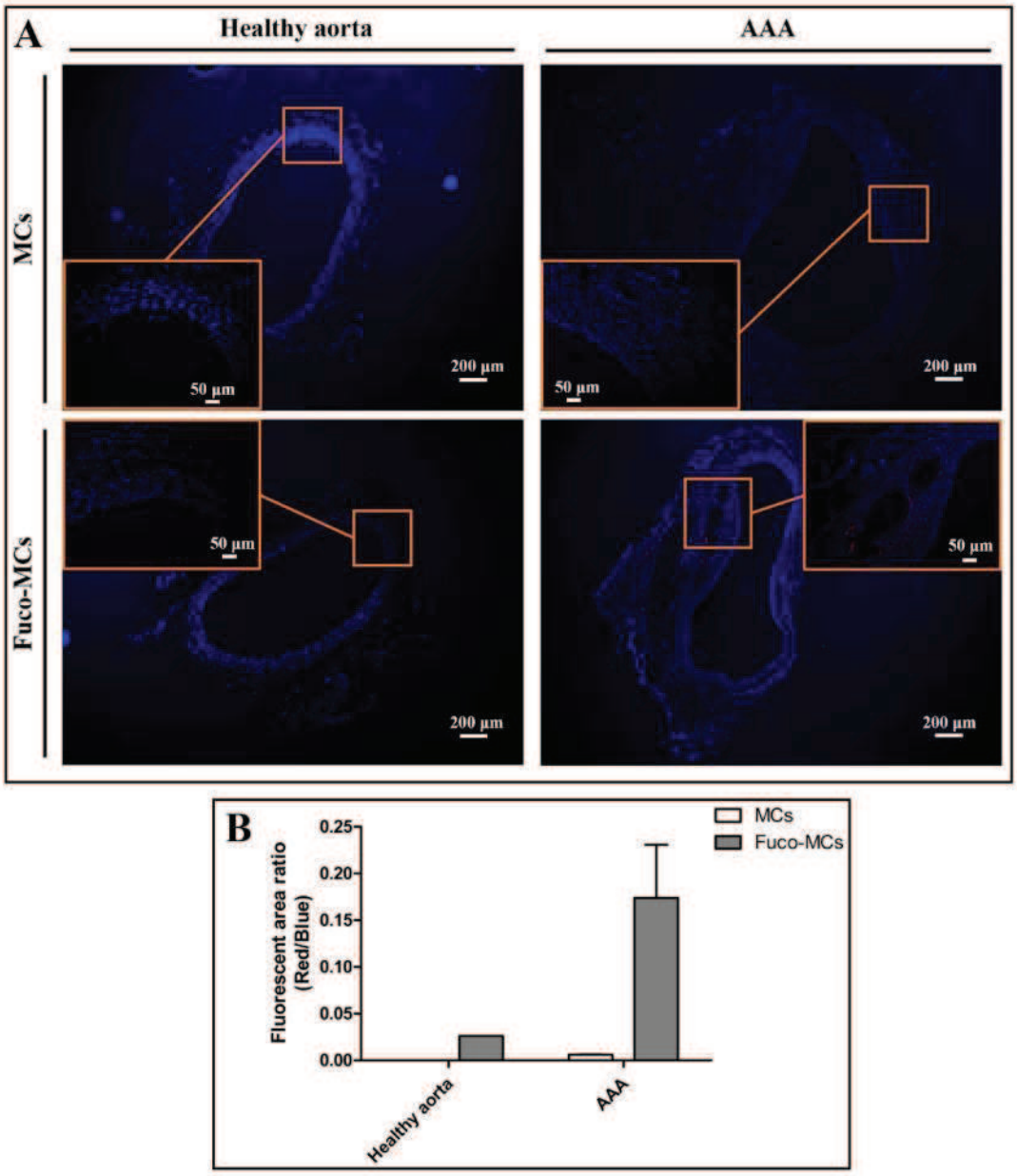

Figure 10. Histological analysis of abdominal aorta sections (**A**). Healthy rats (left) and rat Abdominal Aorta Aneurysms (right). Inserts are magnification of Regions of Interest. Muscle cells appear in blue fluorescence and MCs or Fuco-MCs appear in red. Semi-quantitative analysis of histological sections (**B**). Data are expressed as the proportion of red fluorescent area to blue fluorescent area (x20) on healthy rats or rats with AAA injected with MCs or Fuco-MCs.

4. Discussion

In this study, injectable core-shell polymer microcapsules functionalized with fucoidan were developed as a carrier tool to target P-selectin overexpressed in cardiovascular diseases.

Nanoparticle made of PACA and coated with polysaccharides are promising substrates because of their biodegradability and biocompatibility.[10, 27] We developed here microcapsules composed of a lipophilic liquid core and a PIBCA-polysaccharide mixed membrane. This microcapsule structure was prepared by a new emulsion-evaporation polymerization process performed either in neutral or alkaline conditions. Using this method, the rate of polymerization was controlled by the evaporation rate. This technique allowed for the first time the polymerization of IBCA in emulsion under neutral and alkaline conditions leading to reproducible polymer microcapsules that can be functionalized with polysaccharides such as fucoidan.

Two key conditions must be fulfilled to form stable core-shell microcapsules. First, the water phase should contain water-soluble colloidal stabilizers, such as polysaccharides, that make microcapsules more hydrophilic and helps in avoiding particle aggregation. Second, the pH of the polymerization medium should be well controlled. Acidic condition reduced the initial polymerization rate resulting in insufficient polymer film thickness which did not provide enough surface tension to make droplets. Under neutral or alkaline conditions, the hydroxyl ions in the solution could accelerate the polymerization reaction to form stable shell encapsulating an hydrophobic agent.

For the use as drug carriers, the shell thickness-to-radius ratio (T/R) strongly influenced the embedded drug release behavior. Jiao *et al.* showed that the amount and rate of doxorubicin released in hollow mesoporous silica nanoparticles exhibited shell thickness dependence, decreasing with the increase of the shell thickness.[28] Furthermore, comparing this to undesired burst effect, drug controlled release

prolongs the time of drug action.[29] Interestingly, we found that the polymer thickness could be easily modified from 330 nm to 770 nm depending on the pH of the polymerization medium. This property could be optimized for controlled drug release. In this study, PFOB was used as a reference agent. The theranostic potential of these microcapsules will be investigated in the near future.

As previous studies, we found that Fuco-MCs shown low value of zeta potential compare to MCs. Flow cytometry experiments demonstrated that microcapsules were functionalized by fucoidan. Although the weight content of fucoidan in microcapsules was very low, it was stable at least for one month without obvious release. SEM and TEM analysis along with size measurements showed that the functionalization of microcapsules with fucoidan did not affect the spherical shape or the diameter distribution. Charoenphol *et al.* indicated that spheres exhibiting a diameter of 2.5 μm are optimal for targeting purposes in medium to large vessel walls, which are affected in numerous cardiovascular diseases.[3, 30] The size of our microcapsules from 2.2 μm to 5.8 μm appeared therefore adapted for vascular targeting purposes.

Cell viability assay is a powerful toll in providing valuable information regarding the safety of biomaterials. In this study, the *in vitro* cytotoxicity of microcapsules was evaluated by a colorimetric MTT assay on reference 3T3 cells. Results indicated that both types of microcapsules did not present obvious detrimental effects on 3T3 cells proliferation even at high concentration. Moreover, there was no significant difference between MCs and Fuco-MCs, as both of them had no cytotoxicity and good biocompatibility.

Using flow cytometry, we evidenced that the Fuco-MCs exhibited a stronger affinity for human activated platelets than MCs and that this binding could be inhibited by a P-selectin antibody. Similar results had been published by Bonnard T. *et al.* using fucoidan functionalized polysaccharide microparticles.[31]

Up to now, the design of carrier systems targeting specific molecules and able to bind

them under high velocity blood flow conditions remains a challenge. In this study, an *in vitro* flow adhesion assay onto recombinant selectins confirmed that fucoidan functionalized microcapsules/Fuco-MCs rapidly and specifically bound to P-selectin compared to MCs even under high shear rate conditions (1,500 s^{-1}). Moreover, the number of attached Fuco-MCs was dependent on P-selectin concentration and free fucoidan in solution inhibited the binding of Fuco-MCs to P-selectin. Previous reports indicated that the sulfate ester groups of fucoidan could be recognized by P-selectin and L-selectin,[32] but not by E-selectin.[33] Our results indicated that Fuco-MCs could bind P-selectin but not L-/E-selectins. Moreover, Fuco-MCs revealed a higher ability as compared to MCs to adhere to the surface of activated platelet aggregates under arterial flow conditions. The interaction between the fucoidan coated onto microcapsules and the P-selectin was strong enough to overcome kinetic energy of microcapsules even with their high density (close to 1.3 g/mL) that comes from the presence of liquid PFOB into their core.

Histological and semi-quantitative analysis revealed that Fuco-MCs were localized inside the media layer of the thrombotic AAA wall in rats, whereas very low binding was observed on AAA injected with MCs or on the artery wall of healthy rats injected with Fuco-MCs. Biodistribution studies showed that both types of microcapsules were present in the Mononuclear Phagocyte System (MPS), which is consistent with what is described in the literature, that they were rapidly eliminated during 24 hours and that had no adverse effect on the health of rats. In fact, the rats used in experiment were still alive after a few months. Since microcapsules functionalized with fucoidan accumulated in the inner wall of the AAA, a promising strategy to treat AAA could be to inhibit the proteolytic activity which occurs within the medial layer and leads to the arterial wall degradation.[34] The ability of Fuco-MCs to target the AAA could be associated with the loading of a proteolytic inhibitor in this microcarrier. *In vitro* experiments also indicated that the loading of microcapsules with PFOB allowed ultrasound imaging. Such microcapsules loaded with drugs and functionalized with fucoidan appear therefore as promising molecular theranostic systems.

5. Conclusions

Microcapsules functionalized with fucoidan were developed here for the targeting activated platelets in thrombotic abdominal aorta aneurysm using biodegradable and biocompatible polymer membrane composed of poly(isobutyl cyanoacrylate) and polysaccharides. In this work, we described their elaboration with a new alkaline solvent emulsion-evaporation polymerization process and we confirmed their hydrodynamic diameter distribution, the microcapsule structure and the presence of the targeting agent, fucoidan, at the surface. This work gave the first evidence that functionalized microcapsules can be obtained according to an easy one-step polymerization process of isobutyl cyanoacrylate in neutral and alkaline conditions. *In vitro* cytotoxicity assay showed that the microcapsules exhibited excellent compatibility with cells *in vitro*. Subsequently, we demonstrated *in vitro* by flow cytometry that these fucoidan functionalized microcapsules could specifically bind to the P-selectin expressed by human activated platelets. Flow chamber experiments further confirmed that Fuco-MCs bind to P-selectin and to activated platelet aggregates even at high shear rate. Finally, we showed *in vivo* on rats the ability of Fuco-MCs to bind to thrombotic AAA and evidenced their presence in the AAA wall by histology. We also evidenced that both types of microcapsules were eliminated through liver metabolism function. Future works are required to study the loading of contrast agents or therapeutics to achieve molecular diagnosis and/or treatment of cardiovascular pathologies overexpressing P-selectin.

References

[1] S. Yokoyama, H. Ikeda, N. Haramaki, H. Yasukawa, T. Murohara, T. Imaizumi, *J. Am. Coll. Cardiol.* **2005**, 45, 1280; K. K. Hannawa, B. S. Cho, I. Sinha, K. J. Roelofs, D. D. Myers, T. J. Wakefield, J. C. Stanley, P. K. Henke, G. R. Upchurch, Jr., *Ann. N. Y. Acad. Sci.* **2006**, 1085, 353.

[2] P. A. Barber, T. Foniok, D. Kirk, A. M. Buchan, S. Laurent, S. Boutry, R. N. Muller, L. Hoyte, B. Tomanek, U. I. Tuor, *Ann. Neurol.* **2004**, 56, 116; F. S. Villanueva, E. Lu, S. Bowry, S. Kilic, E. Tom, J. Wang, J. Gretton, J. J. Pacella, W. R. Wagner, *Circulation* **2007**, 115, 345; M. A. McAteer, J. E. Schneider, Z. A. Ali, N. Warrick, C. A. Bursill, C. von zur Muhlen, D. R. Greaves, S. Neubauer, K. M. Channon, R. P. Choudhury, *Arterioscler Thromb Vasc Biol* **2008**, 28, 77; B. A. Kaufmann, C. Lewis, A. Xie, A. Mirza-Mohd, J. R. Lindner, *European heart journal* **2007**; R. Haverslag, G. Pasterkamp, I. E. Hoefer, *Cardiovascular & Haematological Disorders-Drug Targets* **2008**, 8, 252.

[3] P. Charoenphol, S. Mocherla, D. Bouis, K. Namdee, D. J. Pinsky, O. Eniola-Adefeso, *Atherosclerosis* **2011**, 217, 364.

[4] P. Saboural, F. Chaubet, F. Rouzet, F. Al-Shoukr, R. B. Azzouna, N. Bouchemal, L. Picton, L. Louedec, M. Maire, L. Rolland, G. Potier, D. L. Guludec, D. Letourneur, C. Chauvierre, *Mar. Drugs* **2014**, 12, 4851.

[5] F. Rouzet, L. Bachelet-Violette, J. M. Alsac, M. Suzuki, A. Meulemans, L. Louedec, A. Petiet, M. Jandrot-Perrus, F. Chaubet, J. B. Michel, D. Le Guludec, D. Letourneur, *J Nucl Med* **2011**, 52, 1433.

[6] T. Bonnard, J. M. Serfaty, C. Journe, B. Ho Tin Noe, D. Arnaud, L. Louedec, S. M. Derkaoui, D. Letourneur, C. Chauvierre, C. Le Visage, *Acta Biomater.* **2014**, 10, 3535; L. Bachelet-Violette, A. K. A. Silva, M. Maire, A. Michel, O. Brinza, P. Ou, V. Ollivier, A. Nicoletti, C. Wilhelm, D. Letourneur, C. Menager, F. Chaubet, *RSC Advances* **2014**, 4, 4864; M. Suzuki, L. Bachelet-Violette, F. Rouzet, A. Beilvert, G. Autret, M. Maire, C. Menager, L. Louedec, C. Choqueux, P. Saboural, O. Haddad, C. Chauvierre, F. Chaubet, J. B. Michel, J. M. Serfaty, D. Letourneur, *Nanomedicine (Lond)* **2014**, 1.

[7] P. Couvreur, B. Kante, M. Roland, P. Guiot, P. Bauduin, P. Speiser, *J. Pharm. Pharmacol.* **1979**, 31, 331.

[8] I. Bertholon, S. Lesieur, D. Labarre, M. Besnard, C. Vauthier, *Macromolecules* **2006**, 39, 3559.

[9] C. Chauvierre, D. Labarre, P. Couvreur, C. Vauthier, *Macromolecules* **2003**, 36, 6018.

[10] C. Chauvierre, D. Labarre, P. Couvreur, C. Vauthier, *Pharmaceutical Research* **2003**, 20, 1786.

[11] K. Langer, E. Seegmüller, A. Zimmer, J. Kreuter, *Int. J. Pharm.* **1994**, 110, 21.

[12] C. Chauvierre, L. Leclerc, D. Labarre, M. Appel, M. C. Marden, P. Couvreur, C. Vauthier, *Int. J. Pharm.* **2007**, 338, 327.

[13] G. Lambert, E. Fattal, H. Pinto-Alphandary, A. Gulik, P. Couvreur, *Pharm Res* **2000**, 17, 707.

[14] G. Yordanov, *Bulgarian Journal of Chemistry* **2012**, 1.

[15] M. Bagad, Z. A. Khan, *Int J Nanomedicine* **2015**, 10, 3921.

[16] C. Vauthier, C. Dubernet, C. Chauvierre, I. Brigger, P. Couvreur, *J Control Release* **2003**, 93, 151.

[17] K. O. Kisich, S. Gelperina, M. P. Higgins, S. Wilson, E. Shipulo, E. Oganesyan, L. Heifets, *Int. J. Pharm.* **2007**, 345, 154; C. E. Soma, C. Dubernet, D. Bentolila, S. Benita, P. Couvreur, *Biomaterials* **2000**, 21, 1.

[18] C. Chauvierre, M. C. Marden, C. Vauthier, D. Labarre, P. Couvreur, L. Leclerc, *Biomaterials* **2004**, 25, 3081.

[19] M. Liang, N. M. Davies, I. Toth, *Int. J. Pharm.* **2008**, 362, 141.

[20] G. Lambert, *Journal of Dispersion Science and Technology* **2003**, 24, 439.

[21] G. Yordanov, C. Dushkin, *Colloid and Polymer Science* **2010**, 288, 1019; G. Yordanov, R. Skrobanska, A. Evangelatov, *Colloids Surf. B. Biointerfaces* **2012**, 92, 98; G. Yordanov, A. Evangelatov, R. Skrobanska, *Colloids Surf. B. Biointerfaces* **2013**, 107, 115; G. Yordanov, R. Skrobanska, A. Evangelatov, *Colloids Surf. B. Biointerfaces* **2013**, 101, 215; A. Evangelatov, R. Skrobanska, N. Mladenov, M. Petkova, G. Yordanov, R. Pankov, *Drug Deliv.* **2015**, 1.

[22] E. Pisani, N. Tsapis, J. Paris, V. Nicolas, L. Cattel, E. Fattal, *Langmuir* **2006**, 22, 4397.

[23] L. Gustafsson, *Talanta* **1960**, 4, 227.

[24] S. Delbosc, J. M. Alsac, C. Journe, L. Louedec, Y. Castier, M. Bonnaure-Mallet, R. Ruimy, P. Rossignol, P. Bouchard, J. B. Michel, O. Meilhac, *PLoS One* **2011**, 6, e18679.

[25] S. Li, Y. He, C. Li, X. Liu, *Colloid and Polymer Science* **2005**, 283, 480.

[26] M. C. B. Lira, N. S. Santos-Magalhães, V. Nicolas, V. Marsaud, M. P. C. Silva, G. Ponchel, C. Vauthier, *European Journal of Pharmaceutics and Biopharmaceutics* **2011**, 79, 162.

[27] C. Vauthier, C. Dubernet, E. Fattal, H. Pinto-Alphandary, P. Couvreur, *Adv Drug Deliv Rev* **2003**, 55, 519.

[28] Y. Jiao, J. Guo, S. Shen, B. Chang, Y. Zhang, X. Jiang, W. Yang, *Journal of Materials Chemistry* **2012**, 22, 17636.

[29] J. M. Chan, L. Zhang, R. Tong, D. Ghosh, W. Gao, G. Liao, K. P. Yuet, D. Gray, J.-W. Rhee, J. Cheng, G. Golomb, P. Libby, R. Langer, O. C. Farokhzad, *Proceedings of the National Academy of Sciences* **2010**, 107, 2213.

[30] P. Charoenphol, R. B. Huang, O. Eniola-Adefeso, *Biomaterials* **2010**, 31, 1392.

[31] T. Bonnard, G. Yang, A. Petiet, V. Ollivier, O. Haddad, D. Arnaud, L. Louedec, L. Bachelet-Violette, S. M. Derkaoui, D. Letourneur, C. Chauvierre, C. Le Visage, *Theranostics* **2014**, 4, 592.

[32] H. Thorlacius, B. Vollmar, U. T. Seyfert, D. Vestweber, M. D. Menger, *Eur J Clin Invest* **2000**, 30, 804.

[33] C. Foxall, S. R. Watson, D. Dowbenko, C. Fennie, L. A. Lasky, M. Kiso, A. Hasegawa, D. Asa, B. K. Brandley, *J. Cell Biol.* **1992**, 117, 895; A. K. Silva, D. Letourneur, C. Chauvierre, *Theranostics* **2014**, 4, 579.

[34] A. Klink, F. Hyafil, J. Rudd, P. Faries, V. Fuster, Z. Mallat, O. Meilhac, W. J. Mulder, J. B. Michel, F. Ramirez, G. Storm, R. Thompson, I. C. Turnbull, J. Egido, J. L. Martin-Ventura, C. Zaragoza, D. Letourneur, Z. A. Fayad, *Nat Rev Cardiol* **2011**, 8, 338.

CHAPTER III

Polysaccharide decorated Poly (isobutyl cyanoacrylate) microbubbles as potential targeted ultrasound contrast agents

ABSTRACT

Targeted ultrasound contrast agents offer new opportunities to enhance the capabilities of diagnostic ultrasound imaging to detect cardiovascular pathological changes. In this work, a variety of polysaccharide decorated microbubbles consisting of poly (isobutyl cyanoacrylate) shells and air core were fabricated by anionic polymerization method. Several investigations were carried out to determine morphology, size distribution and zeta potential of microbubbles. In addition, the presence of dextran and fucoidan in the microbubbles shell were observed by fluorescence microscopy, and the content of fucoidan in microbubbles were analyzed by methylene blue methods. These microbubbles revealed strong echogenicity in flow conditions and could be destroyed by high ultrasound energies. Furthermore, the fucoidan conjugated microbubbles (Fuco-MBs) showed strong affinity to the surface of white thrombi *in vitro*. The results demonstrated the properties of Fuco-MBs as a molecular ultrasound diagnostic tool for the characterization of arterial diseases expressing P-selectin.

Graphical Abstract

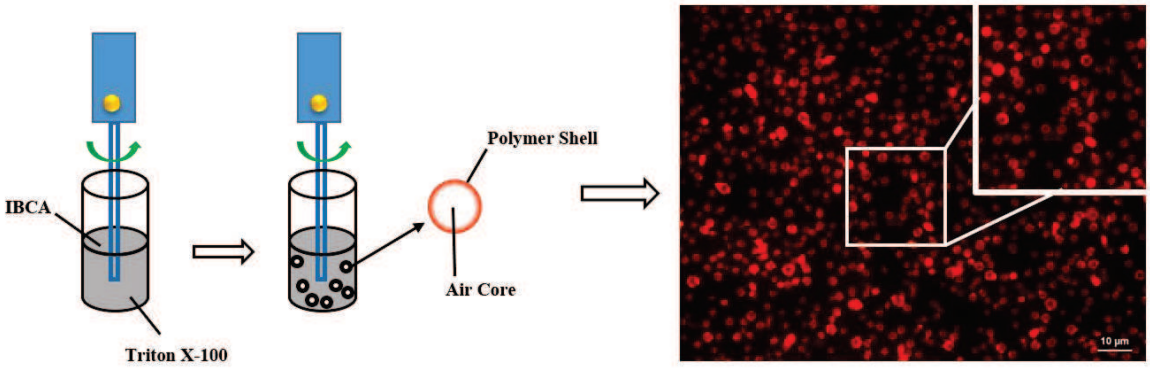

1. Introduction

Ultrasound molecular imaging has been a powerful tool for non-invasive visualization

for the expression of vascular markers during inflammation and physiological process.[1] Air-filled microbubbles (MBs), as one of the most important contrast agents for ultrasound imaging, can help to display diseased locations by specifically binding to activation of functional biomolecules.[2] However, the application of the traditional microbubbles has bound by their inherent defects: instability. To address this problem, many authors have shown interest in development nano-/microcapsules with a single core of liquid perfluorocarbons within a polymer shell.[3] But, as a counterbalance, they exhibit low inherent echogenicity and poor blood contrast under conditions of conventional echocardiography or harmonic imaging.[4] Recently, polymer-based hard-shell microbubbles have become a research hotspot due to their higher stability and enhanced acoustic properties. They succeed the advantages of these two above-mentioned contrast agents and overcome their disadvantages.

Poly (alkyl cyanoacrylate) (PACA) is considered to build contrast agents since it is biomedical materials and widely used for skin adhesives, surgical glues and embolitic materials.[5] Poly (butyl cyanoacrylate) (PBCA)-based microbubbles (PBCA-MBs) have been developed and they exhibit prolonged circulation by reducing the gas-core shrinkage.[6, 7] The potential application of PBCA-MBs is limited by their rather hydrophobic surface and insufficient functional chemical groups in the polymer backbone. Only Few targeting ligands, e.g. short peptide, antibody are combined with PBCA-MBs by hydrolyzing PBCA to produce -COOH group and this approach was quite inefficient and time-consuming.[8, 9]

In this work, poly (isobutyl cyanoacrylate) PIBCA replaced PBCA to formulate microbubbles using the similar method. Moreover, we present here an easy method to modify the surface of PIBCA-MBs by various polysaccharides to prevents opsonization by steric repulsion of blood proteins and to increase the half-life of

microbubbles in plasma.[10] Microbubbles obtained with polysaccharides were incorporated directly in the aqueous phase before forming the microbubbles. Several polysaccharides were reviewed: dextran, CM-dextran, DEAE-dextran and fucoidan. Among them, fucoidan, a type of sulfate and fucosylated polysaccharide, exhibiting *in vitro* a high affinity for immobilized P-selectin and the low nonspecific binding,[11] are considered in detail. We demonstrated that fucoidan was successfully immobilized on the shell of microbubbles. These microbubbles could have clinical uses as an echography diagnostic tool for arterial diseases characterized by the expression of P-selectin.

2. Materials and methods

Materials

Nile Red was provided by Sigma Aldrich (Saint Quantin Fallavier, France). Dextran 20, Dextran 40, FITC-Dextran 40, CM-Dextran 40 and DEAE-Dextran 70 were obtained from TdB Consultancy (Uppsala, Sweden). Fucoidan was a gift from Algues & Mer (Ouessant, France). Isobutyl cyanoacrylate (IBCA) was provided by ORAPI (Saint Vulbas, France).

PIBCA microbubbles functionalized with various polysaccharides

PIBCA air-filled MB were synthesized by a modification of the previously described methods. [7, 8] In brief, 1 mL of IBCA was added to a 60-mL aqueous solution containing 1% triton X-100 and 10% desired polysaccharide at pH 2.5 and stirred vigorously (20,000 rpm) using an Ultra-Turrax for 60 minutes. For fluorescent microscopy studies, 1 mL (1 mg/ml) of Rhodamine B, 1% FTIC-Dextran 20 or 1% FITC-Fucoidan were added to aqueous phase before emulsification, respectively.

Size and zeta potential microbubbles determination

The size distribution of microbubbles was quantitatively obtained using a laser

dynamic scattering particle size-measuring instrument (Mastersizer 3000, Malvern Instruments, Orsay, France).

Zeta potential (ζ) of the microbubbles was measured at 25ºC using quasi-elastic light scattering apparatus (Nano ZS, Malvern Instruments, Orsay, France). Samples were diluted in 1 mM KCl.

All the measurements were performed in triplicate and the results were expressed as mean ± standard deviation.

Scanning Electron Microscopy (SEM)

The surface morphology of microbubbles was imaged using a Scanning Electron Microscopy apparatus (Philips XL 30 ESEM-FEG, Amsterdam, Netherlands) on dried samples coated with a thin gold layer.

Determination of fucoidan in microbubbles by methylene blue

The content of fucoidan in microbubbles was prepared by modifying with dye extraction from stained spot methylene blue-fucoidan complex.[12] Briefly, MBs are hydrolyzed by NaOH, which dropwise and cautiously added on the center of 1×1 cm square chromatography papers, 4 µL of each drop, the next portions were dropped on the same point after drying off the last drop by fan. Finally, the paper with loaded fucoidan drops was dried using the fan, then was treated in mixture of methanol and acetone (6:4) for 3 min. Fucoidan spots on filter paper were visualized after 10 min at room temperature in staining solution containing 50 mM HCl in mixture of methanol/acetone/water (6:4:15). The excess of MB was removed by repeated washing of filter paper with mixed solution containing 5 % acetic acid, 6 % methanol, and 4 % acetone until an appropriate detained background appeared. Filter paper squares were put into 1.5 ml Eppendorf centrifuge tubes with 0.5 ml of 70% methanol containing 2% SDS during 15 min at 50°C. Of this extract, 0.2 ml was transferred into 96-wells plate and absorbance was determined at 663 nm by means of infinite® 200

PRO (TECAN, Switzerland), standard curve was obtained by fucoidan standard solution.

Acoustical characterization of microbubbles

Echocardiographic properties of contrast agent were measured using a high-resolution echocardiography system (Vevo 2100, VisualSonics, Toronto, ON, Canada) equipped with a non-linear probe (MS-200S, 18 MHz). Briefly, 1 ml of 10^7 MBs or MBs-FUCO were injected into flexible plastic tubes, 1.7 mm in diameter, which is similar in size to rat's artery, the peristaltic pump allows the microbubble suspension to circulate throughout the tubes. B-mode movies were acquired for each sample. Destruction of microbubbles were performed in a linear contrast model with a high frequency probe (MS-550D, 40 MHz), 100 µl of 10^6 MB was injected into a gel or under skin of rat, a frame obtained from before and after undergoing the high mechanical index (mechanical index, 1.0; duration, 1 second).

In vitro white thrombus preparation

Whole blood samples (5 mL) from healthy adult volunteers were collected in sodium citrate 3.8% (w/v). White thrombi were prepared using platelet-rich plasma (PRP, 1 mL), which was obtained from centrifuged blood, and mixed with 2 µL of Trap (10 mM), 2 µL of $CaCl_2$ (80 mmol/L) and these solution were incubated at 37℃ for 30 min to form thrombi.

Molecular imaging of thrombus in vitro

White thrombi were washed by saline flushing and then incubated *in vitro* in a 1 mL suspension of 10^6 MBs and a washing step in saline was performed as described previously. Afterwards, thrombi were then imaged in saline at room temperature with contrast imaging mode using a linear transducer (MS-550D, 40 MHz). The thrombi were then insonated with the high MI (Mechanical Index) of ultrasound beam for 1 second to destroy all attached MBs. Another image was taken of the thrombi directly after bubble destruction.

3. Results and Discussion

The aim of this study was to modify the surface of PIBCA microbubbles with various polysaccharides leading to obtaining potential targeting microbubbles. We combined the preparation method of plain PIBCA microbubbles and the surface modification method tested for PIBCA nanoparticles. The size and surface charge were investigated. Particularly, the morphology, echogenicity and targeting efficiency were studied in order to assess its application potential as a targeting contrast agent for echography.

3.1 Preparation and characterization of microbubbles

The MBs size distribution was measured as a function of the various polysaccharide added in the aqueous phase (**Table 1**). After preparation, the size distribution of MBs slightly changed with diverse polysaccharides. Results indicated that the mean size of MBs also increased with increasing of the molecular weight of polysaccharide.

Table 1. Size distribution of microbubbles by modification surface with polysaccharide.

	D_{10} (µm)	D_{50} (µm)	D_{90} (µm)
Non-functionalized (MBs)	1.98±0.01	2.86±0.01	4.00±0.03
Functionalized with Dextran 20 (Dex 20-MBs)	1.78±0.01	2.69±0.01	3.98±0.06
Functionalized with Dextran 40 (Dex 40-MBs)	2.14±0.01	3.04±0.02	4.33±0.08
Functionalized with DEAE-Dextran 70 (DEAE-Dex 70-MBs)	2.41±0.01	3.53±0.01	5.16±0.02
Functionalized with CM-Dextran 40 (CM-Dex 40-MBs)	2.23±0.02	3.30±0.01	4.97±0.03
Functionalized with Fucoidan (Fuco-MBs)	2.23±0.01	3.25±0.03	4.87±0.16

Zeta potential of the MBs are given in **Figure 1**. Negatively charged polysaccharides (CM-dextran and fucoidan) lead to MBs with a highly negative zeta potential (– 28 mV and – 34 mV, respectively), the fucoidan seemly induce more negative zeta potential, the reason may be the negatively charged group of fucoidan largely extend on the MBs' surface due to fucoidan's high molecular weight compared to CM-dextran (around 110 KDa and 40 KDa, respectively). In contrast, MBs prepared with positively charged polysaccharides, DEAE-dextran, showed a highly positive zeta potential (+ 45 mV). Moreover, MBs prepared with dextran (neutral polysaccharide) 20 kDa or 40 kDa showed the similar zeta potential to MBs without polysaccharide (–13 mV, –17 mV and –15 mV, respectively). These results showed that the zeta potential of MBs prepared with different polysaccharides clearly depended on the charge of the polysaccharide used. The results confirm that the polysaccharide was more likely to be located at the nanoparticle surface.

To further visualize the dextran or fucoidan in MBs, a portion of dextran or fucoidan (1% w/w) was substituted during the emulsion process by FITC-dextran or FITC-fucoidan, respectively. Fluorescent MBs suspensions were observed by microscopy (**Figure 2**). The core–shell structure of the microbubbles was perfectly visible; the core composed of air appeared in dark and the shell was well defined and appeared in green color. Similar to the polysaccharide coated PIBCA microcapsules (see Experiment PART II), the fluorescence seems to be homogenous across the shell thickness. The surface morphology of these MBs could be examined by scanning electron microscopy (SEM). Both of them showed rounded and rough bubble surface, a few collapsed of cavities within the spherical particles (**Figure 3, white rectangle**). No obvious difference is found between the Dex-MBs and Fuco-MBs.

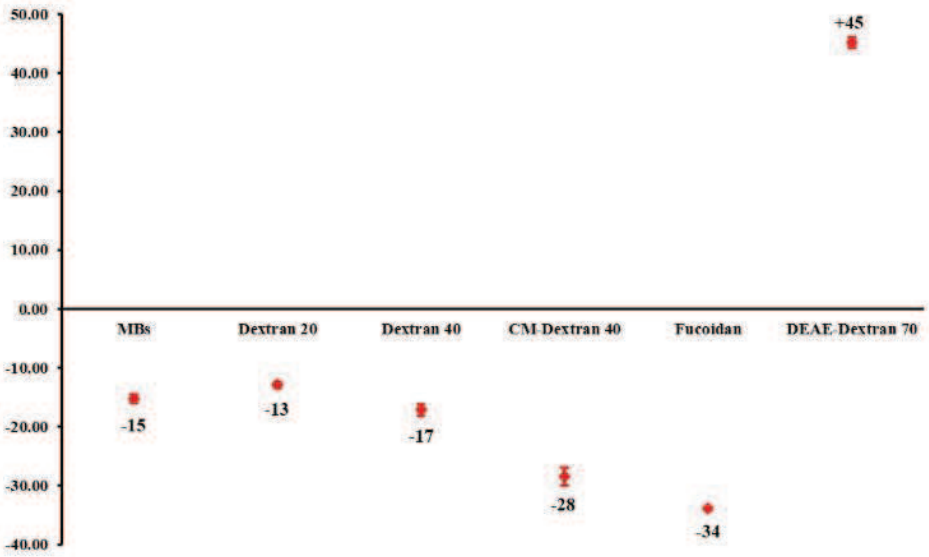

Figure 1. Zeta potentials of PIBCA microbubbles coated with different polysaccharides. Bars represent mean ± SD (n≥3).

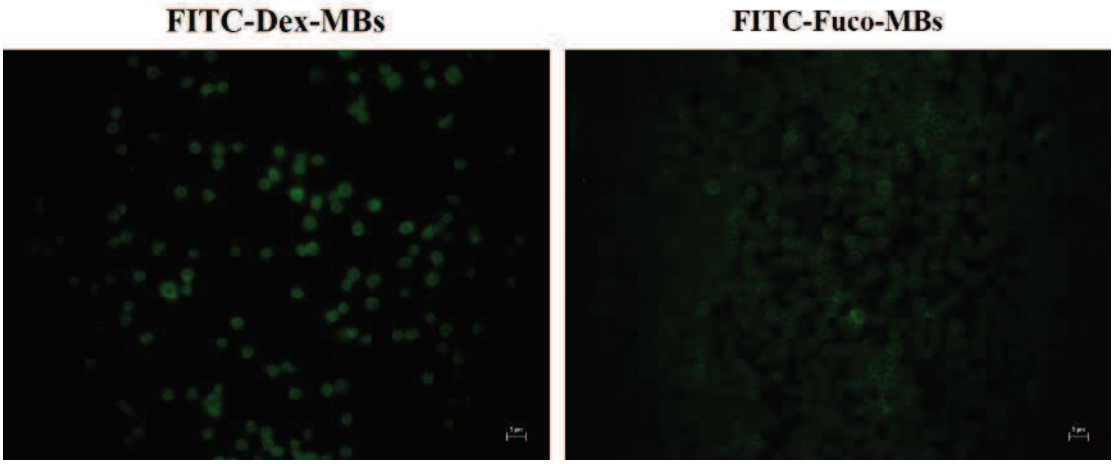

Figure 2. FITC-Dextran and FITC-Fucoidan presence fluorescein on the shell of microbubbles.

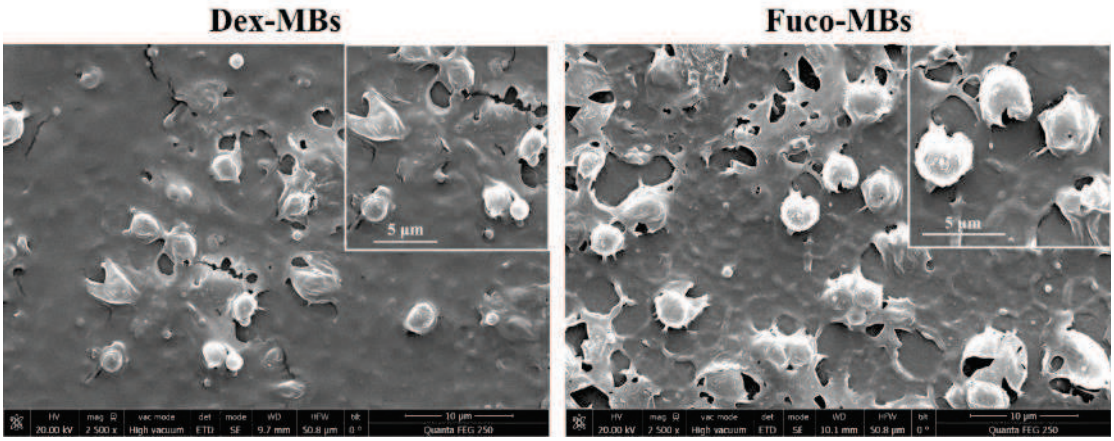

Figure 3. Scanning electron microscopy (SEM) images of MBs.

According to the fucoidan standard solution, the amount of fucoidan per Fuco-MBs was established 197 (**Figure 4**).

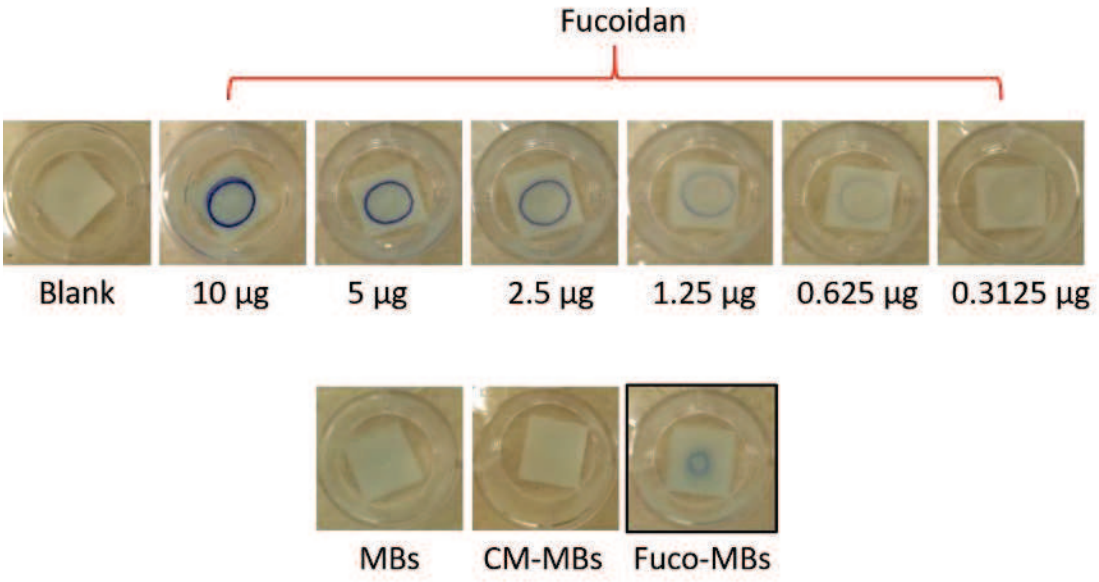

Figure 4. Upper insertion is the fucoidan spot stained with methylene blue. The graph represents the quantity dependents in linear curve.

3.2 *In vitro* ultrasound imaging

For investigating the contrast-intensified ultrasound imaging of microbubbles in flow condition, the same concentration of Dex-MBs and Fuco-MBs in physiological buffer (NaCl 0.9%) were injected into the tube and their echogenicity was detected using a commercial ultrasound imaging system (MS-200D, 18 MHz transducer, VisualSonics

2100), results obtained at the same parameters (**Figure 5**). The images of the 1.7 mm tube show strong contrast enhancements after injection MBs suspensions compared to the 0.9% NaCl-filled tube under the B-mode and non-linear contrast mode. The contrast enhancement arising from both types of microbubbles is not significantly different. In addition, the signal is quite stable with time.

This ability to destroy bubbles with a high MI has been demonstrated in previous studies.[13] Ultrasound-targeted microbubble destruction (UTMD) is also considered a promising technique for non-invasive, targeted drug and gene delivery, and its applications have attracted growing interest.[14] To assess our microbubbles, Fuco-MBs was injected into gel or under the skin of rat. Results showed that almost all of the microbubbles could be destroyed with higher ultrasound energies in either case (**Figure 6**). This indicated its potential as a noninvasive delivery tool in future.

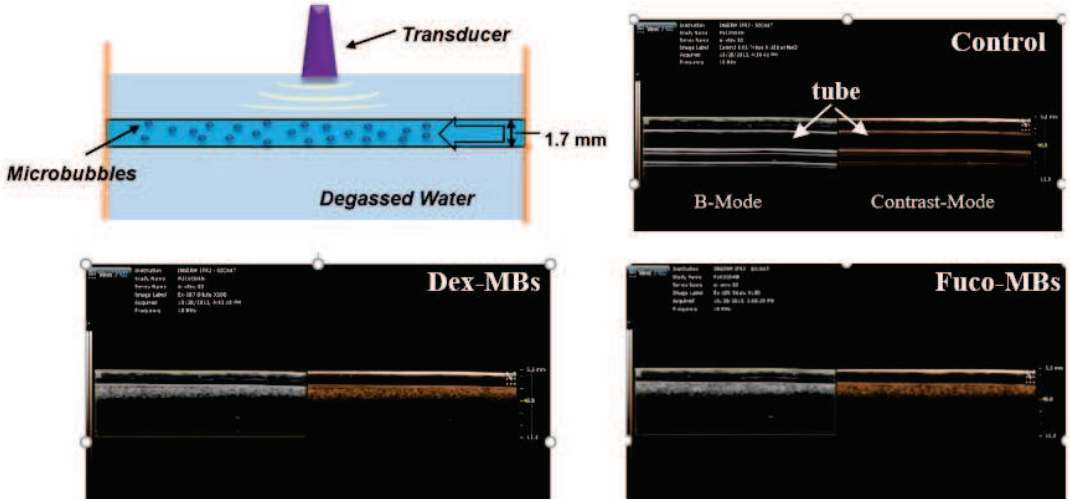

Figure 5. Ultrasound images obtained *in vitro* in B-mode and non-linear Contrast mode. 0.9% NaCl used as a control. Diagram of flow chamber setup used for measurement ultrasonic signals (A). Images of acoustic signal enhancement in the flowing process were recorded (bottom). (transducers: MS-200, frequency: 18 MHz, VisualSonics 2100), microcapsules concentration: 5×10^4 / μL.

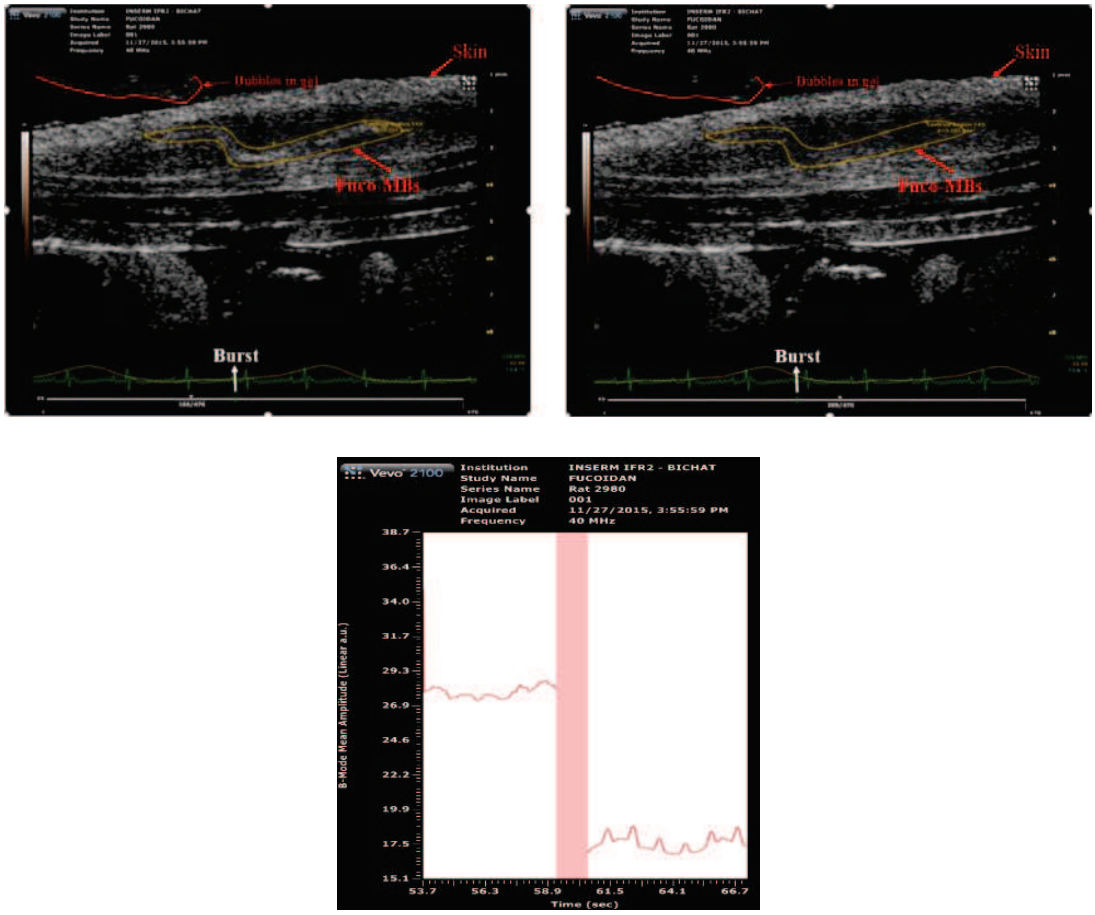

Figure 6. Video showing contrast signal before and after a high mechanical index destructive pulse under skin. Quantitative analysis of signal intensity (Bottom). (transducers: MS-550D, frequency: 40 MHz, VisualSonics 2100), microcapsules concentration: 5×10^4 / μL.

3.3 Molecular imaging of human clots *in vivo*

The highly sensitive contrast agent imaging mode clearly depicted Fuco-MBs attached to the thrombi surface (**Figure 7A**). After bubble destruction for 1 second at a high MI, the contrast enhancement was no longer visible (**Figure 7B**). However, as a control, Dex-MBs showed the same behavior with Fuco-MBs no matter before or after treating with high destructive pluses that may be due to microbubbles absorbed on the surface of thrombi. Thrombi incubated with Fuco-MBs were slightly brighter than control, whereas there were no significant differences. It is difficult to determine enhancement of contrast signals coming from specific binding between Fuco-MBs or from nonspecific absorption. The affinity of Fuco-MBs and P-selectin would be evaluated by new experiment in future.

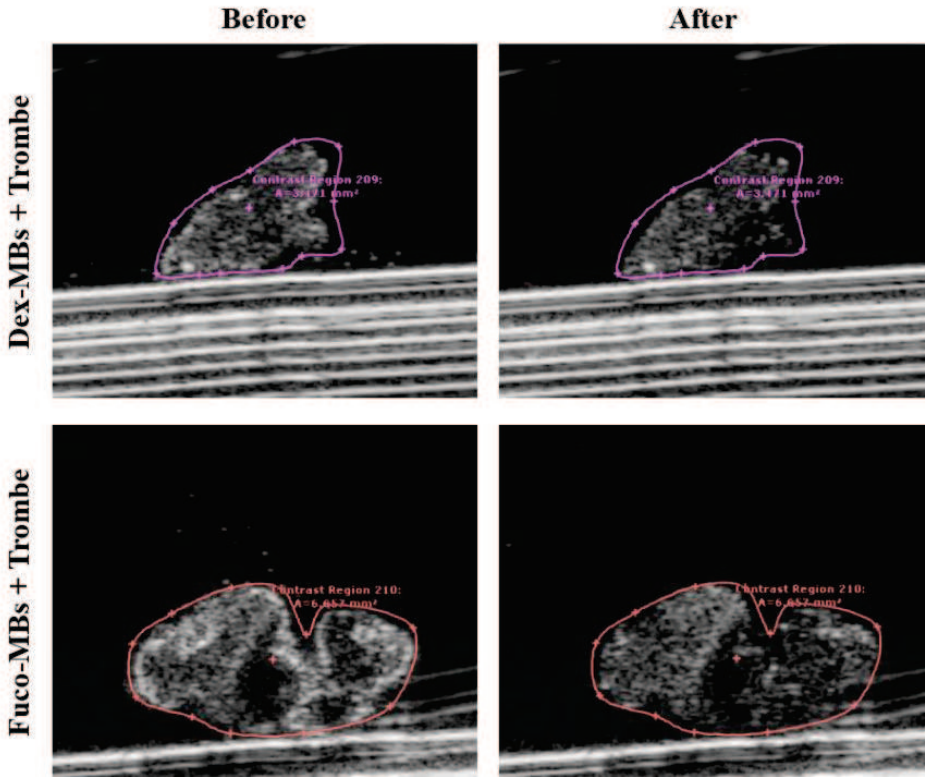

Figure 7. MBs absorption and destruction. Human clot pre-incubated with Dex-MBs (top) and Fuco-MBs (down). Microbubbles attachment to clot surface (left), clot after MBs destruction with a high MI (right). Clot now keeps the position before and after destruction.

4. Conclusion

In this paper, the polysaccharide-coated MBs were fabricated by emulsion polymerization. The method was shown to be very flexible and could be applied with different polysaccharides, which allowed modulating the surface properties of the MBs by choosing the type of polysaccharide. Additionally, these MBs revealed strong echogenicity in the flow conditions and Fuco-MBs showed strong bond on the surface of thrombi. These MBs open very interesting feature for the design of ultrasound contrast agents with surface properties combining the characteristics of several polysaccharides.

References

[1] R. H. Perera, C. Hernandez, H. Zhou, P. Kota, A. Burke, A. A. Exner, *Wiley interdisciplinary reviews. Nanomedicine and nanobiotechnology* **2015**, 7, 593.

[2] D. Cosgrove, *Eur J Radiol* **2006**, 60, 324; E. Stride, N. Saffari, *Proc Inst Mech Eng H* **2003**, 217, 429; F. S. Villanueva, W. R. Wagner, M. A. Vannan, J. Narula, *Cardiol Clin* **2004**, 22, 283; A. Alzaraa, G. Gravante, W. Y. Chung, D. Al-Leswas, M. Bruno, A. R. Dennison, D. M. Lloyd, *Am J Surg* **2012**, 204, 355.

[3] E. Pisani, N. Tsapis, J. Paris, V. Nicolas, L. Cattel, E. Fattal, *Langmuir* **2006**, 22, 4397; E. Pisani, N. Tsapis, B. Galaz, M. Santin, R. Berti, N. Taulier, E. Kurtisovski, O. Lucidarme, M. Ourevitch, B. T. Doan, J. C. Beloeil, B. Gillet, W. Urbach, S. L. Bridal, E. Fattal, *Advanced Functional Materials* **2008**, 18, 2963; R. Diaz-Lopez, N. Tsapis, D. Libong, P. Chaminade, C. Connan, M. M. Chehimi, R. Berti, N. Taulier, W. Urbach, V. Nicolas, E. Fattal, *Biomaterials* **2009**, 30, 1462; R. Díaz-López, N. Tsapis, M. Santin, S. L. Bridal, V. Nicolas, D. Jaillard, D. Libong, P. Chaminade, V. Marsaud, C. Vauthier, E. Fattal, *Biomaterials* **2010**, 31, 1723.

[4] R. Díaz-López, N. Tsapis, E. Fattal, *Pharmaceutical Research* **2010**, 27, 1.

[5] C. Vauthier, C. Dubernet, E. Fattal, H. Pinto-Alphandary, P. Couvreur, *Adv. Drug Del. Rev.* **2003**, 55, 519.

[6] J. R. Harris, F. Depoix, K. Urich, *Micron* **1995**, 26, 103; C. Olbrich, P. Hauff, F. Scholle, W. Schmidt, U. Bakowsky, A. Briel, M. Schirner, *Biomaterials* **2006**, 27, 3549.

[7] S. Fokong, M. Siepmann, Z. Liu, G. Schmitz, F. Kiessling, J. Gatjens, *Ultrasound Med. Biol.* **2011**, 37, 1622.

[8] M. Palmowski, B. Morgenstern, P. Hauff, M. Reinhardt, J. Huppert, M. Maurer, E. C. Woenne, S. Doerk, G. Ladewig, J. W. Jenne, S. Delorme, L. Grenacher, P. Hallscheidt, G. W. Kauffmann, W. Semmler, F. Kiessling, *Invest Radiol* **2008**, 43, 162.

[9] S. Fokong, A. Fragoso, A. Rix, A. Curaj, Z. Wu, W. Lederle, O. Iranzo, J. Gatjens, F. Kiessling, M. Palmowski, *Invest Radiol* **2013**, 48, 843.

[10] O. Diou, N. Tsapis, C. Giraudeau, J. Valette, C. Gueutin, F. Bourasset, S. Zanna, C. Vauthier, E. Fattal, *Biomaterials* **2012**, 33, 5593.

[11] L. Bachelet, I. Bertholon, D. Lavigne, R. Vassy, M. Jandrot-Perrus, F. Chaubet, D. Letourneur, *Biochim. Biophys. Acta* **2009**, 1790, 141; F. Rouzet, L. Bachelet-Violette, J. M. Alsac, M. Suzuki, A. Meulemans, L. Louedec, A. Petiet, M. Jandrot-Perrus, F. Chaubet, J. B. Michel, D. Le Guludec, D. Letourneur, *J Nucl Med* **2011**, 52, 1433.

[12] J. M. Lee, Z.-U. Shin, G. T. Mavlonov, I. Y. Abdurakhmonov, T.-H. Yi, *Appl. Biochem. Biotechnol.* **2012**, 168, 1019.

[13] R. Kern, K. Szabo, M. Hennerici, S. Meairs, *Stroke* **2004**, 35, 870.

[14] H. Chen, J. H. Hwang, *Journal of Therapeutic Ultrasound* **2013**, 1, 10.

GENERAL DISCUSSION AND PERSPECTIVES

In this work, we have designed and synthesized three kinds of ultrasound contrast agents with different structures; all of them can be easily functionalized by fucoidan. Their echogenic properties and binding abilities with P-selectin were also investigated *in vitro* and *in vivo*. This work is the bold trial in the domain of ultrasound molecular imaging of cardiovascular diseases and it provides use for reference experiences for similar projects in future studies.

Since the end of 1970s, liquid perfluorocarbons, such as PFOB, have been tested as contrast agents for ultrasonography and MRI due to its greater stability and low solubility in blood.[1] The challenge of PFOB encapsulation is their low miscibility with organic solvents and high density (1.93 g/mL). Nowadays, the most frequently used method of loading PFOB is an emulsion-evaporation process, which may form nano-/microcapsules. PLGA is used as a polymer shell in this method. However, its application potential is limited by its hydrophobic surface. To address this problem, various hydrophilic matters are considered for surface modification. In this study, polysaccharide modified PIBCA is employed due to its excellent biodegradability and biocompatibility.

- "***Aborted", fucoidan-functionalized PFOB nanoparticles***

In the experimental work, we try to encapsulate PFOB within PIBCA nanoparticles. The nanoparticles were prepared by redox radical emulsion polymerization (RREP) of IBCA using polysaccharide as coating material.[2] Firstly, we attempted to obtain nanocapsules, Zandanel C. *et al.* described hydrophobic fluorescent probe mixed with acetonitrile could be delivered into the core of nanoparticles. Following their work and emulsion-evaporation method, firstly we put PFOB into the acetone and then added them into aqueous phase during polymerization process. We hope the rapid polymerization could capture the PFOB droplets before they escape from acetone. However, due to their high hydrophobic and density, results indicated all of PFOB would be released from acetone before polymerization completed.

Next step, we developed the new method to capture PFOB and it will produce nanoparticles consisting of polysaccharide-PIBCA diblock copolymer core inlaid with PFOB based on RREP process in PFOB emulsion. These nanoparticles could be easily functionalized with fucoidan, but we also found the PFOB content decreased with the increase of fucoidan. This may be due to the negative charge of fucoidan may undermine the nanoparticles stability or the longer fucoidan chains on the nanoparticles obstruct PFOB access and compare to dextran. The intensity of contrast signal is very weak.

This fucoidan functionalized nano contrast agent has a strong affinity for human activated platelets *in vitro*. It is consistent with the results that had been reported by Bonnard T. *et al.* using fucoidan functionalized polysaccharide microparticles to interact with activated platelets.

In vivo ultrasonic images analysis revealed that a fraction of them accumulated in the thrombotic AAA wall where P-selectin is expressed and presented contrast enhancement even after 20 min, but the intensity of contrast signal is very weak. After repeated trials of the same condition *in vivo*, we realized it is difficult to clearly segment signal of contrast agent from vessel wall on ultrasonic imaging.

- Microcapsules bring us closer to the goal

Reviewing the previous part's work, we assumed that the poor echogenicity was due to its low content of PFOB. To address this problem, the structures of core-shell microcapsules are considered to instead of former nanoparticles. We developed microcapsules composed of a core of liquid and a PIBCA-polysaccharide mixed membrane based on modified emulsion-evaporation polymerization process. This was also the first successful synthesis of polysaccharide coated PIBCA microcapsules, and it is also easily functionalized with fucoidan.

We evidenced that these microcapsules specifically bound to P-selectin which is expressed on the human activated platelets, irrespective of being in static conditions

or under high velocity blood flow condition. Histological analysis revealed that fucoidan functionalized microcapsules were localized inside the media layer of the thrombotic AAA wall in rats. Unfortunately, the echogenicity of microcapsules is still insufficient to observe the contrast enhancement from vessel wall signals even when the mass percentage of PFOB is close to 50%.

Previous research identified the shell thickness-to-radius ratio of microcapsules strongly influences their echogenicity and their compressibility.[3] As the absolute shell thickness decreases, microcapsules become more compressible and therefore backscatter ultrasonic waves more efficiently.[4] Here we found the thickness of shell could be easily adjusted by pH condition, but the yield declined rapidly and the size distribution became uneven, which prevents its further development as a commercial contrast agent. Another possible approach for reducing the thickness of the shell is decreasing masses of IBCA during the synthesis process. Mousnier L. *et al.* have demonstrated the decline in polymer proportion would result in microcapsules with a decreasing thickness to PLGA/PLGA-COOH microcapsules.[3] This idea would be tested in the future experiments. Although these microcapsules could not be used as an ultrasound contrast agents at current stage, the specific ability of them to target the P-selectin also could be associated to the loading of antithrombotic drugs in this microcarrier.

- Are the liquid PFCs good contrast agents for ultrasound molecular imaging?

Based on the above results, we found that irrespective of the injection Fuco-TNPs-PFOB or Fuco-MCs, the artery only presented significant contrast for a few seconds, and then the signals disappeared due to reduction of concentration. These results force us to reconsider if PFOB is a good blood poll contrast agent. Moreover, we observed both vessel tissues and PFOB exhibit the similar reflected ultrasound signal in B-mode ultrasound, it is difficult to clearly identify or differentiate the contrast enhancement by accumulated PFOB contrast agents from signal of vessel wall on ultrasonic imaging. Motion artifacts caused by respiratory and

cardiac activities that always can obscure images.

Actually, PFOB is considered to be used as a contrast agents instead of microbubbles mainly because they can withstand pressure changes and mechanical stresses.[5] However, they tend to be less echogenic than gaseous bubbles, in particular when particle size reduce to nano-scale, because they are incompressible and do not oscillate strongly with the passing acoustic wave.

Until now, there have been only few scientific studies to understand the contrast effects of PFOB *in vivo* and the results are not as good as the researchers expected. Pisani E. *et al.* found the contrast enhancement only lasted a few seconds in vessels after PFOB nanocapsules intravenous injection.[4] Díaz-López R. *et al.* also proved echogenic signal in tumor was observed after the intra-tumoral injection PFOB nanocapsules. However, no contrast was observed neither directly after intravenous injection or later, although they confirmed the presence and the accumulation of nanoparticles in tumor tissue.[6] These conclusions reveal the *in vivo* enhancement effects of PFOB ultrasound contrast agent depend mainly on their concentration, which was also confirmed by our experimental results.

Ultrasound molecular imaging techniques require contrast probe which could detect the pathological processes at the molecular level, which means contrast agent should have high signal-to-noise ratio and enable detection at low concentration. However, these features are not present in the PFOB, so it is not reasonable to continue along this path.

- Microbubbles for Future…

In order to solve the low echogenicity totally, we abandoned PFOB, choosing to design functionalized microbubbles. Microbubble has been widely used in human as functional acoustic contrast agent for ultrasonography. They can be visualized due to their high echogenicity in standard B-Mode imaging. Like PFOB, the challenge is that the microbubbles and tissue are comparably bright, resulting in poor contrast between

them. But fortunately, due to their high compressibility, microbubbles will oscillate nonlinearly in an ultrasound field, resulting in the scattered ultrasound echo containing non-linear energy. Non-linear contrast mode imaging techniques could detect this energy from bubbles and segment their signals from the surrounding tissue. The application of the traditional microbubbles was ounded by their inherent defects: instability.

Recently, polymer-based microbubbles have attracted the attention of researchers since their higher stability and enhanced acoustic properties. Particularly, PBCA-MBs have been developed and exhibit prolonged circulation by reducing the gas-core shrinkage.[7] However, the application potential of PBCA-MBs is limited by their rather hydrophobic surface and insufficient functional chemical groups on the surface. Until now, only few targeting ligands, e.g. short peptide, antibody are combined with PBCA-MBs by hydrolyzing PBCA to produce -COOH group and this approach was relatively inefficient and time-consuming.[8]

Here we design a polysaccharide coated PIBCA microbubbles, it had stable structure and exhibited prolonged circulation. Diverse polysaccharides could be fixed on the microbubbles surface and provide lots of reaction groups for further modifications: for example, DEAE-MBs have high positive charge and they could deliver some negative charge particles, like RNA or protein; CM-MBs offer sufficient -COOH group, which could be used to link ligand through EDC/NHS reaction. Meanwhile, fucoidan, as a type of polysaccharide, was successfully immobilized on the shell of microbubbles.

In vitro experiments show strong contrast enhancements after injection MBs suspensions compared to the 0.9% NaCl under the B-mode and non-linear contrast mode, and they could be destroyed by high ultrasound energies. Adding fucoidan didn’t change the echogenic signal of MBs. In addition, the signal is quite stable with time.

We also proved fucoidan functionalized MBs could accumulate on the surface of platelets-rich thrombus, although we haven't established yet, a good method to prove whether these accumulations come from specific binding between fucoidan and P-selectin or from non-specific adsorption. But these results are encouraging and future work will focus on improving experiments to assess their ability to bind on thrombus expressed P-selectin under flow conditions and also detect cardiovascular pathologies in future.

References

[1] M. S. Liu, D. M. Long, *Radiology* **1977**, 122, 71.

[2] C. Chauvierre, D. Labarre, P. Couvreur, C. Vauthier, *Macromolecules* **2003**, 36, 6018.

[3] L. Mousnier, N. Huang, E. Morvan, E. Fattal, N. Tsapis, *Int. J. Pharm.* **2014**, 471, 10.

[4] E. Pisani, N. Tsapis, B. Galaz, M. Santin, R. Berti, N. Taulier, E. Kurtisovski, O. Lucidarme, M. Ourevitch, B. T. Doan, J. C. Beloeil, B. Gillet, W. Urbach, S. L. Bridal, E. Fattal, *Advanced Functional Materials* **2008**, 18, 2963.

[5] R. Díaz-López, N. Tsapis, E. Fattal, *Pharmaceutical Research* **2010**, 27, 1.

[6] R. Díaz-López, N. Tsapis, M. Santin, S. L. Bridal, V. Nicolas, D. Jaillard, D. Libong, P. Chaminade, V. Marsaud, C. Vauthier, E. Fattal, *Biomaterials* **2010**, 31, 1723.

[7] J. R. Harris, F. Depoix, K. Urich, *Micron* **1995**, 26, 103; C. Olbrich, P. Hauff, F. Scholle, W. Schmidt, U. Bakowsky, A. Briel, M. Schirner, *Biomaterials* **2006**, 27, 3549; S. Fokong, M. Siepmann, Z. Liu, G. Schmitz, F. Kiessling, J. Gatjens, *Ultrasound Med. Biol.* **2011**, 37, 1622.

[8] M. Palmowski, B. Morgenstern, P. Hauff, M. Reinhardt, J. Huppert, M. Maurer, E. C. Woenne, S. Doerk, G. Ladewig, J. W. Jenne, S. Delorme, L. Grenacher, P. Hallscheidt, G. W. Kauffmann, W. Semmler, F. Kiessling, *Invest Radiol* **2008**, 43, 162; S. Fokong, A. Fragoso, A. Rix, A. Curaj, Z. Wu, W. Lederle, O. Iranzo, J. Gatjens, F. Kiessling, M. Palmowski, *Invest Radiol* **2013**, 48, 843.

GENERAL CONCLUSION

Cardiovascular diseases, particularly artery diseases such as atherosclerosis, aneurysm, and thrombosis remain major public health problems. Despite tremendous advances in diagnosis and treatment of vascular diseases made recently, currently vasculopathy can only be diagnosed at advanced stages, either by directly revealing the narrowing of the arterial lumen or by evaluating the effect of arterial stenosis on organ perfusion. Non-invasive diagnosis techniques rely on molecular imaging enabling early detection and evaluation of the vascular pathological changes are perceived to have excellent growth prospects. Ultrasonography is widely used as a screening tool in clinic to detect cardiovascular disease based on its several obvious advantages: ease of procedure, low cost and no radiation exposure. Ultrasound molecular technology plays an important part in today's molecular imaging.

The aim of this doctoral project was to develop injectable, low-cost and simple contrast agents, functionalized with fucoidan as efficient acoustic tracers of P-selectin for molecular imaging of arterial pathologies.

Perfluorooctyl bromide (PFOB) was firstly chosen as contrast agent due to its stability and echogenic properties. In the 1st experiment study, we synthesized nanoparticles functionalized with fucoidan and combined with PFOB. They could bind to P-selectin expressed by human activated platelets and we also have observed contrast enhancement in P-selectin expressed area in animal models of arterial disease. However, signal enhancement was insufficient to clearly identify the abdominal aortic aneurysm area, probably because of poor ultrasound signal of nanoparticles due to low content of PFOB and their very small size.

To address the encapsulation efficiency problem, in the next work we developed bigger systems such as fucoidan functionalized microcapsules with PFOB core. These microcapsules exhibited excellent compatibility with cells and they could specifically bind to the P-selectin in static and arterial flow conditions. In addition, we showed *in vivo* on rats the ability of fucoidan functionalized microcapsules to bind to thrombotic

AAA and evidenced their presence in the AAA wall by histology. We also put to evidence that both types of microcapsules were eliminated through liver metabolism function. Unfortunately, the contrast enhancement was still insufficient to be observed. Future works are required to study the loading of contrast agents or therapeutics to achieve molecular diagnosis and/or treatment of cardiovascular pathologies overexpressing P-selectin.

In the 3rd chapter, to improve echogenicity, polysaccharide-coated microbubbles were synthesized by an original emulsion polymerization reaction. These microbubbles revealed strong enhancement contrast signals in flow conditions and fucoidan functionalized microbubbles showed strong binding property to the surface of thrombi. These functionalized microbubbles appear to be very promising molecular ultrasound imaging tools for the diagnosis and the treatment of cardiovascular diseases.

ABSTRACT

ABSTRACT

Cardiovascular diseases due to atherosclerosis remain a major morbidity in developed countries. Their treatment could be substantially improved with early detection of the vascular pathological changes by non-invasive diagnostic techniques. Ultrasonography is widely used as a screening tool in clinic to detect cardiovascular diseases. However, its low resolution requires the development of targeted acoustic tracers to improve the contrast degree. Fucoidan is a sulfated polysaccharide ligand with a high affinity for P-selectin, which was found to be expressed on the activated platelets and endothelial cells and involved in the early pathogenesis of cardiovascular diseases. The aim of this doctoral project was to develop injectable, low-cost and simple contrast agents, functionalized with fucoidan as efficient acoustic tracers of P-selectin for ultrasound molecular imaging of arterial pathologies. Three types of contrast agents have been developed: 1) Fucoidan functionalized nanoparticles loaded with perfluorooctyl bromide (PFOB). They could bind to P-selectin and exhibit contrast enhancement in animal models of arterial disease. However, these products showed poor echogenicity in blood stream due probably to low content of PFOB and their very small size. 2) Fucoidan functionalized microcapsules with PFOB core were developed to improve the PFOB encapsulation efficiency. They could bind to P-selectin in arterial flow conditions, and *in vivo* results revealed that these microcapsules were located in the regional expression of P-selectin. Unfortunately, the contrast enhancement was still insufficient to be observed. 3) To address echogenicity problems, fucoidan functionalized polymer microbubbles were designed to replace PFOB. They showed strong signal enhancement under flow conditions and could accumulate on the surface of platelets-rich thrombus. These results indicated that these microbubbles, as ultrasound molecular imaging tools, could be very interesting for the future study of arterial diseases.

Keywords: Fucoidan, P-selectin, Ultrasonography, Contrast agent, Cardiovascular diseases

RESUME

Les maladies cardio-vasculaires liées à l'athérosclérose sont pourvoyeuses d'une importante morbi-mortalité dans les pays développés. Une détection plus précoce des modifications des parois vasculaires, via des techniques de diagnostic non invasives, pourrait sensiblement améliorer leur prise en charge. L'échographie est largement utilisée comme outil de dépistage des maladies cardiovasculaires. Cependant, sa faible sensibilité limite son utilisation. Le développement d'agent de contraste spécifique permettant de résoudre ce problème semble donc primordial. Le fucoidane est un ligand polysaccharidique sulfaté ayant une forte affinité pour la P-sélectine. Exprimée au niveau de la surface des plaquettes activées et des cellules endothéliales, cette dernière est impliquée dans la pathogénèse précoce des maladies cardiovasculaires. Le but de ce projet de thèse a été de développer un agent de contraste injectable ciblant la P-sélectine via le fucoidane dans le but de réaliser une modalité d'imagerie moléculaire de faible coût, simple et spécifique des pathologies artérielles. Trois types d'agents de contraste ont été développés : 1) Des nanoparticules associées à du bromure de perfluorooctyle (PFOB), fonctionnalisées par du fucoidane. Elles ont été capables de se fixer à la P-selectine et une amélioration du contraste a été observée *in vivo* dans un modèle animal de maladie artérielle. Cependant, ces produits présentaient une mauvaise échogénicité dans la circulation sanguine, probablement en raison de leur faible teneur en PFOB et de leur très petite taille. 2) Afin d'améliorer l'échogénicité, des microcapsules contentant du PFOB dans leur coeur ont été développées. Celles-ci se sont également liées à la P-sélectine même en condition de flux sanguin. Des résultats *in vivo* ont montré que ces microcapsules étaient présentes dans les zones où la P-sélectine était exprimée. Malheureusement, l'augmentation du contraste était toujours insuffisante pour être suffisamment discriminante. 3) Des microbulles (structure polymère contenant un coeur gazeux), également fonctionnalisées par du fucoidane, ont été conçues pour surmonter ce problème d'échogénicité. Elles ont montré une augmentation significative du signal acoustique en condition de flux sanguin. De plus, ces microbulles se sont accumulées à la surface des parois artérielles riches en thrombus. Ces derniers résultats indiquent que ces microbulles, en tant qu'outil d'imagerie moléculaire ultrasonore, pourraient être très intéressantes pour les futures études des maladies artérielles.

Mots-clés: Fucoidane, P-sélectine, Ultrasonographie, Agent de contraste, Maladies cardiovasculaires.